August 2019

The Shape of Soft Matter: Geometry and Defects

Francesco Serafin
Syracuse University

Abstract

How does shape emerge at macroscopic scales from the spontaneous self-organization of building blocks at smaller scales? In this thesis, I will address this question in the context of closed soft two-dimensional membranes with internal order. Soft matter represents a good arena to identify simple universal mechanisms for shape selection. In fact, a distinctive property of soft materials is that they can undergo dramatic changes in geometric conformation at relatively low energetic cost. Thus, shape itself becomes a statistically fluctuating degree of freedom, and in some cases it can be found as the ground state of an appropriate free energy functional. The building blocks of soft materials typically have lower symmetry than elementary point particles and exhibit rich patterns of spontaneous ordering as the free energy of the system is lowered. Order is frustrated if the membranes topology is non-trivial, and topological defects, which typically arise as finite temperature excitations, are forced to exist even in the ground state. Topological defects can play a key role in the selection of the ground state shape. For example, the presence of defects in closed 2-dimensional membranes with liquid-crystalline order enable to predict the existence of surprisingly sharp, faceted yet extremely soft polyhedral ground-state shapes. Upon functionalization of the defect sites, these faceted ground states may provide soft self-assemblable building blocks analogue to atoms but micron-sized, whose valence could be selected according to the internal symmetry of the liquid crystal. Topology plays an important role also in the statistical mechanics of fluid membranes. These closed fluid sacs can have the shape of deformed spheres, one-handled tori, or closed shapes with an arbitrary number of handles. The statistical mechanics of membranes with fluctuating number of handles, encoded in the ensemble's partition function, is dominated by shape fluctutations, and new techniques are required to extract physical information from the sum over arbitrary topologies.

The Shape of Soft Matter:

Geometry and Defects

by

Francesco Serafin

Laurea in Fisica, Università degli Studi di Trieste, 2011

Laurea Magistrale in Fisica, Università degli Studi di Trieste, 2014

DISSERTATION

Submitted in partial fulfillment of the requirements for the degree of

Doctor of Philosophy in Physics

Syracuse University

August 2019

Acknowledgements

I am deeply grateful to the many wonderful people who shared with me the past five years, and who made this journey possible. First and foremost, I am grateful to Mark Bowick for teaching me the value and the practice of perseverance and for his generous encouragement in many occasions. His profound and personal point of view on the physical world has been a constant source of inspiration in these years, and will always be in the future. I am indebted to Cristina Marchetti who was practically a second advisor to me during the final year. She generously shared her perspective and advice on physics and beyond in the numerous conversations we had.

I warmly thank Scott Watson, for his support and encouragement. I am grateful to Sebastian Streichan and Boris Shraiman for all the stimulating conversations at KITP from which I learnt a lot. I would like to thank Sidney Nagel for illuminating conversations about smectic vesicles. Thank you to Jennifer Schwarz for our discussions about membranes.

These five years have been enriched by beautiful friendships. I would like to thank Swetha Bhagwat for being a courageous and very close friend. I would like to thank Suraj Shankar for all the fun, unbounded conversations on the most diverse aspects of science, art and life. Thank you to Gizem Sengör, who can see life as a beautiful painting. I would like to thank Cem Eröncel and his love for adventure, who made so many memorable trips possible. Thank you to Raghav Govind Jha, Nouman Butt, Anam Mano, Sourav Bhabesh, Prashant Mishra for initiating me into the game of 29, and for being fantastic companions in many adventures. Thank you to Ogan Özsoy, whose remarkable sense of humor is truly contagious. I thank Mahesh Gandikota for our photographic trips and beautiful conversations. Thank you to Preeti Sahu for sharing her profound passion for music through memorable duets. Thank you to Jerome for our chess games and all the philosophical conversations we had. I would like to thank Arvind Venkateswaran for the fun music sessions. I thank Kuang Liu

for interesting conversations and fun dinners. Thank you also to Asad, Sarthak, Raj, Gabriele, Arthur, for all the moments we shared. I have truly enjoyed every meeting with Matteo Paoluzzi, from whom I learned a lot. Thank you to David Yllanes and Michael Moshe, whose expertise I deeply admire, for the insigthful comments that they offered me. I also thank Oksana Manyuhina, Matthias Merkel, and Benjamin Loewe for many useful conversations on physics.

I would like to thank Patty Whitmore, Yudaisy Salomón Sargentón, Patty Ford in Syracuse and Bibi Rojas, Lisa Stewart, Lori Staggs, Amy Burgard at KITP for being always smiling welcoming and supportive, and for their crucial work on the administrative side. Merci to Martine White for some memorable dinners and concerts at the Granada theatre in Santa Barbara.

I would like to warmly thank all my friends in Italy, who have gifted me their crucial support during these five years.

Finally, I wish to express my deep gratitude to my parents. Their love has inspired me throughout these five years. I thank them for being always truthful and for teaching me every day how to sail even in stormy seas. Thank you for having made this journey possible.

Contents

Chapter 1

Introduction

1.1 What is shape?

One of the most intuitive ways of experiencing the physical world is to categorize it into shapes. Looking at the remarkable richness of forms around us, a curious observer might be led to ask: what is the origin of shapes? How do natural shapes spontaneously emerge? Investigations on the nature of shape have ancient roots. Between 384 and 322 BC Aristotle argued that the properties and activities (what today we would call functionalities) of physical objects are determined more by shape than by their specific constituents. He further reasoned that shape is inseparable from matter, and is encoded in the relations between elementary building-blocks [5]. In the present language of physics, we can say that the shape of a spontaneously formed material arises from multiple levels of description: the nature of its constituents, the interactions between them, and most importantly how the local information encoded in the interactions is propagated across the material at large scales.

It is useful to rephrase the vague question posed above in more concrete terms: can we identify simple physical mechanisms for shape selection? Sometimes a shape is achieved applying a sequence of moves decided a priori: a gem can be shaped by

a jeweler who performs a sequence of cuts to achieve a desired result. By contrast, the planes of ordered atoms in the crystal were formed *spontaneously* by self-driven processes, without any external direction. The broad theme underlying this thesis is to identify mechanisms of spontaneous self-organization of elementary building-blocks into complex shapes and patterns at larger scales. Clearly patterns and structures exist at every intermediate scale, so the concept of shape is always relative to the magnification we choose (unless we are looking at a fractal). For the scope of this thesis, we will describe shape at the scale of the system size, defined as the radius of the smallest sphere that contains the entire material.

The scale separation between the system's size and its constituents suggests the use of continuum field-theoretic models to study shape. The material will be represented as a collection of fields on a manifold and its shape will be encoded in the geometry of the manifold. This is justified *a posteriori* in the spirit of the Renormalization Group [105, 106]: we imagine that we have coarse-grained the specific properties at the molecular scale by integrating out larger and larger blocks of interacting units, absorbing their effective interactions into few scale-dependent couplings between the long-wavelength fields. The long-wavelength theory is represented by an (infrared)[1] fixed point[2] at which the Hamiltonian contains few relevant operators selected on the sole basis of symmetry and dimensionality. All the microscopic models belonging to the fixed point's basin of attraction flow to the same infrared theory. In this precise

[1]The renormalized Hamiltonian depends only on the low momentum Fourier modes of the fields. By analogy with electromagnetic radiation, *infrared* refers to low momenta. Let $Z = \int \mathscr{D}\psi \, \exp[-\beta H(\psi, g)]$ be the partition function of the theory, where ψ are an ensemble of random fields, $\beta = (k_{\mathrm{B}}T)^{-1}$, g are the bare couplings and $\mathcal{H}(\psi, g)$ is the Hamiltonian. We Fourier-transform the fields $\psi = \sum_k \psi_k \exp(i\mathbf{k}\cdot\mathbf{x})$ and separate the Fourier modes into low momenta $L^{-1} < k^s_< < (sL)^{-1}$ (long wavelength, so infrared) and high momenta $(sL)^{-1} < k^s_> < a^{-1}$ (short wavelength, so ultraviolet) , where L is the system's size, $a \ll L$ is a microscopic cutoff and $s < 1$. The partition function becomes $Z = \prod_{k_<} \int \mathrm{d}\psi_{k^s_<} \prod_{k^s_>} \int \mathrm{d}\psi_{k^s_>} \, \exp[-\beta H(\psi_{k^s_<}, \psi_{k^s_>}, g)]$. After integrating over the high momenta, the renormalized Hamiltonian $\widetilde{H}$ at the scale s is formally given by $\exp[-\beta \widetilde{H}(\psi_{k^s_<}, g(s))] \equiv \prod_{k^s_>} \int \mathrm{d}\psi_{k^s_<} \, \exp[-\beta H(\psi_{k^s_<}, \psi_{k^s_>}, g(s))]$, and it depends only on low momentum 'infrared' modes [3].

[2](if it exists).

sense the infrared model describes universal properties common to all its microscopic realizations.

Understanding how shape emerges in soft materials is challenging because they have many internal degrees of freedom and they undergo large deformations at a relatively low energetic cost. The constituent building blocks of soft matter are typically larger in size than atoms or small rigid molecules, and their interactions are weak, in contrast to the strong electrostatic or covalent bonds that dominate at the atomic scale. For example, ionic interactions between large charged molecules dispersed in water are screened by the presence of latter[3]. Other examples include screened permanent or induced dipolar interactions, short-range steric repulsion due to the Pauli exclusion principle, weak hydrogen bonds and van der Waals forces [56] .

Since the typical interactions are short-ranged and are often comparable with the thermal energy k_BT, many arrangements of neighboring building blocks are possible. At distances larger than few elementary units, the material already exhibits a great number of conformations, all with similar mechanical energy. This means that configurational entropy dominates over mechanical energy. When effective equilibrium descriptions are available, the phase diagram of the system is governed by a Landau *free* energy rather than mechanical energy.

Perhaps counter-intuitively, entropy can lead to ordering. Examples are the spontaneous out-of-equilibrium aggregation of lipids dispersed in a solvent into extended 2–dimensional geometric structures [87] or the low-temperature planar phase of thermally fluctuating polymerized membranes embedded in three dimensions [80]. It is therefore important to use appropriate order parameters obtained by coarse-graining finer details of the system below some length scale of interest.

The coarse-grained geometry of soft matter is often coupled to other internal degrees of freedom that appear as additional order parameter fields. They are not just

[3]The effective weak couplings arise from a trace over the degrees of freedom of the surrounding environment.

scalars, but can be vectors (e.g. polarization), tensors (e.g. elastic stress), or elements of more general spaces (e.g. orientations are elements of the real projective space) depending on the nature of the building blocks underlying the large-scale geometry. Finally, most soft matter systems are immersed in a surrounding environment so their extrinsic geometry is also represented by a set of fluctuating fields, coupled to the intrinsic geometry and the internal order parameters.

1.2 The relevance of shape in Soft materials

Soft materials respond with large deformations to external stresses and so they exhibit a rich variety of both smooth and singular shapes, as well as abrupt changes in their conformation either at zero or at finite temperature. Examples range from fluid lipid bilayers, liquid crystals, gels and colloidal systems to biological membranes and tissues.

Fluid vesicles

Lipid bilayers are simplified versions of more complex biological membranes that form the cell's outer surface, or that enclose various structures in the cell's interior [8, 87]. A cell's outer membrane separates the interior from the environment and regulates the exchange of material and mechano-chemical signals with the external world. Cellular membranes are complex structures: according to the fluid mosaic model [81], they are made of various species of large proteins floating in a lipid bilayer. Lipids, for example phosphatidylcholine, are made of a polar head and an hydrophobic tail. X-rays diffraction experiments shows that lipids (in general amphiphiles) dispersed in a solvent have many phases depending on temperature and lipid concentration. At low concentration, the lipids form micelles, spherical aggregates with tails filling the interior and heads in contact with the fluid. Increasing the concentration,

the micelles first organize in a Body-Centered Cubic lattice and then transition into cylinders. At high concentration, amphiphiles form a bilayer, a nanometric-thin sheet where the hydrophilic heads screen the tails from the solvent on both sides. These structures, which can measure hundreds of microns across, are stabilized by weak van der Waals interactions between the tails. The line energy along the boundary of a raft of lipids increases with the system size, so large lipid bilayers spontaneously form edge-free closed fluid sacs called vesicles or liposomes (see [47] for an overview of vesicle formation).

In the 1970s, Canham [11] and Helfrich [44] proposed a simple geometric model for fluid membranes, based on extrinsic curvature elasticity. We refer the reader to section 4.1 for further details on the Helfrich-Canham effective Hamiltonian. Historically, it was hoped that curvature energy models would explain the discotic shape of red blood cells (RBC). It was later realized that RBC's cytoskeleton affects its elastic properties and it doesn't behave as a simple fluid, but the model found its realization in artificial amphihphilic membranes. Amphiphilic vesicles respond to changes in temperature, pressure, volume-to-area ratio and other parameters with dramatic shape deformations. They can deform from round spheres to ellipsoids, pear and biconcave shapes such as discocytes and stomatocytes [65, 66, 97]. The formation of negative-curvature necks is called budding. It can be induced either by curvature instabilities in vesicles or by line tension between domains in multi-component membranes [52]. A shrinkage of necks may lead to a topological transition (endo- and exo-cytosis) via nucleation of a daughter vesicle, a process resembling the creation of baby-universes in fluctuating gravity. Cells use budding and nucleation of vesicles to exchange and transport chemicals from the external environment.

The Helfrich-Canham model is related to the Willmore functional, an important mathematical object appeared for the first time in the 1810s in the works of Sophie Germain [38] on elasticity, and later forgotten and rediscovered several times. Besides

lipid vesicles, the Willmore functional appears in the theory of elastic plates and shells as the energy associated to flexural deformations [61]. Polyakov [91] found the crumpled ('creased') phase of non-critical strings in $D = 4$ embedding dimensions, by adding a higher-dimensional version of the Willmore functional to the Nambu-Goto string action. The equilibrium shapes of fluid vesicles are minimizers of the Willmore functional. They comprise classic geometric shapes of arbitrary genus g: the sphere ($g = 0$), the Clifford torus ($g = 1$), Lawson surfaces [62] ($g = 2$) and higher genus surfaces. In 1991 Mutz and Bensimon [79] observed toroidal vesicles as predicted by Ou-Yang and Zhong-can in [115]. Soon after (1994-1995) Michelet *et al.* [75, 76] observed that genus-2 vesicles undergo diffusion in shape space. This phenomenon was explained using conformal properties of the Willmore energy [53]. Theoretical and experimental investigations of higher-genus vesicles are reported, for example, in [32, 49]).

Ordered phases of 2-dimensional soft matter

Many soft materials can spontaneously order. At low temperature, lipids' heads in a membrane optimize their attractive interactions by forming a bond-orientationally ordered phase. Liquid crystals (LCs) are anisotropic fluids formed by elongated or branched molecules that can break rotational symmetry (e.g. nematics) by ordering neighbouring molecules along a common local direction, as well as translational symmetry if they organize in stacks or layers (e.g. smectics) [34, 37, 54]. Membranes made of liquid crystalline units (called mesogens) have more degrees of freedom than fluid membranes, because they can partially order. The microscopic fluctuations of the Liquid Crystal molecules can be coarse-grained to build an order parameter ϕ defined so that $\phi = 0$ in the disordered isotropic phase, and $\phi \neq 0$ in the anisotropic ordered phase. The Landau free energy functional in an effective equilibrium description is

schematically composed of two terms:

$$F = F_{\rm el}[\,\phi, \text{Geom.}] + F_{\rm Geom}[\text{Shape}] \quad . \tag{1.1}$$

The first term represents the elastic energy associated to long-wavelength deformations of the coarse-grained order parameter. It depends on spatial inhomogeneities of the order parameter ($\nabla\phi$) and coarse-grained coupling constants, and it dictates how the order couples to the background geometry. The second term depends only on geometric quantities and typically penalizes large curvatures (either extrinsic or intrinsic). This situation is similar to the theory of General Relativity, where matter fields couple to space-time geometry and geometry determines the dynamics of matter. The second term is analogous to the Einstein-Hilbert action and the first is the energy of matter fields in a curved geometry. In soft ordered media, $F_{\rm el}$ is a Landau-type covariant low-gradient expansion of the free energy on long-wavelength deformations of the order parameter field. The fields are coupled to curvature through the covariant derivative which contributes to gradients even for spatially homogeneous fields. The term $F_{\rm Geom}$ is the energy cost for changes in the curvature of the system independently of the order parameter. Typically it is the sum of the integrated Gaussian curvature (a topological term) and the bending energy i.e. the integral of the mean curvature squared $\int_M H^2$ over the manifold M, with H the arithmetic mean of the local principal curvatures $k_1(\mathbf{x}), k_2(\mathbf{x})$. In the following we will assume that the system is a two-dimensional surface embedded in flat Euclidean space ($\mathbb{R}^3$).

(i) Fixed background geometry. If the geometry is a fixed passive background, the equilibrium states of the system are stationary points[4] of (1.1) satisfying $\delta F/\delta\phi = 0$, which typically gives a nonlinear PDE for ϕ. In general the order parameter will develop singular points (*defects*) to screen the background curvature to extremize F. The physics of defects on rigid curved spaces is very rich. Vitelli *et al.* [102] for

[4]States of stable equilibrium are the absolute minima of F.

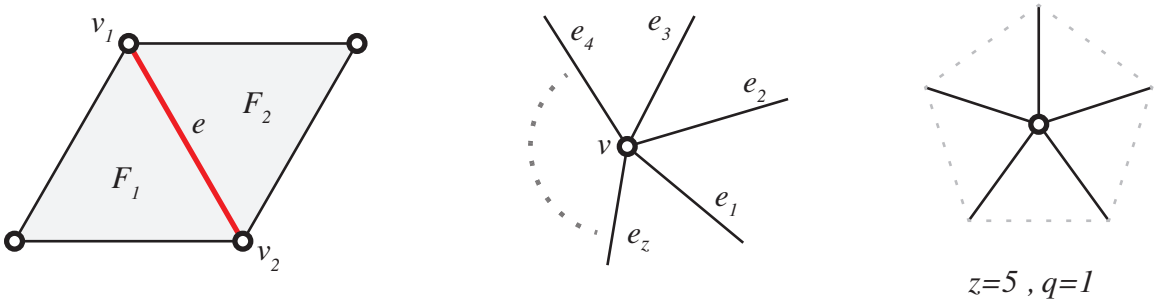

Figure 1.1: Properties of a triangulation: (a) Every edge is shared between two faces and contains two vertices. (b) Coordination number z. (c) A defect with $z = 5$. Its strength is $q = 6 - 5 = 1$.

example showed that a crystal on a rigid Gaussian bump reduces its elastic energy $F_{\rm el}$ by nucleating unbound dislocations. A similar situation holds for smectic liquid crystals confined to a curved substrate [54] where the interplay between a Gaussian bump and the incompressibility condition on smectic layers induces the formation of a semi-infinite straight grain boundary. In this case, the geometry of the substrate induces target self-assembled patterns in the ordered medium.

Closed surfaces made of materials that can spontaneously order are a good arena to study the interplay between topology, geometry and order. To every closed surface is associated the Euler characteristics χ:

$$\chi(M) = V - E + F \quad , \tag{1.2}$$

given by the number of vertices minus the number of edges plus the number of faces of any triangulation of M [28]. Relation (1.2) allows to make predictions on the number of defect in a crystal of given topology. A crystalline triangular lattice on the 2-sphere, for example, cannot have coordination number $z = 6$ everywhere as in flat space. Referring to Fig. 1.1, a triangular face has 3 edges, and every edge is shared between 2 faces, so $3F = 2E$. If z is the number of edges meeting into a vertex, then $2E$ counts the sum of all coordination numbers in the triangulation: $2E = \sum_z z\, V_z$

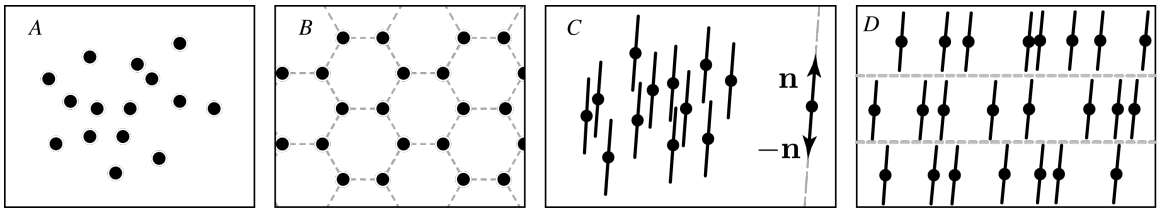

Figure 1.2: Examples of order in 2–dimensions. (A) In a fluid there is no positional order. (B) Positional order in a crystal lattice. (C) and (D) are called mesophases (intermediate between A and B). (C) A (nematic) liquid crystal breaks orientational symmetry selecting one local direction in space, but has translational symmetry. (D) In a smectic liquid crystal translational symmetry is broken across the layers (dashed lines), and it is mantained along the layers.

(V_z is the number of vertices with coordination z). Using these relations and the identity $V = \sum_z V_z$ in (1.2) we find:

$$\sum_z (6 - z) V_z = 12 \quad \text{on } S^2. \tag{1.3}$$

The topological charge $q = 6 - z$ is the deviation from the planar coordination number. If we allow only topological defects of minimal strength ($q = 6 - 5 = 1$) then the sum in (1.3) reduce to the single term $V_5 = 12$: the triangulation will contain 12 pentagonal defects in an otherwise 6–coordinated lattice. In [9] it was shown that the ground state has scars made of dislocations radiating from 12 disclinations or even string-like composite defects made of disclinations and dislocations when the sphere's radius is sufficiently large compared to the lattice constant.

Beyond positionally ordered crystals, relation (1.2) plays a key role in the study of defected states in orientationally ordered (but positionally disordered) materials such as Liquid Crystals (LC), (see Fig. 1.2). Liquid crystals in the ordered phase break rotational invariance of Euclidean space and select a local orientation at every point in the sample. The orientational order parameter is the angle θ that a unit vector $\mathbf{p}$ makes with respect to a pair of orthogonal directions $\{\mathbf{e}_1, \mathbf{e}_2\}$ on the surface. The angle θ is defined modulo p, where p is a positive integer [67] (we refer the reader to

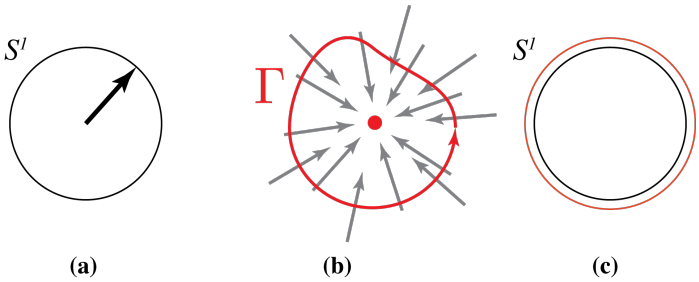

Figure 1.3: Vector order. (a) The order parameter space is a circle (S^1) so it is multi-connected. (b) A defect of strength $s = 1$ in a material with 2–dimensional vector order. As we traverse the closed path Γ in real space, we traverse a closed non-retractible loop in the order parameter space (c). The loop winds once around S^1 in the same direction of Γ, so the strength of the defect is $s = +1$.

chapter 3 for further details)

$$\mathbf{p}(\boldsymbol{\sigma}) = \cos\theta(\boldsymbol{\sigma})\mathbf{e}_1 + \sin\theta(\boldsymbol{\sigma})\mathbf{e}_2 \quad \text{where} \quad \theta + \frac{2\pi}{p} \sim \theta \quad , \tag{1.4}$$

where $\boldsymbol{\sigma}$ is a point of the surface. The order parameter of a liquid crystal with $p-$fold local rotational symmetry ($p-$atic) rotates by integer multiples of $2\pi/p$ around a defect, so the minimal disclination strength is $s = 1/p$. The energy of a disclination scales with s^2 in flat and curved spaces, so the zero-temperature *ground state* of $p-$atic LCs on a sphere will have $2p$ defects of minimal strength $s = 1/p$. Defects on 2 dimensional surfaces repel each other with an effective (logarithmic) Coulomb potential [59, 60], so the ground state will be a solution to the Thomson problem [35] with $2p$ charges residing at the vertices of a regular $2p$-gon. A vector field $p = 1$ (for example the projection of tilted molecules on the surface's normal) will have two elementary disclinations at the poles. Fig. 1.3 illustrates the vector order parameter space and an elementary defect of strength $s = 1$. For $p = 2$ (nematic, see Figs. 1.2,1.4) the 4 elementary defects reside at the vertices of a regular tetrahedron. For $p = 3$ (triatics, see Chapter 3) the 6 disclinations coincide with the vertices of an octahedron, and so on. A more general treatment of spherical nematic ground

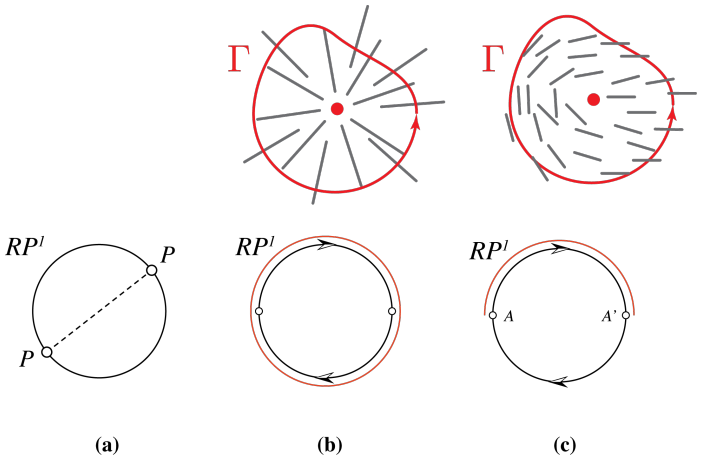

Figure 1.4: Nematic order. (a) The order parameter of a nematic LC is a circle S^2 with antipodal points identified. The resulting space $S^1/\mathbb{Z}_2$ is the Real projective space RP^1. (b) A defect of strength $s = 1$ in the real sample (*top*) and in the order parameter space *bottom*. (c) An elementary nematic defect of strength $s = +1/2$. Note that the path in the order parameter space is a closed loop because A and A' are identified.

states taking into account anisotropies between the bend and splay elastic moduli was treated in [99]. The isotropic defect cores may serve as preferential sites for functionalization (e.g. attaching ligands) which may then realize a spherical *super-atom* capable of directional bonding [83].

The inverse problem, namely to achieve a target geometry prescribing a configuration of the order parameter is addressed by models of thin liquid-crystalline elastomer sheets [1]. A fixed LC configuration 'frozen' into the material by applying an electromagnetic field. The nematic pattern melts at high temperatures, and material shrinks anisotropically with respect to the local director orientation. The material buckles into the target shape to screen the resulting planar stress field.

(ii) Fluctuating geometry. When both the geometry and the order parameter are allowed to fluctuate, the problem of minimizing (1.1) becomes more subtle. We notice that even to write down the free energy, we should integrate over a surface that is the unknown solution to the equilibrium equation! In order to solve for the ground

state, it is often necessary to make good guesses about some global properties of the shape. The case of isolated 5- and 7-coordinated disclinations and 5-7 dislocations in elastic crystalline membranes buckling in the third dimension has been studied analytically and numerically by Seung and Nelson [98]. It was found that beyond a critical membrane size L the elastic energy of a disclination (scaling with L^2) can be reduced by buckling out of plane.

In the context of liquid crystals, the shapes of vesicles depend strongly on in-plane order. The prototype of the Landau free energy of a 2–dimensional $p-$atic Liquid Crystal on a fluctuating geometry is

$$F[\mathbf{p},\Sigma] = \int_\Sigma \sqrt{g}\, d^2\sigma\, [K_1(D\cdot\mathbf{p})^2 + K_3(D\times\mathbf{p})^2] + \frac{\kappa}{2}\int_\Sigma \sqrt{g}\, d^2\,\sigma H^2 \quad , \tag{1.5}$$

where $\mathbf{p}$ is the orientational order parameter[5] and D is the covariant derivative on the surface. The coupling κ is the bending rigidity (also called bending modulus) of the membrane. H^2 is the square of the mean curvature[6]. The elastic constants K_1, K_3 are the elastic moduli associated to splay and bend deformations of $\mathbf{p}$ respectively. We will assume that the effects of thermal fluctuations renormalize the elstic moduli to a common value K (see for example [83]). The first term favors alignment of the director along geodesics ($n^a D_a n^b = 0$). The distortions of the director increase the term $D\mathbf{p}$, so Gaussian curvature is recruited to lower the Christoffel symbols in the covariant derivative. So, disorder attracts Gaussian curvature, while ordered regions expel Gaussian curvature (see [69]). The bending energy favors the formation of planar regions on the membrane, so it tends to expel Gaussian curvature. The frustration between these effects and the boundary conditions leads to the vesicle shape.

[5]For $p = 2$ (nematic) the order parameter is an head-tail symmetric orientation and it is called the director field. It can be represented as a unit vector $\mathbf{n}$ identified with its opposite $-\mathbf{n}$ (see Fig. 1.2).

[6]The definition of H can be found in section 4.1.

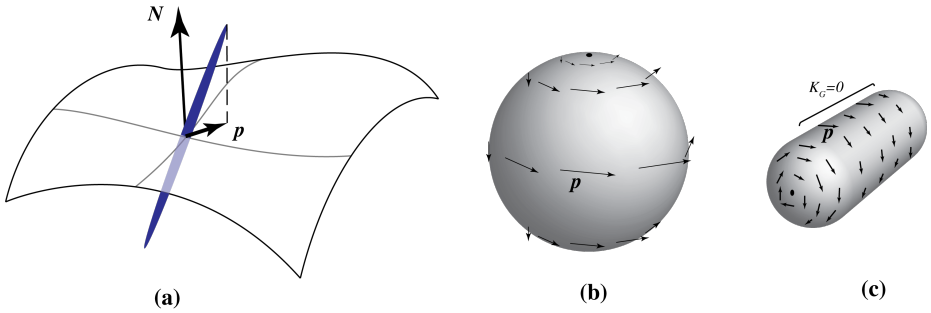

Figure 1.5: An example of the coupling between shape and order in a Smecitc C vesicle. Gaussian curvature is expelled near the equator [69]. (a) Definition of the vector order $\mathbf{p}$ for a smectic C liquid crystal. The local orientation of the liquid crystal in the ordered smectic C phase is represented as a blue needle. The axis of the needle is tilted with respect to the surface normal $\mathbf{N}$. Its projection on the surface is the vector $\mathbf{p}$. (b) Vector order on a 2–sphere. The state with minimal defect strength $s = 1$ contains two vortices at the poles. (c) A flat cylindrical region between the poles lowers the bending energy and supports a uniform vector field (whose covariant derivative vanishes in the cylindrical region).

When $p = 1$ in (1.5) the model describes vetor order on a fluctuating surface. For example, the vector $\mathbf{p}$ may represents the projection of the local tilt order of a Smectic C phase onto the surface (see Fig. 1.5a). MacKintosh and Lubensky [69] considered a vesicle where Smectic-C tilt-order is coupled to geometry. Using (1.5) with $K_1 = K_3$ and introducing a symmetry-breaking term $\mu\mathbf{p}^2/2+\lambda\mathbf{p}^4/4$, they showed that varying the ratio μ/λ the initial symmetry of the 2–sphere can be broken and the vesicle assumes the shape of a cylinder with hemispherical caps at the poles. The two vortices repel through a 2–dimensinal Coulomb repulsion and migrate to antipodal points. The surface near the equator is , leaving a striped ordered region near the equator. Gaussian curvature is expelled from the equatorial region, lowering also the extrinsic curvature energy, which vanishes in the limit of a cylindrical stripe.

Extensions of the 'rigid' $p-$atic model to deformable vesicles were considered in [70, 85]. In [85] the equilibrium shape was found as a perturbation of the round sphere, exploiting a formal analogy between an Abrikosov lattice of vortices in a

superconducting sphere pierced by p quanta of magnetic field and the $2p$ 'vortices' induced by the topological constraint $\chi = 2$.

In order to go beyond small deformations of the sphere and find non-perturbative solutions to the $p-$atic ground state problem, one must make a good guess the optimal shape. The surprise is that at vanishing bending rigidity, the equilibrium shapes are singular, faceted polyhedral shells. The shape selection mechanism of these soft yet sharp vesicles is at the core of Chapeters 3 and 2.

In the case of *tetratic* order ($p = 4$) [70] the liquid crystal state is invariant under local rotations by $\pi/2$. Minimizing the free energy among a family of superellipsoids it was proven that the vesicle's shape is a cube with 8 disclinations located at the vertices. An extension to triatic ($p = 3$) order is the subject of Chapter 3. This is an example of a 'faceting mechanism' that yields ordered vesicles faceted like crystals and yet soft as liquids. We refer the reader to section 1.5 and Chapters 3 and 2 for a complete discussion of this mechanism.

1.3 Modeling Soft materials

The spatial conformations of hard materials are separated by high energy barriers so there is low degeneracy among their states. At low temperature, entropy is small or zero, and their physics is governed primarily by energy. By contrast, soft materials have many states at low energy because they can be deformed at a negligible energetic cost. Flexible polymers or Dna strands for example can be folded easily into very convoluted shapes: conformations that are very far in configuration space are connected by paths of very low energy. Thus the properties of the polymer (for example its macroscopic rigidity) may be dominated by entropy even at low temperature. In order to correctly calculate macroscopic observables of soft materials it is essential to take into account the geometric conformations of the many low-temperature config-

urations. Soft matter systems thus provide a good arena to model shape formation, selection, and transformation.

All the physical systems mentioned above are immersed in an environment: their conformations occupy a portion of a higher dimensional space, so they are physical examples of *embedded* manifolds. Materials with a small thickness-to-width aspect ratio are physical realizations of mathematical two-dimensional manifolds endowed with fields. For example, lipid membranes are effective 2-dimensional membranes. The physics at the thickness scale is absorbed in few phenomenological elastic moduli and/or interactions. Continuum models have been compared to molecular dynamics simulations [41] and have been found to be a reliable long-wavelength description. In order to compare the idealized geometrical model with real systems, a comment is in order. Mathematical surfaces can self-intersect, and self-intersecting configurations occur more frequently in low codimension[7] because there is "less space to explore".

A mathematical surface embedded in 3-dimensions has codimension one. Due to the low value of d_c and the extreme deformability of the surface, self-intersecting configurations are frequent. Real membranes behave differently: if two parts of the object collide, short-ranged repulsive interactions prevent self-intersections. This can be modeled introducing interactions that are non-local in terms of distances measured along the surface. The analysis becomes considerably more subtle and technically challenging than the simple self-intersecting model. At low temperatures regimes and small stresses, however, self-intersecting configurations are disfavored either by entropic or energetic considerations, so that one is still able to extract physical predictions without the complications of self-avoidance. Another possibility is that the membrane is sufficiently sparse or perforated. Then self-intersections become less likely simply because there is less material to collide with [112].

Models of fluctuating two-dimensional manifolds appear in many areas of physics.

[7]The difference $d_c = D - d$ between the dimensions of the ambient space D and the material d is called codimension. It is a measure the amount of space that can be explored by the material.

They appear in the statistical mechanics of domain walls in the 3-dimensional Ising model on a cubic lattice [2, 93], where they appear as 2-dimensional domain walls separating regions of flipped spins. The amplitude of propagation of a closed string involves a sum over all the embeddings of the 2-dimensional worldsheet in $D-$dimensional Euclidean space [92]. In statistical mechanics random interfaces are modeled as random two dimensional surfaces.

Models of atomically thin crystalline membranes at finite temperature offer precise and sometimes surprising predictions of their mechanical and thermodynamic properties. After graphene was first made in 2004 (almost 60 years since Wallace's theoretical proposal) there has been a fast progress in the synthesis of atom-thin crystalline materials even beyond graphene, for example MoS_2. The statistical field theory of thermally fluctuating 2-dimensional elastic solids revealed a striking transition where embedded in D dimensions have been studied in the large D limit to detect the crumpling transition.

1.4 Mechanisms of shape selection

The coupling between local order and geometry, along with topological constraints, controls the properties (in particular the shapes) of many systems in soft matter through the mechanisms of geometric frustration and curvature screening.

1.4.1 Geometrical frustration and topological defects

Geometrical frustration arises when local order cannot be propagated globally across the material, due to geometric or topological obstructions. An example of geometric frustration is the tiling of the plane with regular pentagons. The internal angle of the pentagon (108°) is not an integer fraction of 360°, hence the regular tiling breaks down and order cannot propagate at long distances. This simple observation is at

the origin of the theory of quasi-crystals, as lucidly described by M. Kléman [55]. Another example is the Ising anti-ferromagnet on a triangular lattice: three spins on a triangular plaquette cannot be all mutually anti-aligned.

The idea of geometrical incompatibility [95] is closely related to geometrical frustration. As formalized by Efrati et al. [26, 27] in the context of elasticity, it arises when the intrinsic geometry of an elastic solid cannot be immersed isometrically in the ambient space (usually Euclidean). Since unstrained rest distances cannot be realized in the ambient space, any configuration assumed by the solid contains some residual stress. The wrinkled edges of leaves are a beautiful example where shape arises from geometrical incompatibility. Since the leaf's growth rate increases radially outward, every stripe of material should be longer than the adjacent internal stripe. The preferred rest lengths increase hyperbolically, and a hyperbolic geometry cannot be immersed isometrically in $\mathbb{E}^3$, so the leaf is in a state of residual stress. In order to accommodate at least partially the excess length, the edges bend forming undulating patterns.

The topology of a material with internal order can enforce frustration and cause the order parameter to vanish either at isolated points or on higher-dimensional subspaces. In the 1880s Poincaré proved that the sum of the indices $I_{x_0}(\mathbf{v})$ of a zero of a vector field $\mathbf{v}$ on a closed manifold M is equal to the Euler characteristic $\chi(M)$:

$$\sum_{\{x_0\}} I_{x_0}(\mathbf{v}) = \chi(M) \quad . \tag{1.6}$$

The continuum definition of χ is

$$\chi(M) = \int_M K_{\mathrm{G}}(\mathbf{x}) \sqrt{g}\, d^2x \quad , \tag{1.7}$$

where $K_{\mathrm{G}} = 1/(R_{\max}(\mathbf{x})R_{\min}(\mathbf{x}))$ is the Gaussian curvature of the manifold, ad $R_j(\mathbf{x})$ are the the radii of the largest and smallest osculating circle at the point $\mathbf{x}$. The index

$I_{x_0}(\mathbf{v})$ counts the number of complete rotations of $\mathbf{v}$ around the singular point x_0, at which the vector field vanishes. Poincaré's theorem implies that a vector field on the 2-sphere must vanish at least at one point. In 1926 Hopf generalized this theorem to manifolds of arbitrary dimension. Singular configurations of the order parameter are usually called topological defects in the physics literature. Topological defects can be stable or unstable depending on the topology of the order parameter space. When a material hosts stable topological defects, its ground state is not simply a small perturbation of a non-defected state and it cannot be continuously relaxed to it. Removing defects would require collective and coherent global rearrangements of the system, which are prohibitive either energetically or entropically.

The detection and classification of topological defects requires arguments and techniques from algebraic topology, but these need to be supplemented with suitable energy functionals to describe the physics of systems with defects. Order is favored by local interactions, and a perturbation of the optimally ordered state costs elastic energy. The distortions of the order parameter in smaller and smaller regions around the defect become arbitrarily large, and the long-wavelength description is no longer valid. Local order is destroyed inside a small region of radius a (the defect's core) which is typically of the order the molecular size. To solve for the order parameter inside the defect core, we need a microscopic theory; universality breaks down and the specificity of the interactions becomes important. Far from the core radius, distortions vary slowly in space, so it is possible to calculate the defect's elastic energy inside a region of radius $L \gg a$ surrounding the core. While the core energy is fixed and can be disregarded in the thermodynamic limit, the defect's elastic energy scales with the system size. For example, the energy of disclinations (orientational defects) in planar 2-dimensional crystalline membranes shows a strong quadratic dependence on the system size: $E_{\text{discl}} \sim L^2$. This divergence in the thermodynamic limit $L \to \infty$ is turned into a milder logarithmic dependence $\log(L/a)$ in dislocations [81, 82], which

can be thought of closely bound disclination-antidisclination pairs. The elastic energy of topological defects plays a primary role in shaping soft materials through the mechanism of curvature screening, as will be described in the next section.

1.4.2 Curvature screening

Two-dimensional systems are especially sensitive to the presence of topological defects, because the defect energy and entropy both scale as $\log(L/a)$ where L, a are the system size and the defect core radius, as was pointed out by Berezinskii, Kosterlitz and Thouless in the context of the XY model.

At zero temperature, and in infinite systems with periodic boundary conditions, defects are usually absent due to their large energy of formation. Defects proliferate at finite temperature, leading to the Berezinskii-Kosterlitz-Thouless phase transition in the XY model [7, 60] and to the two-stage melting transitions of crystalline solids as described by the KTHNY theory [20, 43]. If, on the other hand, the ordered material possesses Gaussian curvature, defects are present even at zero temperature. In particular, closed surfaces with order in their tangent plane and $\chi \neq 0$ must contain topological defects, due to the Poincaré-Hopf theorem and its generalizations. Remarkably, in [39] it was found that a perfect toroidal crystal can lower its energy by nucleating pairs of 5- and 7-coordinated defects, even if topology doesn't force their presence, since $\chi(T^2) = 0$.

In a coarse-grained description of the ordered phase, it is convenient to treat the defects as particle-like excitations interacting through the strain field of the surrounding elastic medium. In flat 2-dimensional space, for example, orientational defects interact through a logarithmic 2-d Coulomb potential, and a defected elastic medium can be interpreted as a gas of charged particles. Topological defects on frozen curved surfaces experience an additional coupling to the Gaussian curvature $K_G(\mathbf{x})$ through the covariant derivative. The case is best illustrated for a $p-$atic orientational order

parameter $\mathbf{p}$. Expanding $\mathbf{p}$ in an orthonormal basis $\{\mathbf{e}_1, \mathbf{e}_2\}$ as $\mathbf{p} = \cos\theta\mathbf{e}_1 + \sin\theta\mathbf{e}_2$, the elastic energy can be written as [8]:

$$F_{\text{el}} = \frac{1}{2}K \int_\Sigma \sqrt{g}\, \mathrm{d}^2x\, g^{ij}(\partial_i\theta - A_i)(\partial_j\theta - A_j) \quad , \tag{1.8}$$

where the covariant derivative is written in terms of the spin connection A_i, given by $\epsilon_{kl}A_i = \mathbf{e}_k \cdot \partial_i \mathbf{e}_l$. The orientation field θ is singular, so the curl of $\partial_j\theta$ is sourced by the topological charge density $\rho(\mathbf{x})$:

$$\epsilon^{ij}\nabla_i\nabla_j\theta = \rho(\mathbf{x}) \quad . \tag{1.9}$$

On the other hand, the curl of $\mathbf{A}$ is equal to the Gaussian Curvature $\nabla \times \mathbf{A} = K_G(\mathbf{x})$. Inverting this relation and (1.9) using the Green's function G_Δ of the Laplace-Beltrami operator

$$\Delta_{\mathbf{x}} G_\Delta(\mathbf{x}, \mathbf{y}) = \delta(\mathbf{x} - \mathbf{y}) \quad , \tag{1.10}$$

where $\Delta_{\mathbf{x}}$ acts on a scalar function as

$$\Delta_{\mathbf{x}} f(\mathbf{x}) = \frac{1}{\sqrt{g}}\partial_i(\sqrt{g}g^{ij}\partial_i f(\mathbf{x})) \quad , \tag{1.11}$$

and inserting the result in (1.8) , the elastic energy can be rewritten as

$$F_{\text{el}} = -\frac{1}{2}K \int_\Sigma \mathrm{d}^2x \int_\Sigma \mathrm{d}^2y\, [\rho(\mathbf{x}) - K_G(\mathbf{x})]G_\Delta(\mathbf{x}, \mathbf{y})[\rho(\mathbf{y}) - K_G(\mathbf{y})] \quad , \tag{1.12}$$

where $\sqrt{g}$ has been absorbed in the definition of G_Δ. We find again an effective Coulomb interaction, but with the important difference that the bare topological charge $\rho(\mathbf{x})$ is screened by Gaussian curvature of the same sign. Thus topological defects on a rigid topography tend to occupy regions of non-zero Gaussian curvature in order to screen the curvature charge $K_G(\mathbf{x})$.

The curvature screening mechanism plays a key role also when the surface's geometry is embedded in an ambient space and is allowed to fluctuate out of plane. Buckling of elastic materials is the prototype for all defect-induced changes in shape. The total energy of a continuum solid $E = E_s + E_b$ is composed of in-plane elastic stretching energy and out-of-plane bending energy:

$$E_s = \frac{1}{2}\int d^2x \, (2\mu u_{ij}u^{ij} + \lambda(u^k_k)^2) \tag{1.13}$$

$$E_b = \int d^2x \, \left(\frac{1}{2}\kappa H^2 + \kappa_G K_G\right) \quad , \tag{1.14}$$

where $2u_{ij} = \partial_i u_j + \partial_j u_i$ is the strain tensor, u_i is the in-plane displacement, $H = (k_{\max} + k_{\min})/2$ is the mean curvature and $k_{\max}(\mathbf{x}), k_{\min}(\mathbf{x})$ are the inverse principal radii of curvature [61, 98]. The Lamé elastic moduli λ and μ and the bending rigidity κ measure the energy cost for stretching and bending the material respectively and κ_G is called the Gaussian rigidity. If the topology of the crystal is fixed, the integral of K_G is the constant $2\pi\chi$. Consider a perfect two-dimensional crystal of radius R in the plane, remove a $2\pi/3$ triangular wedge of atoms and glue the edges together. The resulting state has coordination number $z = 6$ of a perfect planar crystal everywhere except for the central atom, which has only 5 neighbors. The disclination density in polar coordinates is $\rho(r) = sr^{-1}\delta(r)$, where $s = (2\pi)/6$ is the aperture angle of the removed wedge. Fix a circle of radius r centered at the origin: its rest length is $(2\pi - s)r$ but now it is stretched to $2\pi r$, so the material is under residual stress. The elastic energy of a planar disclination was calculated in [98]:

$$E_s = \frac{Ks^2}{32\pi}R^2 \quad , \tag{1.15}$$

where R is the system size and $E_b = 0$. When out-of plane buckling is allowed, the system can transfer some stretching energy to bending energy. If the the increase

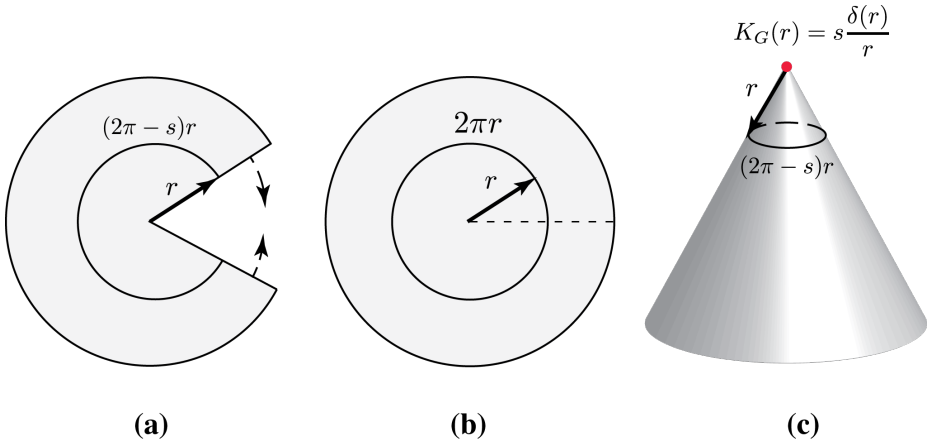

Figure 1.6: Isometric folding of a planar disclination into a buckled cone. (a) The rest length of the circular arc is $(2\pi - s)r$. (b) If the circular sector is deformed and glued in a disk, the material is stretched. The elastic energy is proportional to $(sr)^2$. (c) If the disk is allowed to buckle in the third dimension, its stretching energy can be reduced to zero because every circular section can achieve its optimal length. The Gaussian curvature is localized at the apex.

in bending energy is small compared to the reduction in the stretching energy, the material will settle in a buckled configuration. The stretching energy (1.15) can be lowered to zero if the disclination can buckle *isometrically* into a cone (equivalently, in the limit $\mu, \lambda \to \infty$). A simple way to see this is to compute the Gaussian curvature of a cone with deficit angle $2\pi - s$. Since $\chi_{\text{cone}} = \chi_{\text{disk}} = 1$, the Gauss-Bonnet theorem is

$$\int_\Sigma K_G + \oint_{\partial\Sigma} k_g + \sum_i \alpha_i = 2\pi \quad , \tag{1.16}$$

where k_g is the geodesic curvature of the circular boundary $\partial\Sigma$ and α_i are the rotation angles at the boundary's corners. The cone is developable in the plane, where $\partial\Sigma$ is a circle of radius R so $k_g = 1/R$ and the length of the boundary is $(2\pi - s)R$. Then (1.16) reduces to

$$\int_\Sigma K_G = s \quad . \tag{1.17}$$

The cone has one flat direction, so its Gaussian curvature vanishes everywhere except

at the apex. In view of (1.17) we conclude that

$$K_G(r) = s\frac{\delta(r)}{r} \quad . \tag{1.18}$$

This proves that an isometric embedding of a cone converts the stretching energy of a planar disclination into Gaussian curvature. In the buckled cone all the rings of atoms around the tip attain the preferred rest length so the stretching energy vanishes. A complete calculation of a disclination buckling using the formalism of the Airy stress function was performed by Nelson and Seung in [98].

In chapters 2 and 3 similar arguments will be used to deduce the zero-temperature configuration of liquid crystal vesicles. An important point to note is that in some cases the singular behavior of the defect density can lead to singular extrinsic geometries. Examples are spikes, conical singularities, and sharp edges. The bending rigidity κ is crucial for regulating these singular behaviors.

1.5 Self-assembly and spontaneous faceting

Real physical systems are open: they exchange energy and entropy with the surrounding environment. The spontaneous (self-directed) self-assembly of building blocks in macroscopic structures almost always occurs through a sequence of non-equilibrium steps in which entropy plays a key role. Building a conceptual understanding of the rules of self-assembly is challenging because of the many ingredients that coordinate self-assembly patterns. Short-ranged interactions of the building blocks and their directionality in space direct local assembly but there are also other factors. The shape of the constituents contribute to directional interactions [94] and introduce geometrical frustration during the assembly process through excluded-volume effects, giving rise to patterns of symmetry breaking that are not predictable if one considers only the molecular interactions. Gluing tetrahedral units along their faces, for example, gives

rise to helical chains that spontaneously break chiral symmetry in three dimensional Euclidean space [15]. In order to understand self-assembly rues in controlled experiments, one possibility is to prepare simple building blocks (called *super-atoms*) and then observe how they aggregate into larger-scale structures. Studying how super-atoms spontaneously condense into more complex structures might prove useful as toy models to understand the rules of self-assembly that shape most soft materials. One step forward is to understand how the spatial directionality of interactions arises. This requires the design of functionalized macromolecules of scalable size and tunable interactions. The area of self-assembly provides a lively exchange between theory and experiment, with the potential to indentify new organizational principles that, in a sense by construction, don't have an analogue at the scale of elementary particles [4].

Supra-molecular geometries found in nature might be useful to inspire the design of very anisotropic interacting super-atoms. In [113] elastic crystalline have been shown to collapse into Platonic and Archimedean solids by decreasing their internal pressure. Faceted shapes observed for example in icosahedral viral capsids arise from similar mechanisms [100]. The symmetries of the polyhedral capsid are ultimately determined by the symmetries of the inter-molecular potential. Since the shape is a minimizer of potential energy (and not free energy) the large-scale behavior of the assembled macro-structure, for example its shear rigidity, is fixed by the physics at the Angstrom length scale. One can turn an artificial icosahedral shell into a functionalized super-atom by attaching ligands to the vertices of the polytope. The resulting super-atom is a rigid structure, and the directional ligand-mediated bonds are highly constrained by the symmetries of the potential of the capsid's molecules.

To overcome the limitations of fixed directional-bonds symmetry, as in the example of the viral capsid, a possibility is to use liquid-crystaline order confined in a spherical shell (see for example [30]) and then functionalize the defects [83]. The interactions of the super-atom would arise from the interplay between the mesogens' internal

symmetries and the fixed geometry of the substrate. The use of these shells might prove to be inefficient in the context of assembly of soft materials for two reasons. One is the sequential construction of the individual liquid-crystal shell: first one must make a rigid scaffold, then inject the LC into it and finally functionalize the topological defects. Second, the resulting super-atom is rigid, so it might not be suitable to be used in a biological environment. Biological systems like the cell's membrane are usually very soft and might break or be damaged if they encounter a hard object.

Mechanisms for faceting with liquid crystals

An alternative to the aforementioned hard nematic-shell option is to realize a super-atom unit that self-assembles without external intervention. It it may be faceted and at the same time is soft [10]. This is the theme underlying chapters 2 and 3. This program is feasible using, for example, rod-coil block-copolymers equipped with side mesogens. Rod-coil block-copolymers are polymers composed of a rigid rod and a flexible coil covalently linked (see [84] for a review). Flexible coil chain polymers bend easily into convoluted random-walk-shaped configurations, and thus have large conformational entropy [82]. This makes their thermodynamical behavior quite rich. Extra degrees of freedom can be added to a flexible polymer by dressing it with nanopatterns or nanostrutrures. In most cases, these alterations rigidify the polymer to the point that it becomes an inflexible rod. To retain both good thermodynamical and functional properties, rod and coils can be soldered together to form a coil-rod block-copololymer unit (CRBC). The self-assembly patterns of these units are different in coil-affine or rod-affine solvents. In both cases, CRBC aggregates mimic the morphology of the amphpiphiles: micelles, vesicles, cylindrical rods and so on. Rigid rod blocks segregate from chain-affine solvents so the liquid-crystalline degrees of freedom occupy a molecularly-thin region in the solvent. This realizes a two-dimensional liquid crystal (in the same way that graphene is a 2-dimensional crystal).

As discussed in sections 1.2 and 1.4, the spherical topology of a liquid crystalline vesicle forces the presence of topological defects in the ground state. Although the relaxation of the vesicle into the ground state is an out-of-equilibrium process, heuristic arguments based on an effective equilibrium free energy can guide us to find the zero-temperature configurations. We will take the free energy of a $p-$atic liquid crystalline membrane to be

$$F[\mathbf{X}, \mathbf{p}] = \int_M \sqrt{g}\, d^2x \, [K_1 (D \cdot \mathbf{p})^2 + K_3 (D \times \mathbf{p})^2 + \kappa H^2] \tag{1.19}$$

where $\mathbf{X}$ is the embedding of the manifold M and $D\cdot$ and $D\times$ are the covariant divergence and the covariant curl on the surface. The defects core energy has been neglected in the thermodynamic limit of a large vesicle. The orientation of $\mathbf{p}$ is defined mod p. If we ignored all the constraints, we could argue that $\mathbf{p}$ would attain the lowest elastic energy when its covariant derivative vanishes. This would imply that $\mathbf{p}$ is uniform and the Gaussian curvature vanishes (the Christoffel symbols must vanish identically). This would mean that the surface is flat (in the sense of Gaussian curvature). But the spherical topology (equivalently, an anchoring boundary condition of $\mathbf{p}$ at the edge of a disk) requires, via the Gauss-Bonnet theorem

$$\int_M K_G = 2\pi\chi = 4\pi \quad , \tag{1.20}$$

so that the Gaussian curvature cannot vanish *everywhere*. It must be singular at some isolated points that play the role of conical singularities: $K_G(\mathbf{x}_i) \propto \delta(\mathbf{x} - \mathbf{x}_i)$. Luckily, the order parameter $\mathbf{n}$ has p isolated singularities that can screen the Gaussian curvature, yielding a vanishing elastic energy in view of (1.12). Gaussian curvature and defects of the ordered phase occur at the same points in the vesicle. Three defects are always contained in a plane. In order to specify a three-dimensional vesicle, there must be at least 4 defects. If $p = 2$ (nematic order) four defects of lowest

charge $s = 1/2$ are needed to span a non-degenerate polytope. Moreover, in order to reduce the bending energy term $\kappa \int_M H^2$ the local principal curvatures should vanish. In other words, the bending term wants to expel Gaussian curvature from the surface.

Putting everything together, the energy would be zero if the surface was planar $H = 0$ and flat $K_G = 0$, but the topological constraint $\chi = 2$ forbids it. At this point, we need to make a final assumption. We restrict ourselves to the case of vanishing bending rigidity $\kappa = 0$, where the vesicle is the most soft. The system resolves the frustration by flattening out almost the entire surface, apart from the zero-dimensional defect points and one-dimensional edges connecting the defects. The result is a singular manifold - a polytope - where $K_G \neq 0$ at zero-dimensional vertices, $\kappa = 0$ allows sharp one-dimensional edges at zero bending energy cost, and $H = 0$ on the planar faces bounded by three or more edges. This faceting mechanism holds for generic K_1 and K_3. In view of the preceding argument, it shouldn't sound strange that extremely soft systems make sharp shapes. Experimental evidence of faceted vesicles can be found, for example, in [110].

Chapter 2

Ground States of Smectic Vesicles

2.1 Introduction

From the largest cosmic structures down to the atomic scale, we are surrounded by a rich variety of shapes. Although shape is often the first feature that we identify in a physical system, understanding its origin is in most cases difficult and challenging. Morphogenesis [18] typically requires the collective organization of a macroscopically large number of degrees of freedom, either in or out of thermodynamic equilibrium, moreover the concept of shape itself is often scale-dependent. Here we are interested in characterizing shapes of systems that are large compared to their elementary constituents. For this reason, we will work within a coarse-grained, continuum field-theoretic framework [13], since we expect that the observables of interest will depend only on universal properties of the system and not on its microscopic details.

In this work we consider a closed vesicle of spherical topology formed by spontaneous aggregation of smectic liquid-crystal molecules (a common example is the rod-coil block copolymer structure) [50, 108, 111, 116, 117]. The smectic liquid crystal organizes in a layered structure [37], which we idealize as a set of parallel lines on the vesicle. Because they are very flexible and thin, vesicles are interesting systems in

which to study morphogenesis [97, 107]. Their thickness is of the order of nanometers, while their size can be of the order of 100 micrometers making them a good physical realization of a two-dimensional fluid membrane [13]. We modeled the vesicle shape as a 2-dimensional manifold $\mathbf{X}$ embedded in 3-dimensional space, while the smectic order parameter is described by a 1-form field ω defined on it.

Consider an ensemble of such vesicles. Working in the limit of extremely soft (easily bendable) surfaces, we expect to encounter a large number of low-energy shapes, leading to a large entropic contribution. To each configuration we associate a free energy $F[\mathbf{X}, \omega]$ that measures the energetic cost of bending the surface and of deforming the liquid-crystal layers. The presence of the liquid crystal and its elastic response to deformations has a strong influence on the equilibrium shapes.

We studied the ground state of F, in other words the density of states at zero temperature. This is in general a very hard infinite-dimensional minimization problem, because both the manifold $\mathbf{X}$ and the field ω are allowed to vary. This situation is reminiscent of General Relativity with matter fields, or of classical solutions to some models of two-dimensional quantum gravity [93], where one solves simultaneously for the manifold geometry as well as for the matter fields. We can make a step towards the solution when we notice that the vesicle's spherical topology forces the smectic field to contain topological defects at isolated points, even in the ground state.

A sphere has an Euler characteristic equal to 2, so by the Gauss-Bonnet theorem [23] the total topological charge of the smectic field must add to 2. When the system's shape is allowed to change, and in the absence of topological obstructions [6, 46, 48], the coupling between defects and curvature determines both the equilibrium shape and the smectic configuration. For an extensive review on the interplay of curvature, order and topological defects see [8]. Recent work [110] showed that the ground states of F span a two-dimensional manifold of faceted tetrahedral shells. At a first glance, it seems surprising that, just by coupling to the liquid-crystal order, a very

soft and fluid system can develop sharp edges and vertices. One equilibrium smectic pattern was found to be a set of lines parallel to an edge of the tetrahedron, with four disclinations of charge 1/2 located at the polytope's vertices.

In this work we considered a tilt angle between the smectic layers and the edge of the tetrahedral shell and characterized the degeneracy of such ground-state manifolds. Many of these states contain spiral defects. A complete classification of smectic defects can be found in [109]. It is interesting to note that the smectic vesicle realizes all of them in the ground state.

The lowest-energy manifold displays a number of interesting features: First, the presence of spiral states signals the emergence of chirality in the system composed of achiral building blocks. Second, a smectic state breaks translational invariance to a discrete subgroup. As a consequence, a state exists only if the layer separation h and the vesicle size L are commensurate. For special values of the ratio L/h, a fixed shape supports more than one tilt angle and therefore many distinct topological classes of defects.

In some states the smectic layers are arranged as the latitudes on a globe. In this case, since there is no flow of molecules across layers, a localized perturbation of the fluid within a layer must remain confined on a fixed latitude. In contrast, we expect a spiral state to be much less rigid because a localized deformation would be able to propagate along the spiral and travel long distances from the initial perturbation.

We imagine that smectic vesicles could be used experimentally to self-assemble micro-scale sacks. If the defect sites could be functionalized by anchoring ligands to the defect cores [21, 83], these systems would display highly anisotropic interactions, and the presence of chiral spiral patterns might perhaps open up interesting possibilities in the context of supramolecular chemistry [68].

2.2 The model

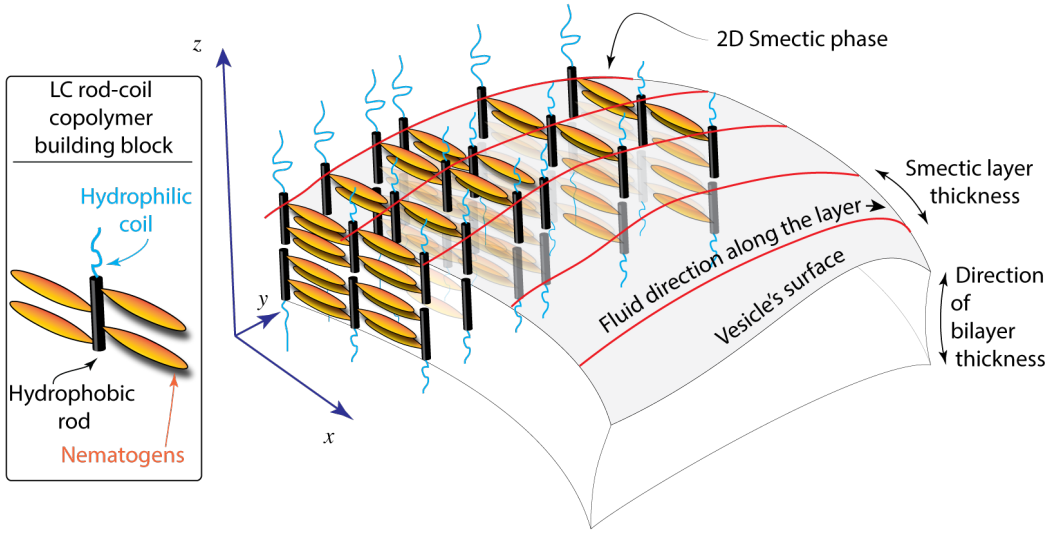

Figure 2.1: (*Left*) Schematic of the molecular building blocks that form the vesicle. (*Right*) Section of an LC membrane with 2-dimensional smectic-A ordered phase on its tangent plane. Notice the interdigitation of the mesogens along the local x direction, as well as their alignment along the y direction.

As mentioned in the introduction, the molecular constituents of the vesicle behave as a liquid crystal. Recently it was shown that certain rod-coil copolymers with side mesogens can spontaneously self-assemble into bilayered membranes in an aqueous environment [111, 117]. A solution made of the side mesogens alone is known to possess a smectic bulk phase. fig. 2.1 (*Left*) shows a schematic of these elementary building blocks. Reference [117] reported that self-assembled liquid crystalline vesicles may have smectic order. Fig. 2.1 (*Right*) shows how the rod-coil copolymers are thought to be arranged to make the membrane. We choose the z direction to be aligned with the rods, i.e. with the normal to the membrane. The x and y directions span the surface of the vesicle. We are interested in the ordered structure in the local tangent plane xy. Consider the plane xz at $y = 0$. The rod-coil copolymers self-organize in a bilayer structure where the mesogens are locked in an inter-digitated

pattern. The rod is normal to the membrane. As we move along the y axis, we find a sequence of stacks containing the same pattern as in the $y = 0$ plane. The key point is that the mesogens (orange in the picture) interact as a smectic liquid crystal along the y direction too. So the mesogens' center of mass in the second layer to the right of the plane $y = 0$ must be aligned with the mesogens' center of mass in the $y = 0$ layer. The same happens for the third layer along the y axis, and so on. The mesogens organize in a layered pattern on the xy plane (the vesicle's surface) where the layer normal coincides with the mesogens. This results in a sequence of stripes on the surface of the vesicle (i.e. the xy plane) that breaks translational symmetry along the x direction [117]. The layer spacing has the same value as in the smectic bulk phase of the nematogens alone. In Ref. [110] the smectic structure on the surface is described as a nematic director field where the in-plane bending constant is large compared to the in-plane splay constant. The positions of the black rods along the y axis is arbitrary, so the membrane is fluid along this direction. Following [110], we consider a minimal model of a liquid crystal coupled to a curved manifold M of spherical topology [1]. Assuming that the vesicle is formed by two symmetric monolayers, the free energy is

$$F[\mathbf{X}, \mathbf{n}] = \int_M \sqrt{g}\, d^2x \, [K_1(D \cdot \mathbf{n})^2 + K_3(D \times \mathbf{n})^2 + \kappa H^2] \tag{2.1}$$

where $\mathbf{n}$ is the director field associated to the liquid-crystal molecules, $\mathbf{X}$ is the embedding of M in $\mathbb{R}^3$, $g = \sqrt{\det g_{\alpha\beta}}$ is the determinant of the induced metric on M, D is the covariant derivative on M, H is the mean curvature [23], K_1 and K_3 are respectively the splay and bending moduli of the liquid crystal, and κ is the bending

[1] By energetic considerations, a large vesicle inhibits the formation of holes. The energy cost for cutting a hole grows proportionally to the hole's boundary, with the line tension as a proportionality factor. In the thermodynamic limit, the energy of the boundary diverges. On the other hand, the bending energy remains constant as we increase the system size, because it is conformally invariant [71, 103]. So we expect that shape fluctuations will close the holes and self-heal the surface, reducing it to a spherical topology.

rigidity of the system. Notice that the surface tension μ is set to zero. We chose a thermodynamic ensemble where the vesicle is coupled to a reservoir of liquid-crystal molecules. The area can freely fluctuate as molecules flow on or off the surface, so $\mu \equiv \delta F/\delta A = 0$. We study the ensemble at zero temperature, in other words we look for minimizers of F.

The functional (2.1) exhibits an interesting set of degenerate ground states. We will study (2.1) in the limit $K_3/K_1 \to \infty$, when the field $\mathbf{n}$ becomes constrained by $D \times \mathbf{n} = 0$, and describes a smectic liquid crystal. In this limit the field configurations contain pure splay modes. The integral lines of the field $\mathbf{t}$ orthogonal to $\mathbf{n}$ will be interpreted as the smectic layers. Equivalently, we can say that they are described by the level sets of a 1-form ω (see next section). In addition, we want to tune the bending rigidity κ to zero, where the membrane is extremely soft. Then the energy density reduces to $K_1(D \cdot \mathbf{n})^2$, and the equations of motion are $D_a(D_b n^b) = 0$, subject to the constraint $\int_M K_G = 2\pi\chi = 4\pi$, where K_G is the Gaussian curvature and χ is the Euler characteristic.

If we ignored the constraint, we would conclude that (2.1) is minimized by a flat manifold ($D = \partial$) covered by a uniform field of straight lines ($\partial^2 \mathbf{n} = 0$). However, this cannot be true when we require that the manifold retain its spherical topology. In order to satisfy the condition $\chi = 2$, we conclude that M must be a developable surface ($K_G = 0$ almost everywhere) and that the director field $\mathbf{n}$ follows parallel straight lines on M, except for isolated singular points. It follows that the smectic layers, represented by the integral lines of $\mathbf{t}$, where $\mathbf{t} \cdot \mathbf{n} = 0$, are also a set of parallel straight lines. The gaussian curvature is localized in a discrete set of points S, identified with the vertices of a faceted polyhedron, and it is screened by the topological defects of the field $\mathbf{n}$.

The minimal number of points that span a non degenerate polyhedron is 4, so the director field will contain four disclinations of charge $s = 1/2$, and the ground state

shape will be a tetrahedron [67] (see also [30, 58] for the nematic analogue). The region of parameter space that we want to study ($K_3/K_1 \to \infty$, $\kappa = 0$) allows many distinct ground state configurations. The analysis developed in [110] showed that the ground state tetrahedra span a two-dimensional moduli space. For a fixed shape, there are many configurations of the field $\mathbf{n}$ (and of the corresponding smectic field) that lie at the same energy. In the following sections we will address the problem of characterizing the degeneracy of these smectic field configurations.

2.3 Geometry of smectic layers

Smectic liquid crystals are composed of apolar elongated molecules that, below a critical temperature, exhibit an ordered phase with broken orientational and translational symmetry [37, 56]. A smectic liquid crystal can break orientational symmetry thanks to local interactions that favor alignment of the molecules. In addition to this nematic order, a smectic state also forms layers, so that it also breaks continuous translational invariance to a discrete subgroup of translations along a direction that coincides (locally) with the average molecule orientation axis. In a smectic-A liquid crystal, within each layer the average molecular orientation coincides with the local layer's normal.

We will consider 2-dimensional closed membranes made of self-assembled molecules that behave as an incompressible smectic liquid crystals on the tangent space of the surface. We will adopt a coarse-grained point of view and parametrize the liquid-crystal vesicle as a 2-dimensional manifold M embedded in $\mathbb{R}^3$ with induced metric $g_{\alpha\beta}$. We will call S the set of points that host topological defects. The smectic layers are then described by a measured foliation [63, 90] of $M \setminus S$ (where the singular points have been removed), that is, a collection of disjoint connected curves on $M \setminus S$ that are equispaced and that cover $M \setminus S$.

2.4 Structure and energetics of defects in smectics

The orientational order parameter associated to the smectic liquid crystal is a nematic-like director field. Topological defects (disclinations) in the orientation of the smectic liquid crystal appear at isolated points, and their charge is an integer multiple of 1/2 [74, 77]. We usually detect their charge by encircling the defect by a closed path, and counting how many times the director rotates back to itself as we complete a revolution around the defect. Every time the director rotates by π, we have closed a loop in the order parameter space [57]. The lowest disclination charge is therefore $q = \pm\pi/(2\pi) = \pm 1/2$. Because the disclination energy is proportional to the square of its charge, both in a flat and in a curved surface, the elementary disclinations with $q = 1/2$ are favored over a $q = +1$ defect [67].

The classification of the field configurations requires knowing the relative energies between the allowed classes of topological defects. Unlike a nematic, one smectic defect of charge $s = 1$ and two defects of charge $s = 1/2$ have the same energy. The proof is contained in [99] and [109]: parametrize the sphere with angular coordinates (φ, θ) and consider the smectic state $\omega = d\theta$ (Fig. 2.2). The smectic layers are the lines $\theta = \pi/N$, where N is the total number of layers. Each layer is a curve of constant latitude. The poles contain two defects of charge +1. Now cut the sphere along the meridian $\varphi = 0$ and divide it in right and left hemispheres. We can rotate the left hemisphere around the y axis by an integer multiple of π/N and split each +1 defect into a pair of 1/2 defects. Notice that the integral lines of $\mathbf{n}$ are again segments of geodesics, and they have zero bending everywhere, so they still describe a smectic state. Since the two hemispheres slid along a geodesic, the energy of the configuration does not change. Although these two states are degenerate in energy, only the one that contains four disclinations is compatible with a faceted tetrahedron. The four defects experience a repulsive effective interaction, so in the ground state they maximize their pairwise geodesic distance by occupying the vertices of a regular

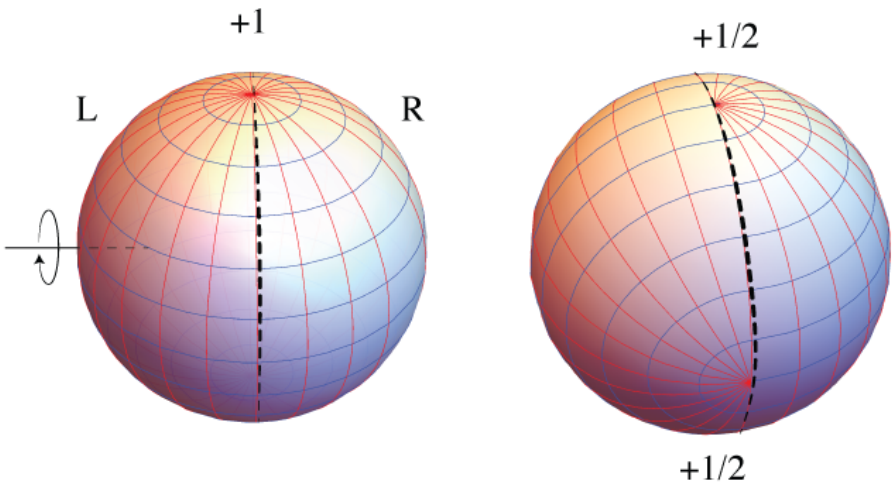

Figure 2.2: Splitting a +1 defect into two 1/2. Cut the sphere along the dotted line (left) and rotate the left hemisphere until the smectic layers (blue lines) are reconnected.

tetrahedron [67].

There is another smectic defect whose charge is $q = +1$ but is topologically distinct from the latitudinal state: it is a single spiral contained between the North and the South pole of the sphere (see the classification of smectic defects in [109]). The spiral defect can be thought of as a closely bound pair of two $+1/2$ disclinations. The energy of this topological defect on a smooth surface of spherical topology ($\kappa \neq 0$) is higher than the latitudinal state, because the geodesic curvature of the director's integral lines cannot vanish everywhere. On a faceted shell however ($\kappa = 0$), the integral lines become rectilinear segments, and the single spiral state becomes degenerate in energy with respect to the latitudinal state. This shows once again that setting $\kappa = 0$ is

different from taking the limit $\kappa \to 0$.

2.5 Ground state degeneracy

Recall that the gaussian curvature is localized at the vertices of a developable tetrahedron where it is screened by the charge of the topological defects. Since the covariant derivative $D\mathbf{n}$ must vanish everywhere except at the vertices, the sum of the angles between the edges around each vertex must be π, otherwise in the developed tetrahedron the smectic lines would bend to fill uniformly the surface. This constraint means that the only those tetrahedra that are developable into a flat parallelogram $\mathcal{P}$ are allowed, and that all the 4 faces must be identical [110]. For later convenience, let us call $\mathbf{e}_1$ and $\mathbf{e}_2$ two vectors that span half of the developed parallelogram (Fig. 2.3). We are interested in the case $\kappa \equiv 0$, where the degeneracy of shapes is maximal. An arbitrarily small deviation of $\kappa \sim 0^+$, however, will select the shape that minimizes the total length of its edges (the bending energy is proportional to the length of a rounded edge) which is a regular tetrahedron. Therefore, for the purpose of classifying states, we will use the regular tetrahedron as the manifold's shape. The same logic applies to non-regular tetrahedra. Notice that the domain $\mathcal{P}$ has the topology of the sphere. The oriented segment $\vec{AC}$ on the left in Fig. 2.3 is identified with $\vec{AC}$ on the right, while the segment $\vec{CD}(\vec{AB})$ is identified with its *reflected* image $\vec{DC}(\vec{BA})$ across the vertex $D(B)$.

Once we fix $\mathbf{e}_1, \mathbf{e}_2$, and the angle between them, we are left with the degeneracy in the configurations of the field $\mathbf{n}$. On a generic surface M, the pure-splay constraint $\epsilon^{ab} D_a n_b = 0$ (where ϵ^{ab} is the Levi-Civita symbol) implies

$$\partial_1 n_2 = \partial_2 n_1 \quad . \tag{2.2}$$

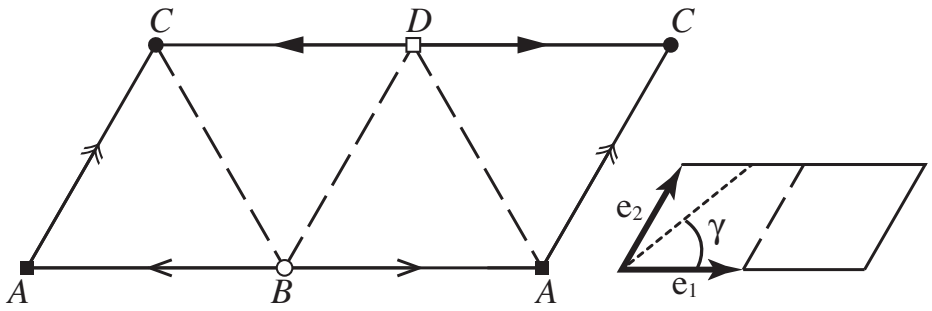

Figure 2.3: *(Left)* The domain $\mathcal{P}$ foldable into a regular tetrahedron. The edges identifications are indicated by arrows and the vertices by letters. The dashed lines indicate the folds. *(Right)* The lattice vectors and the direction γ between a layer and the vector $\mathbf{e}_1$

On the other hand, $n_\alpha n^\alpha = 1$ and $\partial_\beta(n_1^2 + n_2^2) = 0$, we find

$$n_1\partial_1 n_1 + n_2\partial_1 n_2 = 0 \tag{2.3}$$

$$n_1\partial_2 n_1 + n_2\partial_2 n_2 = 0 \quad , \tag{2.4}$$

where we used the relation $\epsilon^{ab}\Gamma^c_{ab} = 0$ thanks to the symmetry of the Christoffel symbols $\Gamma^c_{ab} = \Gamma^c_{ba}$. Combining (2.3) and (2.4) with (2.2), we find

$$(n^a D_a)\mathbf{n} = 0 \quad , \tag{2.5}$$

that is, the integral lines of $\mathbf{n}$ are geodesics on M. Since the tetrahedron is developable into a flat domain $\mathcal{P}$, the integral lines of $\mathbf{n}$ are simple straight lines on $\mathcal{P}$. The smectic layers will also be parallel straight lines, and additionally they must be equi-spaced. Most importantly, the equations of motion $\partial^2\mathbf{n} = 0$ and the energy are left invariant by a global rotation of the layers, so we expect to find a degeneracy of smectic configurations, labeled by the angle γ between a layer and the vector $\mathbf{e}_1$ (Fig. 2.4).

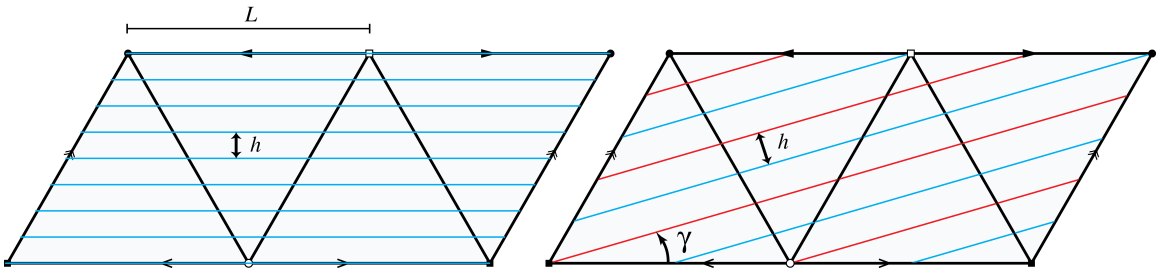

Figure 2.4: (*Left*) Developed tetrahedron of size L covered by a commensurate uniform smectic pattern with layer spacing h. (*Right*) A vesicle where the layers have been tilted by an angle γ.

2.6 Topological classification of the ground states

We are now going to classify the allowed smectic states by drawing suitable sets of parallel lines on $\mathcal{P}$. We must follow two rules when we draw the states: (i) each vertex must be occupied by a smectic disclination, and (ii) the layers are equispaced. Condition (i) is a consequence of the structure of a defect with charge 1/2, and eventually determines the allowed orientations γ of the layers.

The easiest state that can be drawn is a set of equispaced lines parallel to $\mathbf{e}_1$ ($\gamma = 0$) (Fig. 2.4 *Left* and 2.5-I). This is called a Latitudinal state [110], and it has the same topological structure of the state $\omega = d\theta$ on the sphere. The number of independent layers is $\nu = N$. If the edge of the vesicle has length L and the distance between two neighboring smectic layers is h, then we have

$$h = \frac{\sqrt{3}}{2}\frac{L}{N} \tag{2.6}$$

where N is the number of layers on the vesicle.

The next state that we will discuss occurs at $\gamma = \pi/6$. By rule (i) there must be at least two independent layers, one connecting A with D and the other connecting B with C. According to rule (ii), an arbitrary number of layers can be inserted between the first two, as long as they are equispaced. The resulting state is the analogue

of the quasi-baseball state on the sphere (Fig. 2.5-II). Although this layer pattern has the same topology as the $\gamma = 0$ state, we regard them as different states with respect to their tilt angle with the egdes. The layers are perpendicular to an edge. We can either have a layer terminating in the vertices ($L = nh$ with n even) or we can shift the former by $h/2$ and have $L = nh$ with n odd. The latitudinal and the quasi-baseball states are much less frequent than the next set of states that we are going to discuss.

Consider now an angle $\gamma \neq 0, \pi/6$. We will show later that the wedge $\gamma \in [0, \pi/3]$ contains all the states. Following rules (i) and (ii), we cover the domain $\mathcal{P}$ with a measured foliation of parallel lines such that each vertex is occupied by a smectic layer termination. Because of the topology of $\mathcal{P}$, the smectic layers will connect across the edges to form spirals. We can either form a double spiral (Fig. 2.5-III) or a single spiral (Fig. 2.5-IV). This means that these states are organized in two classes according to the spiral's chirality: Left-handed if $\gamma \in (0, \pi/6)$, and Right-handed if $\gamma \in (\pi/6, \pi/3)$. Notice that right- and left- states are in 1:1 correspondence, so we just need to classify, say, the left-handed states i.e. $\gamma \in (0, \pi/6)$. For convenience, the handedness of the spirals is best seen by looking at an axis that goes through the mid point of two opposite edges (e.g., AB and CD in Fig. 2.5-III).

To proceed, consider a state with orientation γ on $\mathcal{P}$ and divide the domain $\mathcal{P}$ symmetrically into two sub-domains $\mathcal{P}_R, \mathcal{P}_L$ spanned by $\mathbf{e}_1$ and $\mathbf{e}_2$ (Fig. 2.7). Rotate $\mathcal{P}_R$ around the vertex D by $+\pi$ keeping fixed the identifications of the edges. This operation is equivalent to the rotation of $\mathcal{P}_R$ around its own center, followed by a translation by $-\mathbf{e}_1 + \mathbf{e}_2$. Call this new domain $\mathcal{P}'$. The smectic field is invariant under translations along lattice vectors as well as rotations by π. This proves that the field is left invariant under this operation and so we conclude that the domains $\mathcal{P}$ and $\mathcal{P}'$ represent the same state.

By discrete translational invariance of the layers along $\mathbf{e}_i$, we also conclude that we

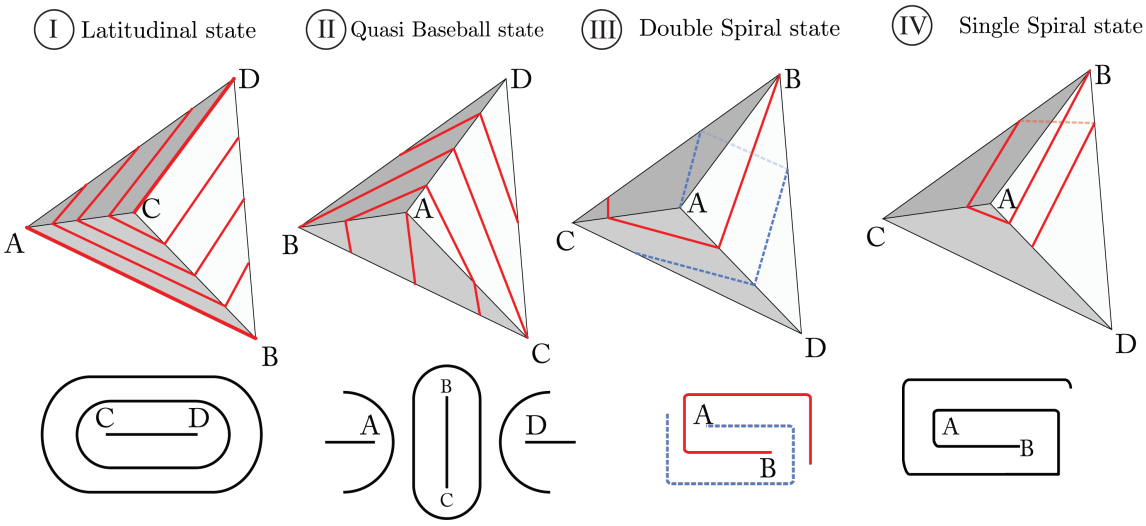

Figure 2.5: Topological classes of smectic states on the vesicle, and their projection onto a plane. The states I and II are homotopically equivalent (same topological class), but they are distinct with respect to the value of the tilt angle.

can translate an individual triangular face by an integer multiple of either basis vector without changing the state. This allows for a great simplification in the counting of states. We can consider an infinite plane tiled with domains $\mathcal{P}$. Using the symmetry operations described above, one concludes that the angles $\gamma \in (0, \pi/6)$,$(\pi/3, \pi/2)$, $(2\pi/3, 5\pi/6)$ represent the same Left-handed states and therefore should not be over-counted. Analogously, the angles $\gamma \in (\pi/6, \pi/3)$,$(\pi/2, 2\pi/3)$, $(5\pi/6, \pi)$ describe the same states (Fig. 2.6). In other words, the angle γ is defined mod $\pi/3$, which is again commensurate with the angles $\pi/3$ contained in the equilateral faces. In conclusion, we just need to consider a wedge of aperture $\pi/6$ in a triangular lattice, count the allowed states in the wedge, and multiply by 2 to account for the right-handed partners.

At first, consider the states that contain two parallel spirals. The triangular lattice provides the optimal setting to classify the allowed angles. Rule (i) implies that we

can find the allowed orientations by drawing rays that connect the origin of the lattice with appropriate lattice vertices in a $\pi/6$ wedge. We label the vertices by pairs of integers (n, m) corresponding to multiples of the lattice directions $\mathbf{e}_1, \mathbf{e}_2$. The position of a vertex from the origin is $\mathbf{r} = n\mathbf{e}_1 + m\mathbf{e}_2$, with $\mathbf{e}_1 \cdot \mathbf{e}_2 = 1/2$. The allowed directions will be labeled by γ_{nm}. See Fig. 2.8.

It is easy to see that, for a fixed ray starting from the origin, all those vertices that are intersected by the ray correspond to the same state. If we imagine an observer at the origin, then a state is labeled by the first vertex in his/her line of sight. In terms of the vertex labels, this means that a state is labeled by a pair (n, m) where m and n are relative primes (or, the fraction m/n is irreducible). This identifies the space of allowed angles as the so-called Euclid's Orchard [78]. The labeling, and therefore the number of states, does not depend on the specific shape of the triangles, a result that is compatible with the degeneracy in the tetrahedral vesicle's shapes.

The values of the angles, on the other hand, depend on the relative size of the edges. For a regular tetrahedron, we find:

$$\tan \gamma_{nm} = \frac{\sqrt{3}\, m}{2n + m} \quad , \ (m, n) \text{ coprimes.} \tag{2.7}$$

$$\sin \gamma_{nm} = \frac{\sqrt{3}\, m}{2\sqrt{n^2 + m^2 + nm}} \quad , \ (m, n) \text{ coprimes.} \tag{2.8}$$

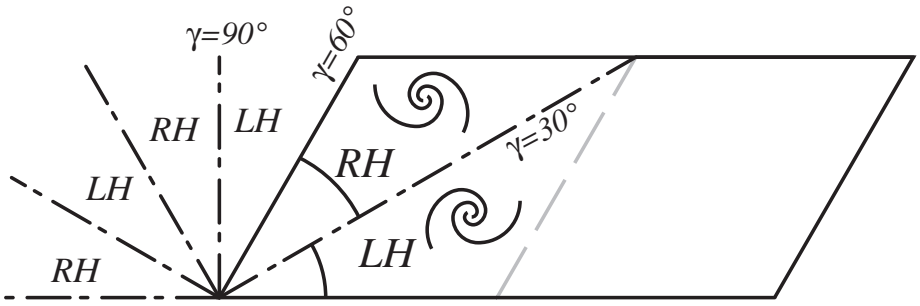

Figure 2.6: The redundancy in the tilt angle γ: the states are labeled by γ mod $\pi/3$. And they split between Left- and right-handed according to $0 < \gamma < \pi/6$ or $\pi/6 < \gamma < (2\pi)/6$.

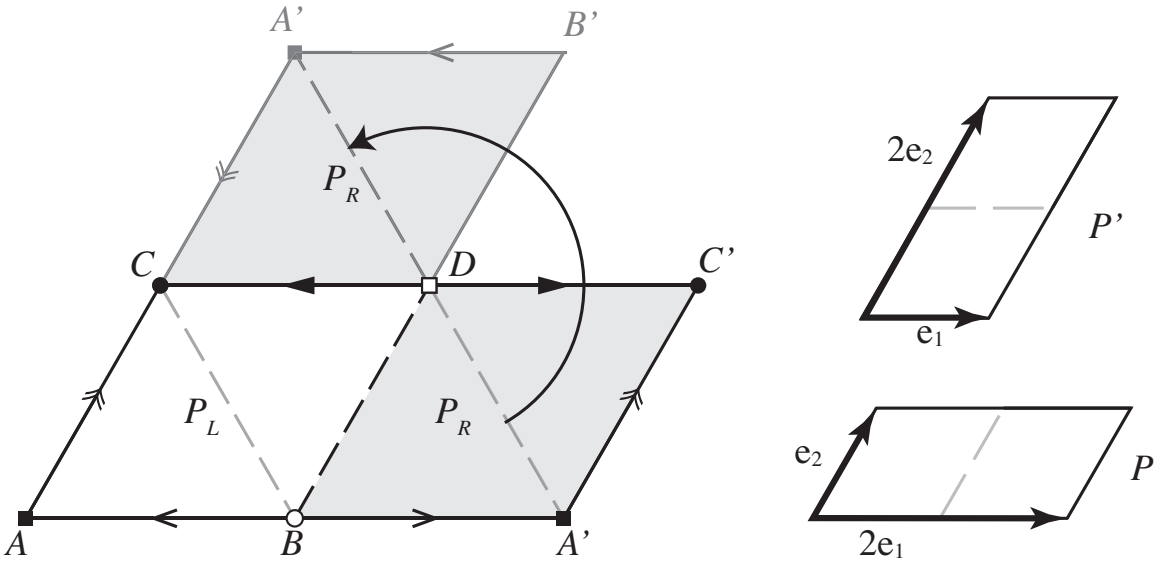

Figure 2.7: Invariance of the fundamental domain under rotations and translations.

The result does not depend on the overall size of the tetrahedron's edge L, which we expect from the scale invariance of the problem. In addition, equations (2.7) and (2.8) depend only on the ratio $q \equiv m/n$, which is consistent with the state counting: non-irreducible fractions lead to the same angles.

Finally, according to rule (ii), we can insert an arbitrary number of equally spaced layers ν between the first and the second spiral (say between the vertices A and B). Therefore, we conclude that a state $S_{m,n,\nu}(\alpha, r)$ is labeled by the integers $m, n, \nu \in \mathbb{N}$ where m, n are relative primes and label the layers tilt angle, ν labels the number of *independent* layers in the foliation [2], and α and r are the angle between $\mathbf{e}_1$ and $\mathbf{e}_2$, and the ratio between their magnitudes. The latitudinal and quasi-baseball states occur for the special values $m = 0$ and $m = n = 1$ respectively.

We will now describe the procedure to draw a smectic state on $\mathcal{P}$ that contains only two parallel spirals: (a) choose a vertex labeled by a pair of coprimes (n, m) on the lattice and draw a line l that joins the origin with (n, m). (b) Occupy every other

[2]The number ν of independent layers is less than or equal to the number N of parallel lines drawn on the developed tetrahedral shell.

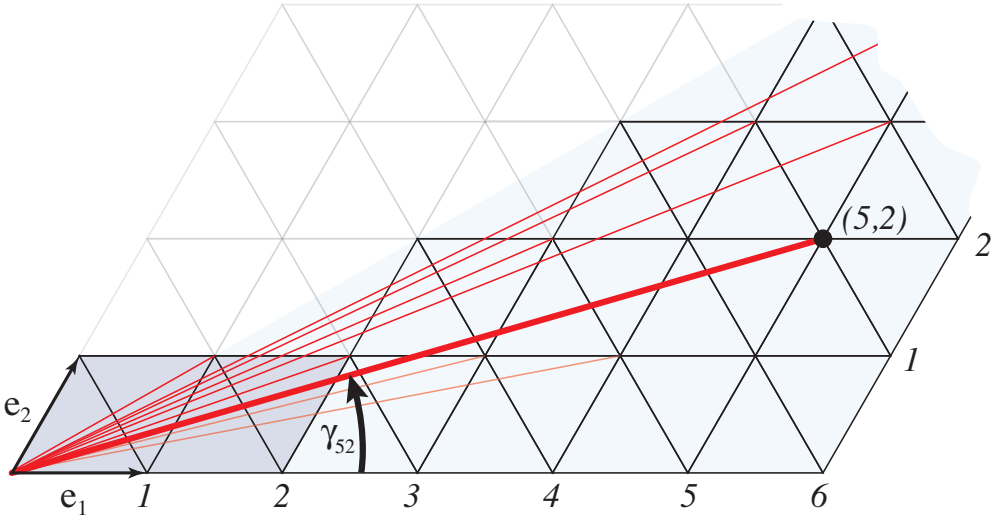

Figure 2.8: The Euclid's Orchard procedure to label the allowed smectic tilt angles γ_{nm}.

vertices in the lattice with lines parallel to l. (c) Choose any fundamental domain in the lattice and fold it. According to this procedure, a choice of γ automatically fixes a layer spacing $h_{\max}$. Notice that the parameter m is also the number of times that the edge $\mathbf{e}_1$ is intersected by the smectic layers, an observation that will be useful later. From the double-spiral state described above, we can form a new class of states by stacking additional layers between the spirals. We can insert an arbitrary number of them, provided that we keep the layers equally spaced (the layer spacing is reduced by an integer factor p: $h_{\max} \to h_{\max}/p$).

In this way, we are increasing the density of smectic layers $\eta \equiv L/h \to p\eta$ on the surface of the tetrahedron by integer multiples. The added layers are parallel to the spirals, but form closed loops, and thus constitute a new class of topological smectic states that is independent from the spirals and the latitudinal states. We will call this new class of smectic patterns as double spiral-loop (2SL) states. We will prove later that such a double-spiral loop state is described by a reducible fraction, where

both n and m have been multiplied by the same integer p.

If we shift any of the patterns described above by half layer spacing along the direction orthogonal to the layers, we obtain another class of states. The structure of the defects at each vertex is a chiral version the quasi baseball defect shifted by a half layer spacing. The single spiral state can be analyzed in a similar way.

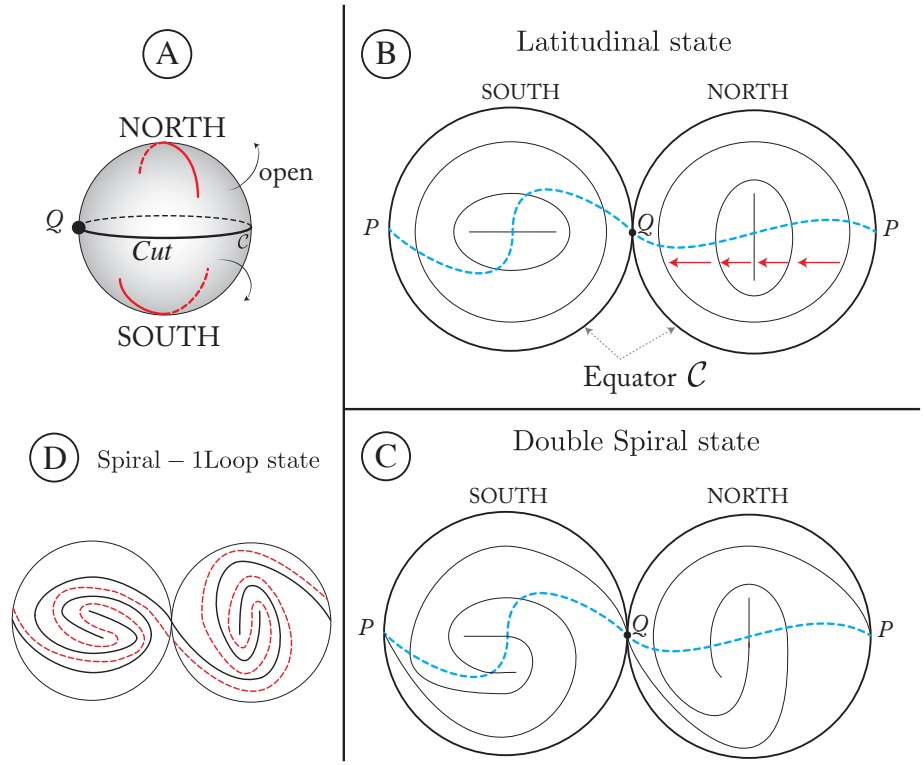

Figure 2.9: The figure proves that the latitudinal state (B) and the double spiral state (C) are topologically distinct. All the layers must be cut along the dotted line and shifted globally by one layer spacing. A shift by 2 layer spacings (D) gives a state containing two spirals and a loop (red dotted line).

2.7 Topology of the spiral states

We will now prove that the pattern of the smectic layers on a spiral state is topologically distinct from the latitudinal state. Notice that distinguishing a single spiral

from a latitudinal state requires more than the usual winding number q around the defect location [74, 109]. In fact, if we enclose a defect core with a loop and we measure the rotation of the tangent vector $\mathbf{t}$ around the loop, we find that for both patterns $q = +1$. We must use another characterization to distinguish a spiral from a latitudinal pattern.

For the purpose of topological classification, we can imagine the smectic pattern as painted on a sphere. Start with a latitudinal state (Fig. 2.9A) on the sphere, where the defects are located away from the equator (as it is in the tetrahedron case). Choose the great circle $\mathcal{C}$ that is equidistant from all four defects and cut all along it except for a single point Q. Then, open the two hemispheres using the common point Q as a hinge, and stereographically project the smectic pattern on the disks (one for each hemisphere) that have $\mathcal{C}$ as its boundary. Draw a line through the hemispheres that cuts every circular layer twice and cuts only once the layers connecting the vertices (see the blue dotted line in Fig. 2.9B). Then cut the layers where they intersect the dotted curve and shift them by one layer spacing in the direction of the red arrows. After the layers are rejoined and the hemispheres have been glued again along $\mathcal{C}$, we find the double spiral state.

This proves that the two states are topologically distinct, although they have the same topological charge ($4 \times 1/2$). Penrose considered a similar discontinuous transformation between similar states in an infinite plane [89]. This is a new manifestation of the fact that in smectic liquid crystals the disclination charge is not sufficient to give a 1:1 characterization of the states. If we shift the pattern by integer multiples of the layer spacing and reconnect them, we obtain the Spiral-Loop (SL) states.

A single-spiral state on the sphere is parametrized by the curve σ:

$$\varphi(t) = p\,\theta(t) \quad , p \in \mathbb{N} \tag{2.9}$$

where φ, θ are spherical coordinates on S^2, $\theta(t) = \pi t$ and $t \in [0, 1]$. The integer p

is the number of times we cross the curve σ if we travel from the north pole to the south pole along a great circle. The winding number of (2.9) around the North pole is $+1$. The double spiral states can be described as bound pairs of $+1/2$ disclinations (see Fig. 2.5-III - the winding number around both vertex A and B is $+1/2$).

2.8 Degeneracy of states at fixed density

In a physical realization of a smectic vesicle, there are two relevant length scales: the vesicle size L (we will consider again regular tetrahedra) and the size of the molecule, which determines the preferred layer spacing h. These two length scales fix the density of layers on the vesicle through the ratio $\eta \equiv L/h$. The parameter η has a lower limit of 2 (when $h = L/2$) and an upper limit of L/a, where a is a microscopic cutoff, comparable with the molecular length scale. We wish to study the number of allowed states $S(\gamma_{nm})$ at fixed η. The parameter η is related to the density of smectic layers in a vesicle of fixed size L.

Consider the plane with Cartesian coordinates x, y and a set $\mathscr{L}$ of parallel lines $y = kh$, where k is an integer and h is a fixed layer spacing. Draw a fundamental domain $\mathcal{P}$ spanned by

$$\mathbf{e}_1 = (L, 0) \quad , \quad \mathbf{e}_2 = \frac{L}{2}(1,\sqrt{3}) \quad . \tag{2.10}$$

In order to find the allowed angles at fixed h/L, we will rotate the domain $\mathcal{P}$ by γ from 0 to $-\pi/6$. By rule (i), an allowed state must have both vertices B, D (See Fig. 2.3) occupied by a layer. These two vertices have positions $\mathbf{e}_1$ and $\mathbf{w} \equiv \mathbf{e}_1 + \mathbf{e}_2$. Rule (i) implies that the tip of the rotated vectors $R_\gamma \mathbf{e}_1$ and $R_\gamma \mathbf{w}$ must simultaneously intersect a line in the set $y = zh$. This condition is satisfied only if the angle γ is the solution to (2.7). Finally, we know that for a given γ_{nm}, the layers $\mathscr{L}$ divide the edge

$\mathbf{e}_1$ into m segments of length $h/\sin\gamma$:

$$L = \frac{mh}{\sin\gamma_{nm}} \quad , \tag{2.11}$$

Using (2.8) into (2.11), we can rewrite (2.11) in terms of n, m to get the relation between the allowed angles and the density:

$$n^2 + m^2 + nm = \frac{3\eta^2}{4} \quad , \quad m < n \quad , \tag{2.12}$$

which is a form of Diophantine equation. The symmetry $n \leftrightarrow m$ of (2.12) exchanges the chirality of the spirals from left to right-handed. When $h \ll L$, we can stack a large number of layers on the tetrahedron's surface, and we expect to find many states with the same density η, labeled by different values of the angles. For example, the density $\eta = 2\sqrt{247}/(3\sqrt{3})$ allows two tilt angles γ_{nm}, one with $(n, m) = (11, 7)$ or $\gamma \approx 22.7°$, the other with $(\bar{n}, \bar{m}) = (14, 3)$ or $\gamma \approx 9.5°$.

Equation (2.12) correctly describes SL states as well. In fact, multiplying equation (2.12) by p^2 we find:

$$(pn)^2 + (pm)^2 + (pn)(pm) = \frac{3(p\eta)^2}{4} \quad , \quad p \in \mathbb{N} \quad , \tag{2.13}$$

where $\bar{\eta} = p\eta$ is the new density. Notice that the angle γ given by (2.8) depends only on the ratio $q = n/m$. The transformation $(n, m) \to (pn, pm)$ leaves q invariant, so we proved that we can increase the density by integer multiples without changing the tilt angle γ, and that the Spiral-Loop states are obtained by rescaling the coprime pairs by an integer number.

Can a Double-Spiral and a Spiral-Loop state have the same layer spacing? Let $\eta > \bar{\eta}$ be the densities of two spiral states whose angles are $\gamma_{nm}, \gamma_{\bar{n}\bar{m}}$ respectively. We increase the density $\bar{\eta}$ by an integer $p \neq 1$, thus obtaining a SL state, and ask: can

$p\bar{\eta}$ be equal to η? The answer is yes if and only if

$$\frac{n^2+m^2+nm}{\bar{n}^2+\bar{m}^2+\bar{n}\bar{m}} = p^2 \quad (p \neq 1) \quad , \tag{2.14}$$

where n, m and $\bar{n}, \bar{m}$ are coprimes. The Spiral and Spiral-Loop states can have the same layer spacing if there exist solutions of (2.14) in $\mathcal{O} \times \mathcal{O}$. The number of independent smectic layers that close into loops is $p-1$. For example, the Spiral state with tilt angle $(n, m) = (20, 17)$ and the SL state with tilt angle $(\bar{n}, \bar{m}) = (4, 1)$ and 6 loops solve (2.14) with $p = 7$, and in fact they have the same density $\eta = 7\bar{\eta} = 14\sqrt{7}$.

This is an important result, because it shows that each state is labeled by a rational number (the angles are still counted by the Euclid's Orchard) and that a fixed value of η can contain states from different topological classes.

Commensurability implies that only special values of the density allow for the existence of ground states. From equation (2.12) we see that the values of η are constrained by the fact that (n, m) are integers. For example, there is no state associated to $\eta = \sqrt{37}$ because for this value (2.12) does not have solutions in the form of a pair of integers (n, m). The number of states at fixed η should be computed by

$$\Omega(\eta) = \sum_{\substack{(n,m)\in\mathbb{N}^2 \\ m\leq n}} \delta\left(\eta - 2\sqrt{\frac{n^2+m^2+nm}{3}}\right) \quad , \tag{2.15}$$

where δ is the Dirac delta distribution and the sum is taken over pairs of natural numbers, to take into account the SL states. Equation (2.15) counts the number of solutions to (2.12) as we sample the pairs (m, n) in the infinite triangular wedge $m \leq n$.

We can solve numerically equation (2.15). Instead of performing the sum (2.15), it is convenient to change variables and look at the degeneracy as function of the auxiliary variable $z \equiv (3/4)\eta^2$. The result is unaffected by the change of variables,

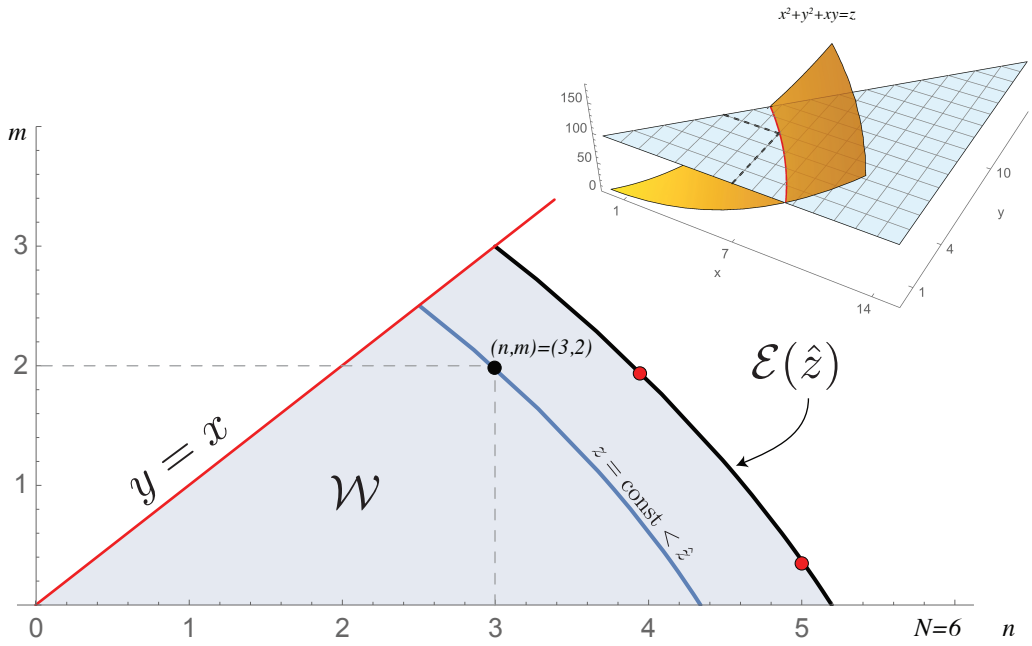

Figure 2.10: Sampling region for the numerical evaluation of $\Omega(z)$.

because all the quantities are positive definite, and the map $\eta \to \eta^2$ is 1:1. For each fixed z, we look at the intersection between the surface $h(x,y) = x^2 + y^2 + xy$ and the plane $h = z$ restricted to the region $y < x$ in $\mathbb{R}^2$. The two surfaces intersect along an arc of ellipse $\mathcal{E}$, as shown in Fig. 2.10. The number of states with density $\eta = \sqrt{(4z)/3}$ is given by the number of points $f_{nm}(z)$ on $\mathcal{E}(z)$ with integer coordinates. In order to sample the pairs (n,m) correctly, we must sum over wedges $\mathcal{W}$ bounded by the x axis, the line $x = y$, and by an ellipse $\mathcal{E}$. First, we introduce a cutoff $\hat{z}$ that parametrizes the elliptic edge of $\mathcal{W}$. This fixes an upper limit $\hat{n}$ on the sum over n. How large should $\hat{n}$ be in order to compute $\Omega(z)$ for all $z < \hat{z}$? At least, $\hat{n}$ should solve $\hat{z} = \hat{n}^2 + \hat{n} + 1$. For convenience, we choose N to be the solution to $\hat{z} + 1 = \hat{n}^2 + \hat{n} + 1$:

$$\hat{n} = \text{Int}\,\frac{1}{2}\left(\sqrt{1 + 4\hat{z}^2} - 1\right) \quad , \tag{2.16}$$

where Int is the integer part, and we keep in mind that the resulting $\Omega(z)$ is accurate

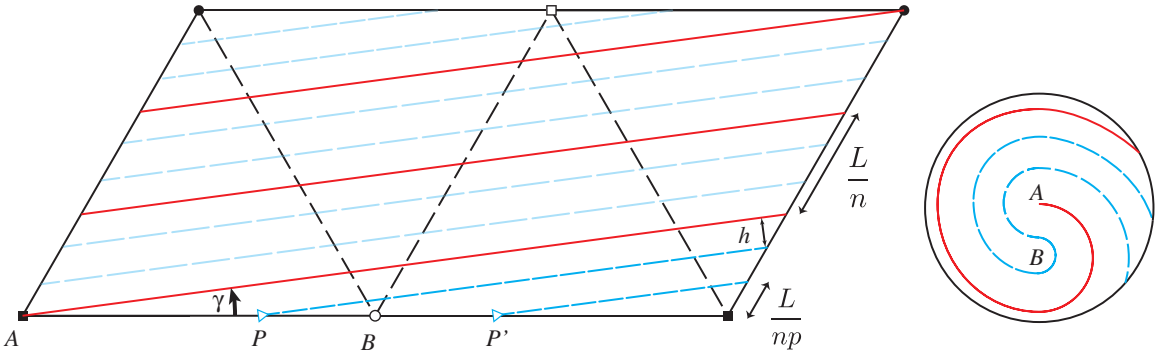

Figure 2.11: *Left:* Construction of a state containing a single spiral (red solid line) and one closed loop (blue dashed line). The points P and P' coincide when the domain is folded. *Right:* The defects structure projected on a sphere, as seen from the South pole.

only for $z < \hat{z}$. The sum over n and m are not independent. As n ranges from 1 to $\hat{n}$, m varies as

$$1 < m < M(n) \equiv \frac{1}{2}\left(\sqrt{\frac{4\hat{z}^2 - 3n^2}{3}} - n\right) \quad . \tag{2.17}$$

Finally, consider the single spiral states. If the tetrahedron contains a single spiral and no closed loops, we have

$$h = 2L \sin \gamma_n \tag{2.18}$$

where

$$\sin \gamma_n = \frac{\sqrt{3}}{2\sqrt{n^2 + n + 1}} \tag{2.19}$$

where n is the number of times that the spiral intersects the edge L of the tetrahedron. Equation (D.2) can be obtained from (2.8) setting $m = 1$. Using D.2 in 2.18 we find

$$3\eta^2 = n^2 + n + 1 \quad , \quad n \in \mathbb{N} \tag{2.20}$$

Suppose we take a single spiral configuration on the developed tetrahedron. We can insert an arbitrary *even* number of equispaced lines below the spiral (see Fig. 2.11). These will reconnect trivially across the edges. We have constructed a state with a

single spiral and a certain number of loops. So we are free to increase the density by odd multiples. This leads to

$$3\eta^2 = p^2(n^2+n+1) \quad , \quad n \in \mathbb{N} \quad p \ \text{ odd} \tag{2.21}$$

p is odd because it measures the number of times that the segment L/n is divided by the new layers. These states are chiral so they have a weighting factor of 2 . If we shift the pattern by $h/2$ in the direction normal to the layers we get the same state again. As we discussed for the double spiral state, we can sample the pairs (n,p) in a suitable region $\mathcal{W}'$ and collect the frequencies of η.

2.9 Numerical evaluation of $\Omega(\eta)$

For a fixed η, we want to count the number of allowed states. It is convenient to rewrite equations (2.6),(2.12),(2.21) and $\eta = n$ (for the quasi-baseball state) in the following form:

$$z = 4n^2 \quad , \quad n \in \mathbb{N} \tag{2.22}$$

$$z = 3n^2 \quad n \in \mathbb{N} \tag{2.23}$$

$$z = p^2(n^2+n+1) \quad , \quad n \in \mathbb{N} \quad p \ \text{ odd} \tag{2.24}$$

$$z = 4(n^2+nm+m^2) \quad , \quad m < n \in \mathbb{N} \tag{2.25}$$

where $z \equiv 3\eta^2$ and n, m, p range in suitable domains. We have to count every density of the type (2.24) two times for chirality, and every density of type (2.25) four times - two for chirality and two for a rigid shift of the lines by $h/2$. As we sample the integers n, m, p in the appropriate domains, we collect the frequencies of z, and produce the

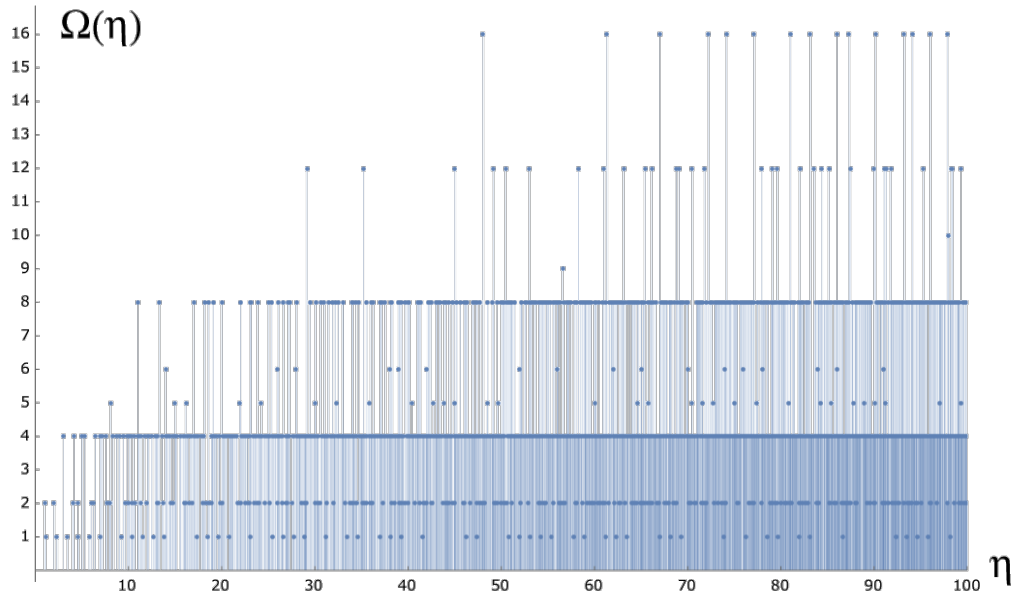

Figure 2.12: Degeneracy $\Omega(\eta)$ of tilted smectic states as function of $\eta \equiv \frac{L}{h}$ computed numerically for $\eta < 100$.

set of pairs:

$$\left(\sqrt{\frac{z}{3}}, \text{freq}(z)\right) \tag{2.26}$$

where $\sqrt{z/3} = \eta$. The result for $\eta < 100$, is shown in Fig. 2.12. The degeneracy is a highly irregular function of the density. As η increases, we meet higher and higher peaks, a result that we expect from (2.12), because the arclength of the ellipse grows and can allow more points (n, m) on it (see also Fig. 2.10).

2.10 Conclusions

We studied the ground state ($T = 0$) degeneracy of a vesicle made of smectic A liquid-crystalline building blocks. The shape of the vesicle and the configuration of the smectic layers were inferred from an equilibrium model where the smectic order and the embedding of the shape are coupled in a Landau-De Gennes free energy. In

order to find a solution to this infinite-dimensional minimization problem, we used the fact that the vesicle topology requires the presence of topological defects in the smectic layers.

Focusing on the case of four $s = +1/2$ defects, we argued that at vanishing bending rigidity the vesicle's ground states are faceted tetrahedral shells and the layers must be parallel straight lines. The layers form topologically distinct patterns depending on the tilt angle γ between the layers and an edge of the shell. We found that the system realizes all the topological defect configurations allowed by smectic order (we refer the reader to section 2.6 for a detailed discussion). Two of them, the latitudinal (i.e. $\gamma = 0$) and the quasi-baseball (i.e. $\gamma = \pi/6$) states are topologically indistinguishable, but geometrically very different. In all other cases ($\gamma \neq 0, \pi/6$) the layers form either two parallel spirals or a combination of spirals and closed loops that wind around the shell. Because a spiral can be either right- or left- handed, these states reveal the breaking of chiral symmetry, an interesting result considering that the smectic A building blocks are achiral in nature. Table 2.13 summarizes the classes of smectic states on a tetrahedral shell.

It is possible that the vesicles could be functionalized by making use of the isotropic defect cores as preferred sites for ligand attachment. A single tetrahedral shell would then be approximated as a tetravalent unit [83]. The spiral states and their chiral nature might allow interesting possibilities for supramolecular chemistry.

The topology of the smectic layers should also affect the global material parameters of the vesicles. For example, if all layers form closed loops (zero tilt angle) the length of each loop cannot be deformed and molecules cannot easily flow between the layers. We therefore expect the system to have a relatively large rigidity to an external compression. When the state contains only spirals, a localized compression can propagate a long distance along the spiral. Thus, a vesicle composed of spiral state should be softer than one composed of latitudinal state because it is able to ac-

Figure 2.13: The table summarizes the ground states of a smectic vesicle organized in 3 topological classes.

commodate shape deformations more easily. Consequences of these properties should be experimentally observable. For example, we expect that the diffusion coefficient through a perforated membrane should increase as the concentration of spiral states over latitudinal states increases because vesicles with spiral states can squeeze trough the membrane pores more easily.

Chapter 3

Triatic Liquid Crystals

3.1 Introduction

The design of new materials depends on the ability to transfer the properties of the microscopic constituents to the macroscopic scale. Particularly interesting in this context is the synthesis of building blocks of pre-assigned shape, such as "super-atoms", nanoparticles, and colloids. Self-assembly of these elementary blocks can be seen as a generalisation of atomic chemistry at larger scales, with the important difference that here the landscape of the resulting large-scale materials and their properties (chemical, structural, thermodynamic) is much richer, because they often possess novel symmetry. Many techniques have been employed in recent years to obtain supramolecular shapes [40]. Here we present a purely physical mechanism for naturally generating polyhedral shells. In particular we show that a sufficiently floppy vesicle or spherical interface with long range orientational order in the constituent three-fold symmetric building block [22], [50] inevitably relaxes to an octahedral shell as it equilibrates (for other examples see [33], [85]). The final shape depends only on the ratio of bending rigidity to liquid crystalline elastic moduli and is scale independent, as opposed to

buckling phenomena. This mechanism for shape formation is relatively unexplored.[1] The conceptual framework described can lead to a wide variety of self-assembling polyhedral building blocks. The design rules for anisotropy-driven self-assembly are only just beginning to be understood [40]. We also relate the macroscopic polyhedral symmetry group of the "super-atom" to the microscopic point-symmetry group of the generalized liquid crystal needed for its formation.

3.2 Triatic Liquid crystals

The behavior of a Liquid Crystal (LC) results from the interplay between its fluid properties, such as response to shear forces, and the intrinsic anisotropy of its microscopic constituents. The tendency to preserve local orientational order arises from the shape of the liquid crystal molecules and their mutual interactions. The oldest case studied is a nematic LC, which models a fluid of rods. The order parameter, an element of $\mathtt{RP}^1$, can be viewed as a unit vector field $\mathbf{p}(\mathbf{x})$ identified with its image under a rotation by π: $\mathbf{p} \simeq -\mathbf{p}$. It is then natural to ask if there exist models of LC with higher symmetry, such as three, four, and in general $p-$fold symmetry under local rotation of the order parameter. In what follows we will concentrate on the case $p = 3$, which will be called triatic.

It is convenient to adopt a coarse-grained description of the system, and introduce an order parameter, $\mathbf{Q}$, whose properties under spatial rotations model the anisotropic character of the liquid crystal. We will restrict our analysis to perfectly regular molecules in $d = 2$ dimensions. The nature of the microscopic interactions between molecules is left unspecified, but it is assumed to produce average alignment of the molecules in macroscopic (yet small compared to the characteristic correlation length) portions of the system. The symmetries of the order parameter must be consistent

[1] See `http://www.sacannagroup.com/home` for examples of the wide variety of novel structures being created by chemists.

with the resulting anisotropy within a given region. We therefore identify a given state of the system with its images under the action of the cyclic group C_p, which means under rotations by multiples of $(2\pi)/p$. Hence, from the point of view of symmetry, a liquid crystal represents a fluid in which the full rotation group in d dimensions, $SO(d)$, is locally broken to a discrete subgroup of order p. An alternative, but equivalent, point of view, is to require that at each point in the system, the group $SO(d)$ acts on $\mathbf{Q}$ modulo $\mathbb{Z}_p$. In most cases, the order parameter is built from a unit vector $\mathbf{p}$ and from the probability density $\rho(\mathbf{x}, \mathbf{n})$ for it to be found along a particular orientation. The lowest non constant moment of the distribution ρ consistent with the symmetries is taken to be the order parameter, which in general is a tensor. The appropriate tensor for the triatic will be found to be

$$\mathbf{Q} = \sum_{k=0}^{2} R^k \mathbf{p} \otimes R^k \mathbf{p} \otimes R^k \mathbf{p}, \tag{3.1}$$

where R^k is the rotation of a reference unit vector $\mathbf{p}$ by $k(2\pi)/3$ Third rank tensors have been used as order parameters to describe tetrahedral LC in 3-dimensional space, see for example [29]. For experimental realizations of three-fold symmetric LC, see [114].

The dynamics of the system is governed by a free energy $F = \int_\Sigma f(\mathbf{Q}) d^2\sigma$, functional of the order parameter, that will be constructed according to the framework of Landau theory: it is the most general expression formed from the invariants of the $\mathbf{Q}$ tensor, and each term must be compatible with the local symmetries of the system.

We want to determine the equilibrium (or ground) state of the system at zero temperature. In particular, we are interested in the structure of the minimally defected ground states allowed by the symmetries. We will do it in two settings: at first, the triatic will be confined to an infinite flat space. Then we will study a closed fluid membrane whose surface supports triatic LC order. The latter system has interesting

ground state configurations, resulting from the coupling between the order parameter and the geometry of the substrate, as now the free energy contains interaction terms between $\mathbf{Q}$ and the metric tensor $g_{\mu\nu}$ on the surface. The structure of the defects plays a crucial role in determining the optimal shape of the membrane.

3.3 Order parameter for triatic

In this section we will discuss the origin of the order parameter suitable for triatic liquid crystals. We will work in analogy with the nematic $Q-$tensor. Nematic order in $d = 2$ is described by an element of $\mathtt{RP}^2$, identifying antipodal points of the unit circle: $\mathbf{p} \simeq -\mathbf{p}$, $\mathbf{p} \in S^1$. The probability of finding $\mathbf{p}$ aligned with, say, z, satisfies $\rho(\mathbf{r}, \mathbf{p}) = \rho(\mathbf{r}, -\mathbf{p})$. For this reason, the first non vanishing moment of ρ is $\mathcal{M}_2 = \int_{S^1} \mathbf{p} \otimes \mathbf{p}\rho$, which is taken to be the order parameter of nematic. We will define an order parameter for the triatic following the same logic, although there will be some differences. The tensor will be of rank 3, and the trace is not a well-defined operation when the rank is not 2. We will have to look for other invariants that signal the phase transition. In the following, ρ is a positive-definite probability density on S^1. Other approaches that use a non-positive ρ can be found in [101].

At each point $\mathbf{r}$, triatic configurations are identified up to local rotations R^k by $k(2\pi)/3$, and under reflections $H_k \equiv H(R^k\mathbf{p})$, $k = 0, 1, 2$ across the legs of the triad. Correspondingly, the probability density has to satisfy four conditions: $\rho(\mathbf{r}, \mathbf{p}) = \rho(\mathbf{r}, H_1\mathbf{p}) = \rho(\mathbf{r}, H_2\mathbf{p})$ and

$$\rho(\mathbf{r}, \mathbf{p}) = \rho(\mathbf{r}, R\mathbf{p}) = \rho(\mathbf{r}, R^2\mathbf{p}). \tag{3.2}$$

Introducing an angular coordinate α on S^1, and writing $\mathbf{p} = (\cos\alpha, \sin\alpha)$, we find that (3.2) can be rewritten as $\rho(\mathbf{r}, \alpha) = \rho(\mathbf{r}, \alpha + k\frac{2\pi}{3})$, $k = 1, 2$. The first moment is $\mathcal{M}_1(\mathbf{r}) = \int_0^{2\pi} \rho(\mathbf{r}, \alpha)\,(\cos\alpha, \sin\alpha)\,d\alpha$. For later convenience we define the integration

measure $\mathtt{d}\mu \equiv \rho(\mathbf{r}, \alpha) d\alpha$. As a consequence of (3.2), $\mathtt{d}\mu$ is invariant under shifts of α by multiples of $(2\pi)/3$. We then split the integration interval in 3 sub-intervals from 0 to $(2\pi)/3$ to $(4\pi)/3$, so that $\mathcal{M}_1(\mathbf{r}) = \vec{I}_0 + \vec{I}_1 + \vec{I}_2$, with

$$\vec{I}_j = \int_{j(2\pi)/3}^{(j+1)(2\pi)/3} d\mu(\cos\alpha, \sin\alpha) \quad j = 0, 1, 2 \tag{3.3}$$

Now we make the change of variable $\alpha \to \alpha - j(2\pi)/3$. This doesn't affect the measure but brings the integration range to $[0, (2\pi)/3]$ and rotates $\mathbf{p}$ by $j(2\pi)/3$. The first moment is thus the sum of three vectors: $\mathcal{M}_1(\mathbf{r}) = \vec{I}_0 + R\vec{I}_0 + R^2\vec{I}_0 = 0$. Notice that the symmetry under rotations alone was sufficient to constrain the first moment completely. A similar argument shows that the second moment $(\mathcal{M}_2)_{ij} = \int_{S^1} d\mu\, p_i p_j$ is a constant: $\mathcal{M}_2 = \frac{1}{2}\mathtt{Id}$. Since the second moment is independent of the state of the system we go on to look at the third moment. This is not constant, and can be taken as the triatic's order parameter:

$$\mathbb{T} \equiv \mathcal{M}_3 = \int_{S^1} d\mu\ \mathbf{p} \otimes \mathbf{p} \otimes \mathbf{p} \quad . \tag{3.4}$$

For a completely disordered (or isotropic) phase, $\rho = \mathtt{constant} = (2\pi)^{-1}$. This gives $\mathbb{T}_{\mathtt{iso}} = 0$. On the other hand, the probability distribution of a perfectly ordered state cannot be $\rho = (2\pi)^{-1}\delta(\mathbf{p} - \mathbf{p_0})$, because it does not satisfy condition (3.2):

$$\delta(\mathbf{p} - \mathbf{p_0}) \neq \delta(R\mathbf{p} - \mathbf{p_0}) \quad \text{and} \quad \delta(\mathbf{p} - \mathbf{p_0}) \neq \delta(R^2\mathbf{p} - \mathbf{p_0}) \quad . \tag{3.5}$$

This was not the case with a uniform nematic, because the Dirac delta function is even under inversion of its argument. The analogy with nematics ends here, also because the trace is defined only on tensors of rank 2. A possible solution is to define

the density in the isotropic phase as a sum of 3 delta functions:

$$\rho_{ord} \sim \delta(\mathbf{p} - \mathbf{p_0}) + \delta(\mathbf{p} - R\mathbf{p_0}) + \delta(\mathbf{p} - R^2\mathbf{p_0}) \tag{3.6}$$

which is analogous to a distribution of three point masses if $\mathbf{p}$ was to represent a position in physical space. When we use (3.6) in (3.4), we find that $\mathbb{T}$ is automatically invariant under reflections across the three vectors of the triad. We will take the order parameter to be

$$\mathbf{Q} = \mathbf{p} \otimes \mathbf{p} \otimes \mathbf{p} + R\mathbf{p} \otimes R\mathbf{p} \otimes R\mathbf{p} + R^2\mathbf{p} \otimes R^2\mathbf{p} \otimes R^2\mathbf{p} \ . \tag{3.7}$$

The order parameter (3.7) describes accurately an ordered phase. Phase transitions and loss of orientational order are instead described by a scalar order parameter $S \equiv \langle (\mathbf{l} \cdot \mathbf{n}) \mathrm{mod}(2\pi/3) \rangle_\rho \equiv \langle (\cos 3\alpha) \rangle_\rho$, where $\mathbf{l}$ is the orientation of a single molecule, $\mathbf{n} = \langle \mathbf{l} \rangle_\rho$, with the average taken over a ball of radius $a \ll R \ll L$ (a, L here are the molecular and system sizes respectively), and ρ satisfies (3.2). S is obtained from the *microscopic* $\mathbf{Q}$-tensor $\mathbf{l} \otimes \mathbf{l} \otimes \mathbf{l}$ by writing $\mathbf{l} = e^{i\alpha}$ and averaging over a ball: $S = \mathrm{Re} \langle e^{i3\alpha} \rangle_\rho$. A disorder-order phase transition would be described by a Landau free energy of the form

$$f(S) = \frac{1}{2}|\nabla S|^2 + \frac{1}{2}a(T)S^2 + BS^4 \quad . \tag{3.8}$$

Phase transitions, however, are not the focus of this paper.

3.4 Free Energy

The ordered phase of the system is described by minimizers of a suitable free energy functional

$$F[\mathbf{Q}, D\mathbf{Q}] = \int_\Sigma f(\mathbf{Q}, D\mathbf{Q}) d\mu(\Sigma) \quad , \tag{3.9}$$

where the integration is taken over the space Σ to which the liquid crystal is confined. The measure $d\mu(\Sigma)$ contains the determinant of the metric tensor on Σ. The free energy density is a scalar with respect to a change of coordinates, and thus it must be written in terms of invariants of the tensors $\mathbf{Q}$ and $D\mathbf{Q}$. The lowest order term f_0 containing $D\mathbf{Q}$ is [2]:

$$f_0 = \frac{1}{2} K \; D_a Q_{bcd} D^a Q^{bcd} \quad . \tag{3.10}$$

For simplicity we choose to work in the one Frank constant approximation K, as the essential principles are revealed for $K_1 = K_3$. The elastic modulus K is of the order $k_B T_m/a$, where T_m is the melting temperature of the triatic and a is the molecular size. Consider flat 2−dimensional space, choose polar coordinates $\{\mathbf{e}_1, \mathbf{e}_2\} \equiv \{\mathbf{e}_r, \mathbf{e}_\varphi\}$, and write $\mathbf{p} = \cos(\psi)\mathbf{e}_1 + \sin(\psi)\mathbf{e}_2$. There is only one independent component of the $\mathbf{Q}$−tensor (3.7): $\frac{3}{4}\cos(3\psi) = Q_{111} = -Q_{122} = -Q_{221} = -Q_{212}$, $\frac{3}{4}\sin(3\psi) = Q_{112} = Q_{121} = Q_{211} = -Q_{222}$. When expression (3.10) is computed in flat polar coordinates (r, φ), and assuming that ψ depends on φ only, the result is $f_0 = \frac{81}{16} K \; r^{-2}(\partial_\varphi \psi + 1)^2$. In terms of the angle θ between $\mathbf{p}$ and an horizontal cartesian axis,

$$f_0 = \frac{81}{16} K \; r^{-2}(\partial_\varphi \theta)^2 \quad . \tag{3.11}$$

We will consider only the term $(\partial_\varphi \theta)^2$ because the prefactor contributes only to the core energy of the defect. Can other invariants be included in the free energy? By computing the lowest order ones, we see that no invariant formed from contractions of $\mathbf{Q}$ alone has dynamical content. The reason lies in the symmetries of the order parameter, which forces any contraction to vanish: $Q_{a\nu\nu} = Q_{a11} + Q_{a22} = 0$ for any choice of $a = 1, 2$. Hence, terms like Q^2 or Q^4 vanish.[3] Furthermore, contractions

[2] Notice that there are no cross-contractions between indices of D and those of Q. Any other contraction between D and $\mathbf{Q}$ vanishes because of the symmetries of $\mathbf{Q}$.

[3] This argument applies generally to any odd-rank tensor. For a 3rd rank tensor in three space dimensions, see [29], Sec. IIIA.

between D and $\mathbf{Q}$ alone are not allowed, since D and $\mathbf{Q}$ belong to different spaces. In view of this fact, we start our analysis of the ground state in flat space from the simple quadratic free energy functional

$$F = K \int d\mu (D\mathbf{Q})^2 = K \int_0^\infty r dr \int_0^{2\pi} d\varphi (\partial_\varphi \psi + 1)^2 \quad . \tag{3.12}$$

Notice that, in terms of the unit vector $\mathbf{p}$, expression (3.12) is equivalent to the functional $F = \frac{1}{2}\int_\Sigma d\mu(\Sigma) G_{ab} \partial_\mu p^a \partial^\mu p^b = \frac{1}{2}\int_\Sigma d\mu(\Sigma)(D\mathbf{p})^2$, that is usually encountered in nematic liquid crystals as well as in the non linear sigma model with a flat geometry ($G_{ab} = \delta_{ab}$) in the field space. It can be proven that for any orientational order parameter of rank p, describing a $p-$fold symmetric LC, the free energy density f_0 always reduces to the nematic expression $(D\mathbf{p})^2$. We thus find that the free energy does not distinguish between different discrete symmetries of the order parameters, and the quadratic term f_0 is the same for all $p-$atic liquid crystals. This has an interesting consequence when we consider the class of odd-rank order parameters, including the triatic. These OP are odd under inversion of $\mathbf{p}$: $\mathbf{Q}(-\mathbf{p}) = -\mathbf{Q}(\mathbf{p})$. In fact inversion seems to produce a distinct configuration of the LC. The free energy, however, is quadratic in $\mathbf{Q}$, and therefore shows an accidental symmetry under the same operation, suggesting that states related by inversion have at least degenerate energies. We will see in the following discussion that inversion in the OP space is equivalent to a proper rotation in physical $2-$dimensional space, so there is no degeneracy for the ground states, and both $\mathbf{Q}$ and $-\mathbf{Q}$ represent the same physical state.

3.5 Ground states and defects

The Euler-Lagrange equations for (3.12) reduce to Laplace's equation in one dimension:

$$\partial_\varphi \partial_\varphi \psi(\varphi) = 0 \tag{3.13}$$

The solutions in terms of the angle ψ between $\mathbf{p}$ and $\mathbf{e}_r$ are linear functions of φ:

$$\psi(\varphi) = a\varphi + \psi_0 \quad , \tag{3.14}$$

where $a \in \mathbb{R}$ and ψ_0 gives the initial orientation of $\mathbf{p}$ at $\varphi = 0$. We can always choose coordinates in space such that $\psi_0 = 0$, so that $\mathbf{p}$ is parallel to the line $\varphi = 0$.

We can classify solutions to (3.13) according to their winding number, or topological charge, s, which measures the number of full revolutions of the director $\mathbf{p}$ along a closed path Γ encircling the location of the defect. To do so, we must measure the angle φ and the revolution angle of $\mathbf{p}$ with respect to the same reference axis. We thus introduce the angle $\theta(\varphi)$, related to $\psi(\varphi)$ through[4] $\theta(\varphi) = \psi(\varphi) + \varphi$. The winding number is then defined as $\oint_\Gamma d\theta = (2\pi)s$. For $s = 0$ the solution is free of defects, and describes a uniform distribution of triads: $\theta(\varphi) = \texttt{const}$. The integral curves of the director are straight lines, which need to be identified with their images under $(2\pi)/3$ rotations (see Fig.1d). Notice that, unlike nematics, where the integral lines of $\mathbf{p}$ don't have an orientation, here each line carries a direction, dictated by the associated member of the triad. Orientation of the lines lifts the accidental $\mathbf{p} \to -\mathbf{p}$ symmetry of F, as was anticipated, because reversing orientations would require a rotation by $\pi/3$ in the OP space, which is not in the symmetry group of $\mathbf{Q}$. As was noticed before, there are two choices for the orientation of the integral lines but they are in fact the same configuration, because they can be made to coincide by rotating the physical space by $\pi/3$. So it is not surprising that the free energy associated with opposite orientations is the same.

The lowest, or elementary, topological charge allowed by the 3−fold symmetry of triatics is $s = 1/3$, because when φ is rotated by 2π around a closed loop, the angle θ must come back to itself modulo an integer multiple of $1/3 \cdot (2\pi)$: $\theta(\varphi + 2\pi) = \theta(\varphi) + s(2\pi) \quad , s = \frac{1}{3}m$, $m \in \mathbb{Z}$ When this uniqueness condition is rewritten in terms

[4]The analysis of the defect structure follows the treatment of Landau and Lifshitz [61].

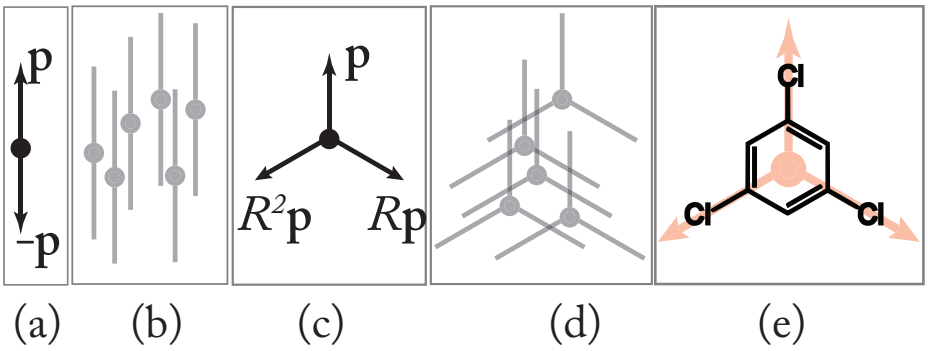

Figure 3.1: **(a)** Nematic frame, consisting of the vector **p** and its image rotated by π. **(b)** Perfectly ordered nematic state in the plane. **(c)** Triatic frame, consisting of **p** and its images rotated by $(2\pi)/3$ and by $(4\pi)/3$. **(d)** Perfectly ordered triatic state in the plane.**(e)** A possible realization of a triatic LC with 1,3,5-Trichlorobenzene.

of ψ, we find that the coefficient a of equation (3.14) is related to the charge by $a = s - 1$. The smallest charge is $s = +1/3$, and the corresponding defected state is $\psi(\varphi) = -\frac{2}{3}\varphi$. For future convenience, we write explicitly the solutions ψ and θ for an $s = 1/3$ defect: $\theta(\varphi) = s\varphi = \frac{1}{3}\varphi$ and

$$\psi(\varphi) = (s-1)\varphi = -\frac{2}{3}\varphi = \frac{s-1}{s}\theta(\varphi) = -2\theta(\varphi) \quad . \tag{3.15}$$

The integral lines of $\mathbf{p}(r, \varphi)$ are found by requiring that **p** is parallel to the line element $d\mathbf{l}$. In polar coordinates, this reduces to

$$\frac{dl_\varphi}{dl_r} \equiv \frac{r d\varphi}{dr} = \frac{\sin\psi}{\cos\psi} = \tan\psi(\varphi) \quad , \tag{3.16}$$

together with the condition that ψ has the correct periodicity $\psi(\varphi + 2\pi) = \psi(\varphi) + (s-1)(2\pi)$. Substituting (3.15) into (3.16), we find

$$\frac{d\varphi}{d\log r} = \tan\left(-\frac{2}{3}\varphi\right) \quad . \tag{3.17}$$

We can integrate (3.17) by separating variables. We have to be careful about the

sign of $\tan\psi$ as we complete one full revolution around the defect core. From (3.15), we find that as φ changes from 0 to $(2\pi)/3$, ψ changes from $-(4\pi)/3$ to 0. Within this interval, the function $\tan\psi$ changes sign 3 times. In particular *i*) $\tan\psi < 0$ for $\psi \in [-(4\pi)/3, -\pi] \cup [\pi/2, 0]$ while *ii*) $\tan\psi > 0$ for $\psi \in [-\pi, -\frac{\pi}{2}[$. As r increases, the integral lines bend clockwise in case *i*), and counterclockwise in case *ii*). The function $\tan\psi$ can change sign in two ways. It can cross $\tan\psi = 0$ at $\psi = -\pi$ and at $\psi = 0$, in which case $d\varphi = 0$. This means that the integral curve is a straight line, which will be called an *Asymptote*. Or, it can jump from $+\infty$ to $-\infty$ at $\psi = -\pi/2$. This is a regular point for the differential equation, because $d\varphi/\tan\psi \to 0$, so r tends to a constant finite value.

The integration of (3.17) can be organized efficiently once we know the directions in the plane $\varphi = \widetilde{\varphi}_m$ at which the tangent changes sign. These are found by inverting (3.15): $\widetilde{\varphi}_m \equiv \varphi(\psi_m) \equiv -\frac{3}{2}(-m\frac{\pi}{2})$, $m = 0, 1, 2$. For completeness, we observe that as we close the path Γ, $\varphi \to 2\pi$, and $\psi \to -(4\pi)/3$. Hence the region below $x > 0$ is regular, and the slope of the integral lines on the $x-$axis is everywhere equal to $\theta = (2\pi)/3$, which is what we expect for a 1/3 defect. From the previous discussion we conclude that:

a) $\varphi \to 0^+$ is an asymptote ($\tan\psi \to 0^-$)

b) $\widetilde{\varphi}_1 = \frac{3\pi}{4}$ divides behavior *i*) from behavior *ii*), and the curves are regular here

c) $\widetilde{\varphi}_2 = \frac{3\pi}{2}$ is an asymptote

d) For $\varphi \to 2\pi$ the integral curves are regular, and their slope approaches $(2\pi)/3$ independently of r.

Let us identify 3 regions in the (r, φ) plane: region I for $0 < \varphi < (3\pi)/4$, region II for $(3\pi)/4 < \varphi < (3\pi)/2$ and region III for $(3\pi)/2 < \varphi < 2\pi$. Integration of (3.17) is easiest in region II, as here $\tan\psi$ is positive, so we can integrate $d\psi/\tan\psi =$

$d\log(\sin\psi)$. The integral line containing the base point (r_0, φ_0) is given by:

$$r_I(\varphi) = r_0 \left[\frac{\sin(-2/3\varphi)}{\sin(-2/3\varphi_0)}\right]^{-3/2}, \; \varphi, \varphi_0 \in \left[\frac{3\pi}{4}, \frac{3\pi}{2}\right] \tag{3.18}$$

In regions I and III the tangent is negative, so we use the following procedure to integrate equation (3.17). We take region I as example. According to (3.17), here the derivative of φ with respect to r is negative. We define an auxiliary variable $u(\varphi)$ such that the value $\tan u$ is positive and $\frac{d\varphi}{d\log r} = \tan\psi(\varphi) \equiv -\tan u(\varphi)$. According to (3.16), the variable ψ changes as $\psi(\varphi) = -2/3\varphi$. Inside region I, φ changes between 0 and $(3\pi)/4$. The function $\tan x$ is odd under inversion of x. Hence, we define u as the symmetric of ψ with respect to the origin $(u(\varphi) = +2/3\varphi)$, so that $\tan u > 0$.In terms of the variable u, the differential equation (3.17) becomes

$$-\frac{3}{2}\frac{du}{\tan u} = d\log r \quad , \tag{3.19}$$

which integrates to $r_{II}(\varphi) = r_0 \left[\frac{\sin(2/3\varphi)}{\sin(2/3\varphi_0)}\right]^{-3/2}$ for $\varphi, \varphi_0 \in [0, \frac{3\pi}{4}]$. Analogous considerations allow to solve (3.17) in region III as well. The solution is identical to r_{II}, but the interval of definition for φ, φ_0 is now $[3\pi/2, 2\pi]$. The pattern of the full solution is represented graphically in Fig. 2 (Left panel). Each curve is the integral line of one leg $\mathbf{p}$ of the triad. Once the orientation of $\mathbf{p}$ is chosen along an integral curve, the orientation of the remaining two legs is uniquely determined. Imagine to draw $\mathbf{p}$ in region I, on the curve which is closest to the $x-$axis. We can choose to orient $\mathbf{p}$ to the right, so that $\theta = 0$. As for the uniform, non-defected ground state, we observe again that each integral line carries an orientation,but an oriented pattern and its reflected image are connected by a rotation by $\Delta\varphi = \pi/2$ of the physical space, so there is no degeneracy, and no chirality associated with the pattern.

Now imagine a closed path Γ that encircles the origin, and follow $\mathbf{p}$ along Γ.

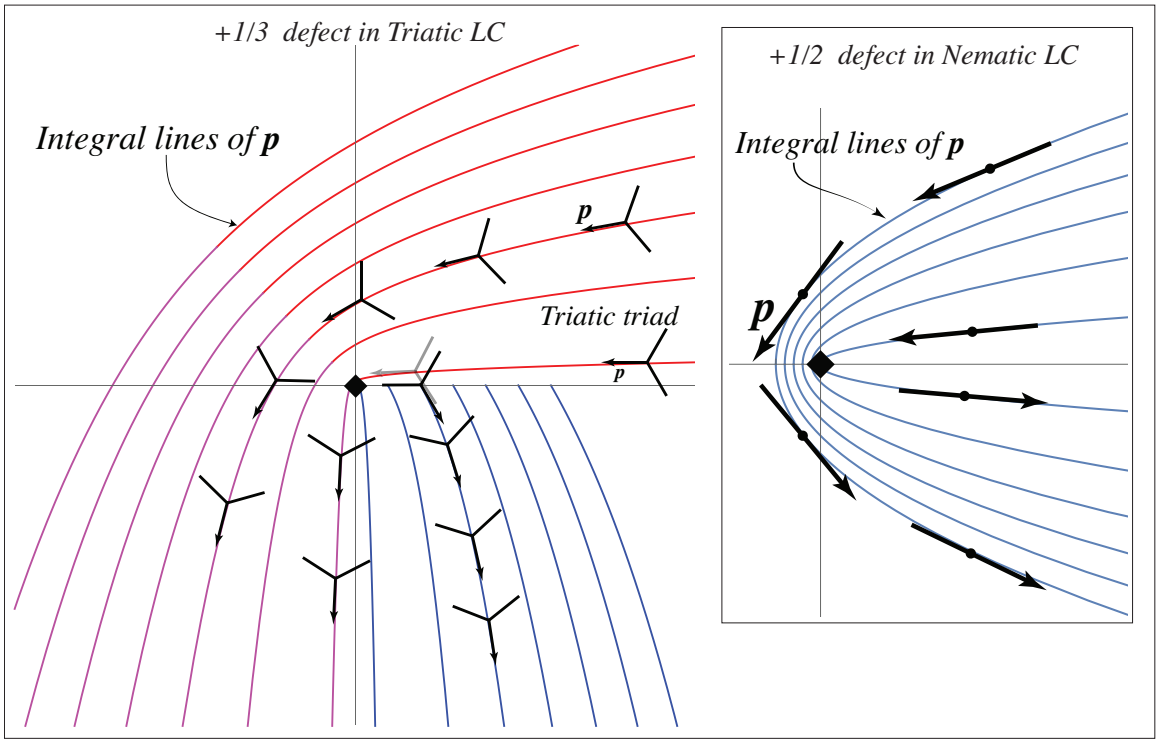

Figure 3.2: $s = +1/3$ (Left panel): the defect structure of a triatic. (Right panel) The structure of a strength $+1/2$ nematic disclination. The vector $\mathbf{p}$ is used to solve (3.16) and then identified with the other two legs of the frame.

As Γ crosses the negative y axis, $\mathbf{p}$ has rotated by $\Delta\theta = \pi/2$. When the loop Γ is approaching the starting point on the x-axis from below, the orientation of $\mathbf{p}$ approaches the limiting value $(2\pi)/3$. The reason is that the slope of the integral curves is precisely the angle θ, see eq. (3.16). On the $x-$axis, the value of θ is $\theta(2\pi) = (2\pi)/3$, because the defect has charge $s = +1/3$. All the integral curves that approach the $x-$axis from below have slope $(2\pi)/3$ at $y = 0$. The core profile $S(r)$ of the defect can be computed in polar coordinates (r, φ) using the scalar order parameter $S = \langle \cos(3\alpha) \rangle_\rho$ and imposing $S(r = 0) = 0, S(r \to \infty) = 1$. The core energy scales with $2\log(L/a)$, so it is negligible compared to the bulk energy in the limit $L \to \infty$.

In the following section we discuss triatic order in confined planar geometries, and make several predictions for the resulting equilibrium states of topological defects. These could be tested experimentally.

3.6 p-atics confined to a disc

A $p-$atic LC confined to a disk of radius R will develop p defects of strength $1/p$ to screen the topological charge of the disk $\chi = 1$. Thus, nematic and triatic LC will respectively form two $s = 1/2$ and three $s = 1/3$ defects that mutually repel each other. The location of these defects also depends on the boundary conditions. Strong anchoring of the prescribed orientation on the disk boundary is modeled by image charges s' that push the bulk defects s into the disk, away from the boundary. In equilibrium, the nematic is arrayed along a diameter at distance d from the center (Fig.3b), while the three $+1/3$ defects of the triatic are positioned at the vertices of an equilateral triangle (see Fig.3c). The resulting equilibrium distance $d < R$ of the defects from the center of the disc depends on the precise number and configuration of interacting defects. The disk boundary is given by $z \cdot \bar{z} = R^2$ in complex coordinates

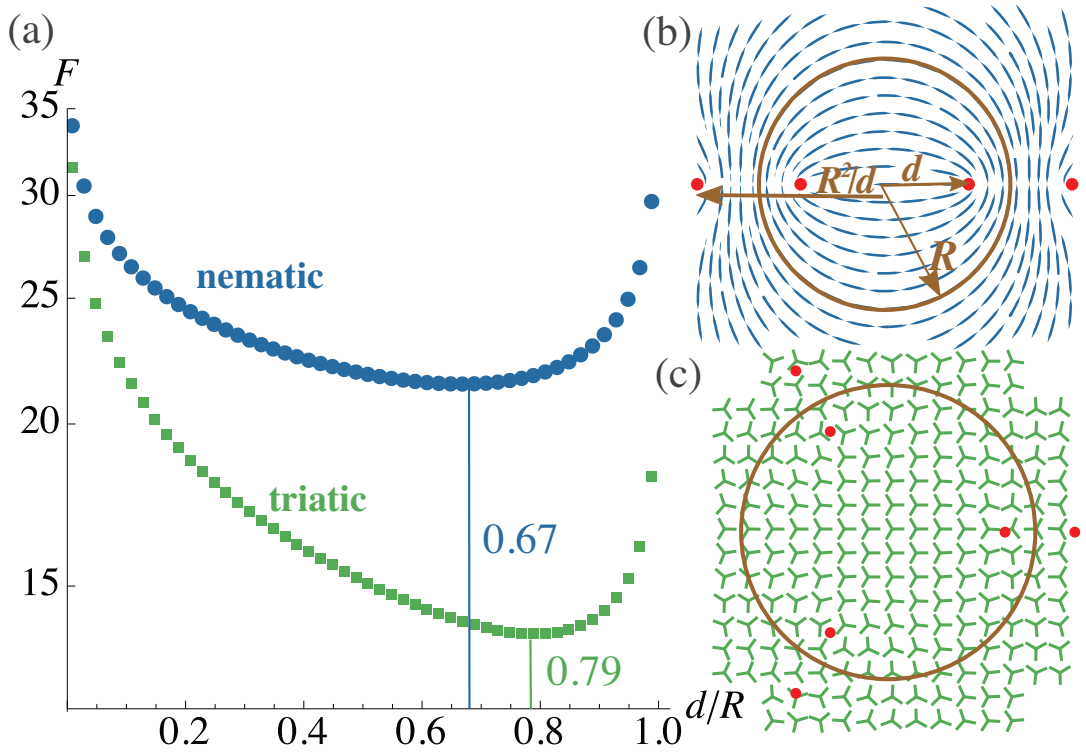

Figure 3.3: (a) The calculated free energy (3.10) for nematic and triatic liquid crystals confined to a disc. The tangential boundary conditions are achieved by placing $p = 2, 3$ charges of strength $+1/p$ at distances $d < R$ inside a disc and image charges at R^2/d outside the disc of radius R (3.20). The equilibrium configurations for nematic (b) and triatic liquid crystals (c) occur for defects placed at $d/R = \{0.67, 0.79\}$, respectively.

$z, \bar{z} \equiv x \pm iy$. The orientation $\psi(z, \bar{z})$ of $\mathbf{p}$, satisfies Laplace's equation $\partial_{\bar{z}}\partial_z\psi = 0$ (see (3.10)) and the tangential alignment at the boundary $\psi|_{r=R} = \pi/2 + \varphi$ is:

$$\psi(z, \bar{z}) = \arg\left[(z^p - d^p)^{1/p}\left(z^p - (R^2/d)^p\right)^{1/p}\right]. \tag{3.20}$$

The argument, arg, of the complex function is continuous everywhere except at the points $de^{i2\pi k/p}$ and $R^2/de^{i2\pi k/p}$, with $k = 0, 1, 2, \ldots, p-1$, located inside and outside the disc of radius R, where we place disclinations of charge $+1/p$ for a generic p-atic field. The free energy of the configuration (3.20) is minimized for $d/R = 0.67$ for a nematic ($p = 2$) and $d/R = 0.79$ for a triatic ($p = 3$) - see Fig.3a. The value of the integrated energy (3.10) depends on the cut-off around the core of the defect (chosen to be $0.01R$), but the location of the minimum depends only on the order p. This robust prediction was already verified experimentally for the nematic case, where elongated spindle cells [25] organize in a structure analogous to Fig.3b with the position of $+1/2$ disclinations at $d/R = 0.67$. Experiments with triatic LCs, for example using 1,3,5-Trichlorobenzene or Clathrin, would be highly desirable to verify the form of the equilibrium configuration and the structure of $+1/3$ disclination.

3.7 Triatic LC confined to closed shells

We have seen that the ground states of the free energy (3.12) in flat space are ordered states that minimize bend and splay of their integral lines. When a liquid crystal is confined on the $2-$dimensional surface of a vesicle, the substrate is also a dynamical variable, since it can adjust its shape to achieve the state of minimum energy. The energy cost to deform the surface is modeled through the Willmore functional F_W, that measures the energy required to increase the mean curvature $\vec{H}$ of the surface:

$$F_W[\mathbf{g}] = \frac{1}{2}\int_\Sigma \vec{H}^2\, d\mu(\Sigma) \quad . \tag{3.21}$$

The dynamical variable is the metric tensor on the surface $\mathbf{g}$, which is implicitly contained in the measure and in $\vec{H}$. The total free energy of a vesicle covered with a liquid crystal is therefore the sum of (3.12) and (3.21) [5]:

$$F[\mathbf{Q},\mathbf{g}] = \frac{1}{2}\int_{\Sigma}[K(D\mathbf{Q})^2 + \kappa\vec{H}^2]\,d\mu(\Sigma) \quad . \tag{3.22}$$

The order parameter and the metric tensor are minimally coupled through the covariant derivative $D_a = \partial_a + \mathbf{\Gamma}_a$, where $\mathbf{\Gamma}(\mathbf{g})$ are the Christoffel symbols on the surface, and depend on the metric tensor. The action of D on the third rank tensor $\mathbf{Q}$ is $D_aQ^{bcd} = \partial_aQ^{bcd} + \Gamma^b_{ai}Q^{icd} + \Gamma^c_{ai}Q^{bid} + \Gamma^d_{ai}Q^{bci}$. The core energy of defects is not included in (3.22) because it is negligible for large system sizes. We imagine forming a vesicle with a triatic bilayer membrane immersed in a reservoir, so the surface tension is tuned to zero ($\delta F/\delta A = 0$) thanks to micro-transport (the area can freely fluctuate). According to expression (3.21), flat surfaces are favored by the Willmore energy, since $\Gamma^a_{bc} = 0$ and $\vec{H} = 0$ everywhere. A deformable closed vesicle with the topology of a 2-sphere, however, is subject to a topological constraint: the integrated Gaussian curvature must equal the Euler characteristic of the 2-sphere $\chi(\Sigma) = 2$ Since $\mathbf{p}$ is taken to be a vector field in the tangent space of Σ, it must also contain a total topological charge equal to 2. Hence, the ground state of the order parameter on Σ must necessarily contain defects whose sum is 2. Since the core energy of each defect is proportional to the square of the charge, s^2 (see [14]), the least energetic configuration contains 6 defects of charge $+1/3$. If we imagine to force the surface to be a sphere ($\kappa \to \infty$), and allow the defects to move on it, they will repel and try to maximize their mutual geodesic distance, occupying the 6 vertices of a regular octahedron (see [67]). If the shape is now allowed to deform, the Willmore term will favor the formation of flat areas on the surface. In the limit $\kappa = 0$, where the formation of

[5] As with (3.10), the one Frank constant approximation $K_1 = K_3$ suffices to establish the existence of a polyhedral shell as the ground state.

sharp edges has no energy cost, we achieve a regular octahedron with $+1/3$ defects on each vertex. It is useful to check that there is no energy stored in the integral lines of $\mathbf{p}$ across the edges: as for Fig.1, the pattern is determined by the orientation of $\mathbf{p}$ with $\theta \in [0, (2\pi)/3]$. If we imagine to unfold the octahedron on a flat plane (Fig.4a), we will see that the lines are straight across the edges, hence they have zero bending energy into the tangent plane. We expect a variety of shapes for anisotropic bending rigidities. Thanks to the freedom to choose either orientation along the integral lines, we conclude that equation (3.22) allows two degenerate ground states. However, they have to be counted as the same object, because they are connected by a rigid proper rotation of the vesicle in $3-$dimensional space. At each of the 6 vertices of the octahedron resides a $1/3$ defect in the triatic field, whose charge s can be detected by travelling along a loop Γ that encircles vertex V, and measuring the net rotation of a reference leg in the triad, as explained in Fig.4b.

3.8 Conclusions

We have constructed the order parameter describing a liquid crystal that breaks the isotropic group $O(2)$ down to $O(2)/\mathbb{Z}_3$ in the space of directions $\mathbf{p}$, finding that, unlike the nematic OP, it has vectorial properties. This distinction is a general feature of generalized liquid crystals. When the configurations of $\mathbf{p}$ are identified modulo $\mathbb{Z}_p$, the OP behaves like an element of the projective space for p even, and as an ordinary vector when p is odd. When the rank of the $\mathbf{Q}-$tensor is odd, we find that $\mathbf{Q}(-\mathbf{p}) = -\mathbf{Q}(\mathbf{p})$. Using this property, we have shown that the functional expression of the free energy reduces to the simple quadratic form $(D\mathbf{p})^2$, where D is the covariant derivative. This expression is common to all $p-$atic LC. For odd-symmetric LC, we have interpreted the accidental symmetry of the free energy under $\mathbf{p} \to -\mathbf{p}$ as the invariance of the system under proper rotations in the embedding

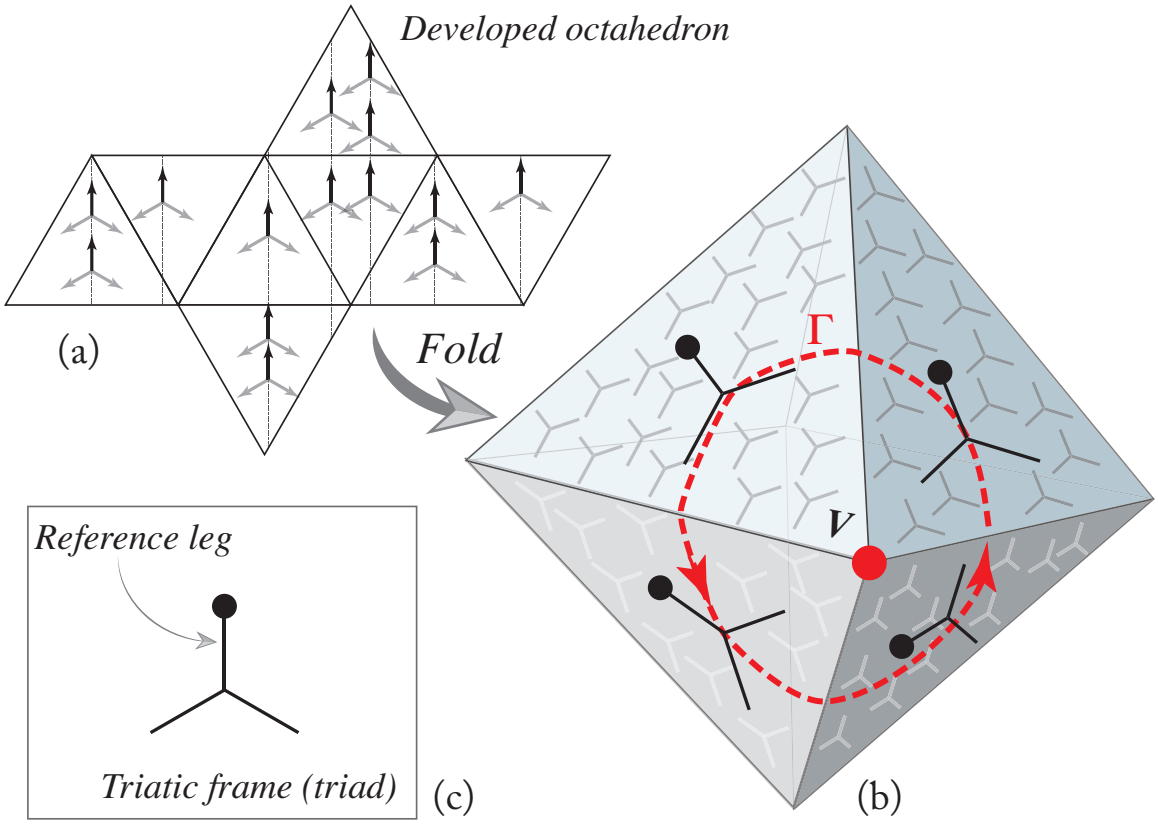

Figure 3.4: **(a)** Unfolded octahedron with triatic order on its faces. The triatic LC is represented by a frame with 3 identical legs. The orientation of the frames is uniform within each face. **(b)** Folded octahedron supporting triatic order. The triatic LC forms a defect of charge 1/3 around each vertex V (red dot). Let Γ be a closed path (red dotted line) encircling the vertex V. Choose a reference leg of the frame (indicated by a black dot in inset **(c)**), and follow its orientation as you travel around Γ. By the time we return to the starting point, we find the reference leg rotated by an angle of $(2\pi)/3$.

space. In the specific case of triatics, the three-fold symmetry under rotations of $(2\pi)/3$ of the reference vector allows to construct an elementary defect of charge $+1/3$. We then considered a closed $2-$dimensional membrane coated with a triatic LC. We assumed that the total free energy takes into account both bending of the membrane, and elastic deformations of the vector $\mathbf{p}$ across the system. The state of minimum energy shows frustration between the constraint $\chi = 2$ due to the spherical topology of the vesicle, and the tendency of $\mathbf{p}$ to be uniform across the surface. The energy is minimized by screening the total curvature charge with six elementary defects in the LC pattern ($2 = 6 \cdot (1/3)$), whose locations maximize their mutual geodesic distance, as observed by Prost and Lubensky [67] in 1992. In the limit of vanishing bending rigidity ($\kappa = 0$), it is energetically favorable to form sharp straight edges between pairs of defects, and develop flat faces bounded by these edges through expulsion of gaussian curvature. The resulting shape is an octahedron. The analysis employed to reach this conclusion, which was adopted earlier in [110], can be easily generalized to any $p-$fold symmetric liquid crystal. For example, in [70] was constructed a non linear free energy for a vesicle covered with a four-fold symmetric LC, the tetratic (See also [64],[36],[24]), which gives rise to a cubic shape. Hence, we expect that the ground states of generalized LC vesicles at zero bending rigidity realize all possible polyhedral shapes as one varies $p \in \mathbb{N}$. Precise predictions have been be made about the position of triatic LC defects confined to a disk. We hope that this work will encourage the design of experiments with biological and non-biological molecules of three-fold symmetric shape confined to two-dimensional layers to test such predictions. Clathrin or BTA molecules might be good candidates to test the unusual behavior of triatic LCs. Recent developments in DNA nanotechnology [12] have made possible the synthesis of molecules of various shapes, and triatic behaviour could be expected whenever an ensemble of such molecules exhibits local three-fold symmetry. Experimental tests of the effects of an anisotropic bending rigidity on

the polyhedral shells would be highly beneficial to guide an extension of the present theory to less idealized situations. Emphasis should be put on the assembly of these polyhedral building blocks, through the functionalisation of the defects sites at the vertices.

Chapter 4

Statistical Mechanics of surfaces with fluctuating topologies

In this chapter we consider the statistical mechanics of fluid membranes embedded in 3–dimensional flat space. We will distinguish fluid membranes from interfaces. Interfaces are 2–dimensional regions Σ that separate two bulk phases. A simple example is provided by the surface of separation between oil and water. The equilibrium shape of the interface is found by minimizing a free energy $F[\Sigma] = \gamma A$ proportional to the total interface area A. The variable γ conjugate to the area is called the interfacial or surface tension [19]. Another example is given by the Nambu-Goto action of the bosonic string embedded in $D = 3$ dimensional space. The action is proportional to the area of the $2-$dimensional string world-sheet and is therefore analogous to an interface model, where the inverse of the string coupling constant plays the role of the surface tension.

Membranes, unlike interfaces, have a very low, sometimes even vanishing, effective surface tension [86]. The Landau-type energy functional associated to shape fluctuations is written in terms of Gaussian and mean curvatures , and depends on fourth-order spatial derivatives of the deformation. Since derivatives up to third or-

der are not suppressed, the configuration space of fluid membranes contains highly non-planar geometries often rich of handles. If fluctuations are unconstrained, the partition function involves the sum over non-trivial topologies and conformations.

In the rest of this chapter we will justify and study a model that allows topology changes in the partition function of fluid membranes. This could be regarded as a statistical model of handle formation. In some physical systems like microemulsions the effective surface tension vanishes, so the statistics of different topologies is controlled by curvature energies H only. We can model the formation of handles via a Gibbs measure $\exp(-H/k_BT)$. We then construct the partition function by summing over all topologies. Using some exact lower bounds on the curvature energy of closed surfaces, we deduce an upper bound for the partition function.

4.1 Models of fluid membranes

The constituents of a fluid membrane are free to diffuse within the surface, in other words their positions have zero correlation length. In this case, the shear modulus vanishes and the physical states of the membrane are controlled by shape deformations alone. This is in contrast to the case of crystalline membranes (more generally, membranes with internal order) where the shear modulus is finite and configurations are labeled by the local arrangement of the membrane's constituents in addition to the global shape. In a coarse-grained geometrical description, the fluid membrane is modeled as a mathematical surface Σ. We label every element of the fluid surface by a pair of internal coordinates $\boldsymbol{\sigma} = (\sigma^1, \sigma^2)$. The position of a fluid element in the 3–dimensional 'ambient' space is a vector $\mathbf{X}(\boldsymbol{\sigma})$ with components

$$X^\mu(\boldsymbol{\sigma}) \quad , \quad \mu = 1, 2, 3 \quad . \tag{4.1}$$

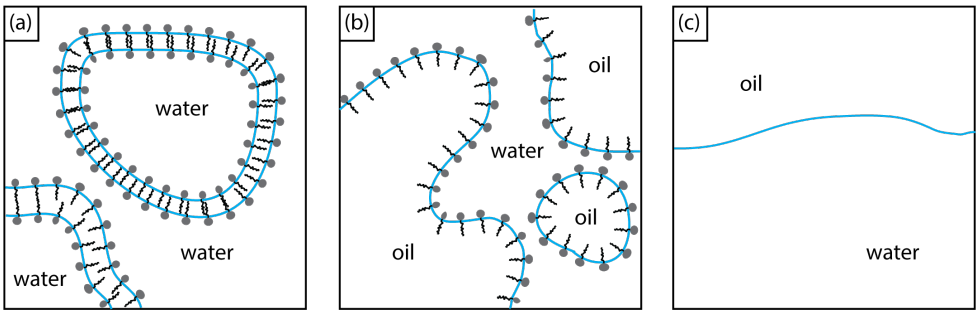

Figure 4.1: Three kinds of fluctuating surfaces: (a) and (b) are 2–dimensional fluids: (a) Bilayer membranes made of amphiphilic molecules. Hydrophilic heads are dispersed in water, while hydrophobic tails are screened from water. (b) Emulsion stabilized by a surfactant. The surfactant molecules forming the membrane are in a fluid phase (the bulk modulus along the surface is finite, and the shear modulus is zero). (c) Interface between two immiscible fluids. The shape of the surface is determined by the surface tension γ conjugate to the total area A.

The absence of positional order in the fluid elements implies that the thermodynamic potential describing the ensemble must be invariant under reparametrization of the internal coordinates. The tangent vectors to the surface are defined as

$$\mathbf{t}_a = \frac{\partial \mathbf{X}}{\partial \sigma^a} \quad , \quad a = 1, 2 \tag{4.2}$$

and the metric tensor induced by the embedding $\mathbf{X}$ is defined as

$$g_{ab} = \partial_a \mathbf{X} \cdot \partial_b \mathbf{X} \quad . \tag{4.3}$$

The covariant derivative on the surface acts on a tangent vector $\mathbf{t}_b = \partial_b \mathbf{X}$ as

$$D_a \partial_b \mathbf{X} = \partial_a \partial_b \mathbf{X} - \Gamma^c_{ab} \partial_c \mathbf{X} \quad , \tag{4.4}$$

where the Christoffel symbols (connection coefficients) are

$$\Gamma^c_{ab} = \frac{1}{2} g^{cj} (\partial_a g_{bj} + \partial_b g_{aj} - \partial_j g_{ab}) \quad . \tag{4.5}$$

At every point on the surface we can define a unit normal vector

$$\mathbf{N} = \frac{\mathbf{t}_1 \times \mathbf{t}_2}{||\mathbf{t}_1 \times \mathbf{t}_2||} \quad . \tag{4.6}$$

The surface can bend in the 3–dimensional 'ambient' space. The extrinsic curvature tensor K_{ab} measures the rate of change $\partial_a \mathbf{t}_b = \partial_a \partial_b \mathbf{X}$ of the tangent vectors with respect to the ambient space projected on the normal to the surface. The vector $\partial_a \partial_b \mathbf{X}$ can be decomposed in components tangent and normal to the surface:

$$\partial_a \partial_b \mathbf{X} = \Gamma^c_{ab} \partial_c \mathbf{X} + K_{ab} \mathbf{N} \quad . \tag{4.7}$$

where Γ^c_{ab} are the Christoffel symbols of the curved surface. Since the covariant derivative on the vector $\partial_b \mathbf{X}$ is given by (4.4), we can write

$$K_{ab} \mathbf{N} = D_a \partial_b \mathbf{X} \quad . \tag{4.8}$$

Sometimes it is convenient to absorb the normal vector $\mathbf{N}$ in the definition of K_{ab}, and write the extrinsic curvature tensor as a vector in 3–dimensions

$$K^\mu_{ab} \equiv D_a \partial_b X^\mu \quad . \tag{4.9}$$

The trace of (4.9) with respect to the surface's metric gives a 3–dimensional vector called the mean curvature vector:

$$H^\mu \equiv \frac{1}{2}\, g^{ab} K^\mu_{ab} = \frac{1}{2} K^{a\mu}_a \quad . \tag{4.10}$$

4.1.1 Fluctuating membranes as statistical ensembles

The geometric description described in the previous section is valid only averaging over a macroscopic number of molecules up to a certain scale $\ell_g \gg a$, where $a \sim 10^{-10}m$ is the typical size of a molecule. Even at this length scale, the extreme flexibility of the membrane requires that it be treated as a statistical ensemble. It is therefore of primary importance to define what are the constraints on the ensemble and what macroscopic variables are free to fluctuate. Suppose N is the number of molecules making the membrane. If a_m is the effective area occupied by a single lipid molecule, and the membrane is incompressible, then the total area is simply

$$A = Na_m \quad . \tag{4.11}$$

The thermodynamic variable γ conjugate to A is called the surface (interfacial) tension.

The irregularity of the configurations means one must distinguish the total intrinsic area A of the membrane from its projected area A_p. This quantity is best defined if we imagine taking a square membrane and attaching its edges to a rigid frame [17]. As the name suggests, A_p is the projection of a configuration in the plane of the rigid frame. The ratio of projected area and the intrinsic area is a measure of the roughess of the surface. The limit $A_p/A \to 1$ corresponds to a planar undistorted phase, while $A_p/A \to 0$ signals a highly corrugated 'crumpled' surface. If the frame is rigid, the projected area is kept fixed (and is equal to the area enclosed by the frame). The variable τ conjugate to the projected area is called the film tension.

We can define four different statistical ensembles depending on what variable we keep fixed [17].

1) If (A, A_p) are held fixed, the system is isolated (no exchange of molecules with the environment) and is anchored to a rigid frame.

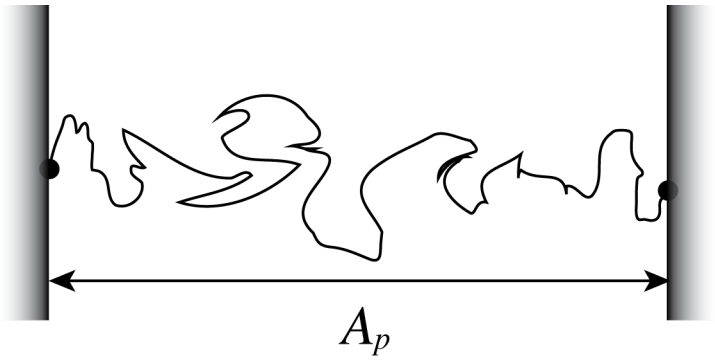

Figure 4.2: A one-dimensional version of a membrane anchored to a rigid frame. The projected area is fixed by the dimensions of the frame. Here is shown the case where the intrinsic area (measured along the contour) is larger than the frame width.

2) If (γ, A_p) are fixed, the system is framed and open: the total area can fluctuate. This can be done by coupling the system to a reservoir of molecules.

3) If (A, τ) are fixed, the system is closed and unframed: the projected area is not constrained.

4) If (γ, τ) are fixed, the system is open and unframed. Both intrinsic area and projected area are unconstrained.

We will start from the framed, open ensemble (γ, A_p). At the scale ℓ_g where the geometric description (4.2) is valid, area fluctuations are governed by the effective Hamiltonian

$$H[\mathbf{X}] = \gamma A + H_c \quad , \tag{4.12}$$

where the first term is proportional to the total area of the membrane

$$A = \int_\Sigma d^2\sigma \, \sqrt{g} \quad , \tag{4.13}$$

and γ is the surface tension. The second term in (4.12) is a curvature Hamiltonian H_c. The term H_c in (4.12) is an effective Hamiltonian that depends on the membrane's

shape $\mathbf{X}$. Since it arises from a first level of coarse-graining, it is constructed from a Landau-type low-gradient expansion in $\partial_a \mathbf{X}$. It must be invariant under translations and rotations in $\mathbb{R}^3$ and under reparametrizations of the internal coordinates[1]. We further require the energy density to be local, thus neglecting self-avoidance. The most general Hamiltonian that meets these criteria is a function of the mean curvature H^μ and the Gaussian curvature $K_{\rm G}$

$$H_{\rm c}[\mathbf{X}] = \frac{\kappa}{2}\int_\Sigma H^2\, dA + \kappa_{\rm G}\int_\Sigma K_{\rm G}\, dA \quad , \tag{4.14}$$

where $H^2 = H^\mu H\mu$ and the area element is $dA = d^2\sigma\sqrt{g}$. The mean and Gaussian curvatures are given by

$$H \equiv \frac{1}{2}\left(\frac{1}{R_1}+\frac{1}{R_2}\right) \quad K_G \equiv \frac{1}{R_1 R_2} \tag{4.15}$$

where R_1, R_2 are the principal radii of curvature of the surface at the point $\boldsymbol{\sigma}$. The parameter κ is called the bending modulus (or rigidity) and $\kappa_{\rm G}$ is called the Gaussian rigidity. The bending rigidity κ controls shape fluctuations. A typical value of the bending rigidity for phospholipid membranes is $\kappa \sim 10^{-19} J$ [96], which must be compared to the thermal energy $k_B T_{\rm r} \sim 4\times 10^{-21} J$ at room temperature $T_{\rm r} = 300K$. Since the bending energy is only two orders of magnitude larger than $k_B T_{\rm r}$, surface deformations (called thermal undulations) strongly affect the thermodynamic behavior of the membrane. A direct consequence of thermal undulations is the reduction of the ratio A_p/A of projected area relative to intrinsic area (see Fig. 4.2). If the membrane is asymmetric, a spontaneous curvature term H_0 should be added to the energy (4.14) by replacing H with $H - H_0$. In the following we will assume that there is no spontaneous curvature. The symmetric model with $H_0 = 0$ was first proposed

[1] In particular, it cannot depend on terms of the form $g_{ab} - \bar{g}_{ab}$, where $\bar{g}_{ab}$ is some reference metric. These terms would assign an energetic cost to deviations δg_{ab} from $\bar{g}_{ab}$ therefore selecting a preferred molecular arrangement in the membrane.

by S. Germain in 1810 [38] and later by Helfrich and Canham [11, 45].

The partition function of the ensemble is a sum over the configurations $\mathbf{X}$ of the membrane. Each configuration at fixed genus h is weighted according to the Gibbs distribution with a probability

$$p[\mathbf{X}] = Z^{-1} \exp\left(-\frac{H[\mathbf{X}]}{k_{\mathrm{B}}T}\right) \quad , \tag{4.16}$$

where $H[\mathbf{X}]$ is given by (4.12) and $k_{\mathrm{B}} = 1.38 \times 10^{-23} JK^{-1}$ is the Boltzmann constant. Z is the partition function. We will consider an ensemble of closed orientable surfaces, which are completely classified in terms of the genus h. Using this fact, we can organize the partition function Z as a functional integral over the shapes at fixed genus $\mathbf{X}_h$, followed by a sum over genera h:

$$Z(\gamma, A_p) = \sum_{h=0}^{\infty} \int \mathscr{D}\mathbf{X}_h \, \exp(-\beta H) \quad , \quad \beta \equiv \frac{1}{k_{\mathrm{B}}T} \quad . \tag{4.17}$$

The free energy of the ensemble is

$$G(\gamma, A_p) = -k_{\mathrm{B}}T \log Z(\gamma, A_p) \quad . \tag{4.18}$$

The thermodynamic potential for an isolated, framed system (A, A_p) is given by the Legendre transform of (4.18):

$$F_{i,f}(A, A_p) = G(\gamma, A_p) - \gamma A \quad . \tag{4.19}$$

By a second Legendre transform, we find the thermodynamic potential for an isolated, unframed system

$$F_{i,u}(A, \tau) = F_{i,f}(A, A_p) - \tau A_p \quad . \tag{4.20}$$

Since $F_{i,u}(A, \tau)$ doesn't depend on A_p, we can take the derivative of (4.20) and find

that the film tension τ is given by:

$$\tau = \left.\frac{\partial F_{i,f}(A, A_p)}{\partial A_p}\right|_A \quad . \tag{4.21}$$

Following [17] we define the area ratio and the free energy density

$$a_p = \frac{A_p}{A} \quad , \quad f = \frac{F_{i,f}}{A} \quad . \tag{4.22}$$

The equilibrium value $\langle a_p \rangle$ of the projected area minimizes the free energy density f. There are three possible behaviors of the free energy f, represented schematically in Fig. 4.3. In case (A) f has a minimum for a non zero value of $\langle a_p \rangle$. At the equilibrium value of the projected area, the film tension (4.21) vanishes and the membrane is an extended 2–dimensional object. In case (B) the free energy has its minimum at $\langle a_p \rangle = 0$ then the membrane is crumpled: its area does not scale with the square of its lateral size. In this case, the film tension is the slope of f at the origin. In general, the slope is not zero (Fig. 4.3 B(i)), so the membrane has a finite surface tension. *Free* liquid membranes are crumpled at all temperatures [81, 88] so in general they have a non zero film tension. If we add interactions however, for example introducing a surfactant in an oil-water mixture or a self-avoiding potential, the projected area can be forced to have $\langle a_p \rangle \neq 0$ as in (A) so its film tension vanishes.

Shape fluctuations in fluid membranes renormalize the bare values of the bending modulus κ and of the surface tension γ. In 1985 Peliti and Leibler [88] computed the renormalized bending rigidity and surface tension under the assumption that the average membrane configuration is planar and that the initial value of the surface tension is small. F. David generalized these results for fluctuations around a non-planar state [17]. We report here the argument used in [17] that showed that in special cases the surface tension γ can be renormalized to zero by thermal fluctuations.

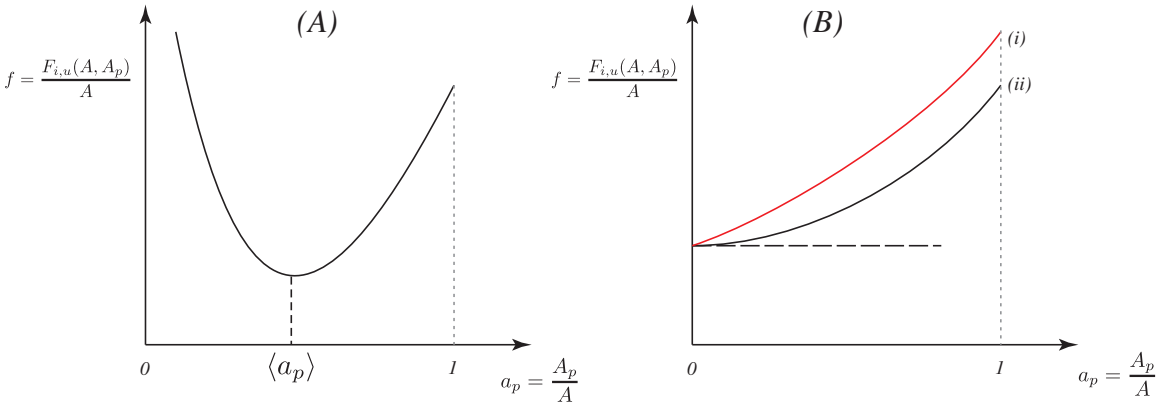

Figure 4.3: Schematic free energy density of a closed, framed membrane ensemble as function of the projected-intrinsic area ratio $a_p = A_p/A$. (A) The equilibrium value $\langle a_p \rangle$ is non-zero and the film tension τ vanishes. (B) f is minimum at $\langle a_p \rangle = 0$. Free fluid membranes are always crumpled and behave as (i). The film tension can vanish in the marginal case (ii).

Starting from a bare Hamiltonian

$$H_0 = \int dA \left(\gamma_0 + \frac{\kappa_0}{2} H^2 + \kappa_{\rm G0} K_G \right) \tag{4.23}$$

one can integrate out all the shape fluctuations with momenta contained in a shell of width

$$q \equiv \frac{\Lambda}{s} < |\mathbf{k}| < \Lambda \quad , \tag{4.24}$$

where Λ is the inverse of the geometric scale $\Lambda \sim \frac{1}{\ell_g}$ and the scale parameter $s > 1$. After rescaling the distances $\mathbf{X} \to s\mathbf{X}$ and momenta $|\mathbf{k}| \to |\mathbf{k}|/s$, the renormalized effective Hamiltonian can be expanded in powers of the extrinsic and Gaussian curvature

$$H_s = \int dA \left(\gamma(s) + \frac{\kappa(s)}{2} H^2 + \kappa_{\rm G}(s) K_G + ... \right) \quad , \tag{4.25}$$

where $\gamma(s)$, $\kappa(s)$, $\kappa_G(s)$ are the scale-dependent surface tension, bending modulus and Gaussian rigidity. They satisfy the renormalization group equations (valid at one

loop order)

$$\frac{\partial\kappa(s)}{\partial\log s} = -\frac{3k_BT}{4\pi}\left(1+\frac{\gamma(s)}{\Lambda^2\kappa(s)}\right)^{-1} \tag{4.26}$$

$$\frac{\partial\gamma(s)}{\partial\log s} = 2\gamma(s) + \frac{k_BT\Lambda^2}{4\pi}\log\left(1+\frac{\gamma(s)}{\Lambda^2\kappa(s)}\right) \tag{4.27}$$

$$\frac{\partial\bar{\kappa}(s)}{\partial\log s} = \frac{5}{3k_BT}\left(1+\frac{\gamma(s)}{\Lambda^2\kappa(s)}\right)^{-1} \quad . \tag{4.28}$$

We refer the reader to the review [87] and [17] for the derivation. The second equation allows the solution with vanishing surface tension $\gamma = 0$. Then the bending rigidity satisfies the equation

$$\frac{\partial\kappa(s)}{\partial\log s} = -\frac{3k_BT}{4\pi} \qquad (\gamma = 0) \quad . \tag{4.29}$$

Integrating (4.29) between $s = 1$ and s the result is [17, 86, 88]

$$\kappa(s) = \kappa_0 - \frac{3k_BT}{4\pi}\log s \quad , \tag{4.30}$$

where κ_0 is the microscopic (bare) bending rigidity. We now use the fact that $s = \Lambda/q$, where q is a momentum smaller than Λ. Identifying the highest momentum with the inverse of the cutoff scale ℓ_g and the lowest momentum with the inverse of some macroscopic length scale L, we can write the renormalized bending modulus measured at the scale L as

$$\kappa(L) = \kappa_0 - \frac{3k_BT}{4\pi}\log\left(\frac{L}{a}\right) \qquad \text{and } \gamma = 0 \quad . \tag{4.31}$$

where a is the microscopic cutoff. This means that thermal shape fluctutations lower the bending rigidity of fluid membranes at zero surface tension. The thermally induced softening of the bending rigidity suggests that these tensionless membranes can undergo violent shape fluctuations. Local protrusions can coalesce into handles and change in the topology of the membrane. In the next section we briefly describe

microemulsions as physical realizations of tensionless membranes.

From (4.31) we can find the persistence length of the membrane. This is defined as the length scale ξ_p at which the renormalized bending rigidity $\kappa(\xi_p)$ is of the order of k_BT. Using $\kappa(\xi_p) \simeq k_BT$ we can rewrite (4.31) as

$$\kappa_0 - k_BT \simeq \frac{3k_BT}{4\pi} \log \frac{\xi_p}{a} \quad . \tag{4.32}$$

At the molecular length scale, we take the bare bending rigidity to be much larger than the thermal energy, and we neglect k_BT on the left hand side of (4.32). Then, we find that the persistence length

$$\xi_p \simeq a \exp\left(\frac{4\pi\kappa_0}{3k_BT}\right) \quad . \tag{4.33}$$

At this scale, the membrane's shape is highly corrugated due to thermal fluctutations, and the correlation between the normals $\mathbf{N}$ to the surface decays exponentially. We notice that at low temperatures, the persistence length becomes large, and diverges at $T = 0$, where it becomes an extended 2–dimensional object [81, 82].

4.1.2 Microemulsions and vanishing surface tension

The result (4.26) indicates that if one starts with a small but non vanishing value of the surface tension, the area term in the renormalized Hamiltonian will dominate over the curvature terms at large length scales [16, 87]. This is confirmed by dimensional analysis. Consider the Hamiltonian (4.23) divided by k_BT, and define the reduced parameters

$$\widetilde{\gamma}_0 \equiv \frac{\gamma_0}{k_BT} \qquad \widetilde{\kappa}_0 \equiv \frac{\kappa_0}{k_BT} \tag{4.34}$$

The area A has dimension $[A] = L^2$. By dimensional analysis, the surface tension conjugate to the area in the expansion (4.23) has dimension L^{-2} and it is strongly

relevant [16]. From (4.15), the mean curvature has units of inverse length. Thus, since $[dA] = L^2$, the integral of $H^2 dA$ is dimensionless. The bending rigidity has dimension zero and therefore it is marginal. This means that unless the surface tension is fine tuned to zero, the long-wavelength theory will contain only the area term.

There are physical systems where the renormalized surface tension is zero. This is the case of microemulsions. A microemulsion is obtained by stabilizing a mixture of oil and water with a surfactant [19]. The surfactants are molecules composed by a polar head that is soluble in water and an hydrophobic tail that is soluble in oil. The presence of the surfactants at the interface between oil and water decreases the interfacial surface tension γ.

In most cases, the surface tension cannot be decreased indefinitely by adding surfactants. This happens because beyond certain bulk limiting concentration, the surfactants don't localize at interfaces but form bulk micellar phases (a micelle is a spheroidal aggregate of surfactants where polar heads are at the surface and the tails are in the interior).

By using some special surfactants however it is possible to decrease the surface tension to zero. The difference from the first case is that the surfactants enter the bulk phase without forming micellar structures. This phase is called microemulsion. The microemulsion phase (sometimes called sponge phase) tends to increase the interfacial area. Oil and water are mixed in all proportions, with the surfactants residing at the interface between the two liquids. Since in microemulsions the interfacial tension γ vanises, we are in the situation (4.31), and the interface has a low bending rigidity that allows large shape fluctuations. In fact, microemulsion interfaces develop handles and typically have very complex topologies. Fluctuations of the interface are controlled only by the curvature energies (4.14).

4.2 Partition function including arbitrary genus membranes.

We will now consider a statistical ensemble of a membrane with vanishing surface tension and with a fluctuating number of handles. We take as effective Hamiltonian

$$\beta H_{\text{eff}}[\mathbf{X}_h] = \frac{\widetilde{\kappa}}{2}\int_{\Sigma_h} H^2\, dA + \frac{\widetilde{\kappa}_{\text{G}}}{2\pi}\int_{\Sigma_h} K_G\, dA \quad . \tag{4.35}$$

As discussed in section 4.1.1, the Hamiltonian (4.35) arises from a first level of coarse-graining, so the elastic moduli $\widetilde{\kappa}, \widetilde{\kappa}_G$ are the renormalized bending and Gaussian rigidities divided by $k_B T = \beta^{-1}$. The normalization $(2\pi)^{-1}$ in front of $\widetilde{\kappa}_G$ is chosen for later convenience of notation. We consider the regime where the renormalized surface tension vanishes. The fluctuations given by the spectrum of (4.35) can describe, for example, the tensionless interface of microemulsions. For future convenience of notation, we identify

$$W[\mathbf{X}_h] \equiv \int_{\Sigma_h} H^2\, dA \tag{4.36}$$

with the Willmore functional (or Willmore energy) of the embedding $\mathbf{X}_h$. By the Gauss-Bonnet theorem, the second term in expression (4.35) doesn't depend on the embedding $\mathbf{X}$ but only on the genus h. It is a topological invariant proportional to the Euler characteristic $\chi = 2(1-h)$:

$$\int_{\Sigma} K_{\text{G}}\, dA = 2\pi \times 2(1-h) \quad . \tag{4.37}$$

where h is the genus of the surface. The sphere has no handles $h = 0$, the torus has one ($h = 1$) and so on. Using (4.36) and (4.37), the Hamiltonian (4.35) is rewritten as

$$\beta H_{\text{eff}}[\mathbf{X}_h] = \frac{\widetilde{\kappa}}{2} W[\mathbf{X}_h] + 2\widetilde{\kappa}_{\text{G}}(1-h) \quad . \tag{4.38}$$

In the following sections, we will be interested in the value of H_{eff} for the ground states $\mathbf{X}_h^0$. Expression (4.38) for the free energy suggests that H_{eff} becomes increasingly more negative as the genus grows and that we must distinguish two regimes for the Gaussian rigidity. If $\kappa_{\text{G}} > 0$, the model favors the formation of handles, while $\kappa_{\text{G}} < 0$ disfavors the formation of handles. The question is more subtle however, because although it is known that W must be larger than 4π for all genera above 0, a minimizing shape is not known to exist for every genus above 0. The ground state energies $W[\mathbf{X}_h^0]$ might for example increase with h, so to compensate the negative energy $-4\pi h$ associated to the handles.

In order to generate all the topologies in the ensemble, we associate a Gibbs distribution (4.16) to every configuration $\mathbf{X}_h$. We wish to generate only connected surfaces of arbitrary genus because we don't regard disconnected surfaces (for example disjoint spheres) as allowed configurations. For this reason, we calculate a free energy which we denote by $\log Z$ by summing only over connected configurations of the ensemble. The sum over configurations then consists of the integration over embedded shapes at fixed genus $\mathscr{D}\mathbf{X}_h$ and then a sum over all genera $h \geq 0$:

$$\log Z \equiv \sum_{h=0}^{\infty} \int \mathscr{D}\mathbf{X}_h \, \exp(-\beta F[\mathbf{X}_h]) \quad \text{with } \mathbf{X}_h \text{ connected}, \tag{4.39}$$

where H_{eff} is given by (4.38). The first few terms of the sum contain surfaces with the topology of the 2–sphere ($h = 0$) the torus ($h = 1$) and so on. We can make a formal analogy between these surfaces and the diagrams of closed oriented interacting bosonic strings. A membrane configuration of genus h is represented by a string diagram with h loops. By adding a source term $-\int \mathbf{J} \cdot \mathbf{X}_h$ to F, the function $\log Z[J]$ is the generating function of connected diagrams (each diagram is a membrane con-

figuration). Substituting (4.38) in (4.39) we obtain

$$\log Z = \sum_{h=0}^{\infty} \int \mathscr{D}\mathbf{X}_h \, e^{-\frac{\tilde{\kappa}}{2} W[\mathbf{X}_h]} \, e^{-2\tilde{\kappa}_{\mathrm{G}}(1-h)} \tag{4.40}$$

$$= e^{-2\tilde{\kappa}_{\mathrm{G}}} \sum_{h=0}^{\infty} e^{2\tilde{\kappa}_{\mathrm{G}} h} \int \mathscr{D}\mathbf{X}_h \, e^{-\frac{\tilde{\kappa}}{2} W[\mathbf{X}_h]} \quad . \tag{4.41}$$

In the second line the genus-dependent factor $e^{2\tilde{\kappa}_{\mathrm{G}} h}$ is independent of the geometry of the configuration and can be extracted from the integral $\int \mathscr{D}\mathbf{X}_h$. The overall factor $e^{-2\tilde{\kappa}_{\mathrm{G}}}$ can be absorbed in the normalization of $\log Z$ and is not physically relevant.

Since the genus increases by discrete units, we can interpret the Gaussian rigidity in (4.41) as a chemical potential for the formation of one handle. The factor $e^{2\tilde{\kappa}_{\mathrm{G}} h}$ plays the same role as the fugacity in a thermodynamical system with a fluctuating number of particles. For every handle, there are two factors of $e^{\tilde{\kappa}_{\mathrm{G}}}$. The total energy of the handle, of course, depends on its geometry via $W[\mathbf{X}_h]$ but, independently of the handle's shape, the addition of a handle on a surface of genus h always requires cutting two disks from the surface and connecting them with a tube. The limiting case of an infinitesimal handle is a string that connects to the surface at two points. We can associate to each disk or point a factor of $e^{\tilde{\kappa}_{\mathrm{G}}}$ that is analogous to a coupling constant g for the interaction of a tube emitted and reabsorbed from the surface

$$g \equiv e^{\tilde{\kappa}_{\mathrm{G}}} \quad . \tag{4.42}$$

Using the notation (4.42), the free energy (4.41) may be written in the final form

$$\log Z = \sum_{h=0}^{\infty} g^{2h} \int \mathscr{D}\mathbf{X}_h \, e^{-\frac{\tilde{\kappa}}{2} W[\mathbf{X}_h]} \quad . \tag{4.43}$$

We must specify the meaning of the functional measure $\mathscr{D}\mathbf{X}_h$ in (4.43). Distinct configurations of the membrane correspond to distinct shapes. An unrestricted sum

over all possible embeddings would over-count some configurations. Global rotations, translations and scale transformations of a given shape should not be counted as new states. The measure should also be invariant under reparametrizations of the internal coordinates. Two embeddings $\mathbf{X}$ and $\mathbf{X}'$ describe the same state if they differ only by a displacement of the fluid particles in the tangent plane of the surface:

$$\mathbf{X}' = \mathbf{X} + V^a \mathbf{t}_a \quad a = 1, 2 \tag{4.44}$$

where $\mathbf{t}_a$ are tangent vectors on the surface $\mathbf{t}_a = \partial_a \mathbf{X}$. An infinitesimal change in the internal coordinates

$$\sigma^a \to \sigma'^a = \sigma^a + \epsilon^a(\boldsymbol{\sigma}) \tag{4.45}$$

generates the relation (4.44) between the embeddings. In fact, the vector $\mathbf{X}$ transforms as

$$\mathbf{X}'(\boldsymbol{\sigma}) = \mathbf{X}(\boldsymbol{\sigma}) + \epsilon^a \frac{\partial \mathbf{X}(\boldsymbol{\sigma})}{\partial \sigma^a} \quad a = 1, 2 \tag{4.46}$$

A genuine change of shape from a given state is therefore induced by deformations normal to the surface. The invariance of the measure under local diffeomorphisms requires adding a Fadeeev-Popov determinant. The constraint that projects a generic embedding onto the class of normal deformations is [81]

$$\epsilon^a \frac{\partial \mathbf{X}(\boldsymbol{\sigma})}{\partial \sigma^a} = 0 \quad . \tag{4.47}$$

4.3 Fluid membranes and the Willmore functional

The integral of H^2 over a surface Σ_h of genus h appearing in (4.35) is a functional of the surface's embedding $\mathbf{X}_h$, and it is known in mathematics under the name of Willmore functional [72]:

$$W[\Sigma_h] = \int_{\Sigma_h} H^2 dA \quad , \tag{4.48}$$

where dA is the area form of Σ. Being the integral of a positive quantity, the value of the Willmore energy is non-negative. Stationary solutions of (4.48) are called Willmore surfaces and satisfy the Euler-Lagrange equations $\delta_{\mathbf{X}} W = 0$:

$$\Delta H + 2H(H^2 - K_G) = 0 \quad . \tag{4.49}$$

Appendix C gives a detailed derivation of equation (4.49). Note that there is an equation of the form (4.49) for every value of the genus h. For $h = 0$, we can check that the round 2–sphere of radius R defined by the equation

$$|\mathbf{X}(\sigma^1, \sigma^2)|^2 \equiv X^2 + Y^2 + Z^2 = R^2 \tag{4.50}$$

solves (4.49). In fact the mean and Gaussian curvatures of the sphere are constant and equal to $H = R^{-1}$ and $K_G = R^{-2}$. Therefore the Laplacian ΔH and $H^2 - K_G$ are both zero. We can also compute the Willmore energy of the round 2–sphere. Since the area element of the round 2–sphere in polar coordinates is $dA = R^2 d\phi d\cos\theta$, its Willmore energy is

$$W[S^2] = \int_0^{2\pi} d\phi \int_{-1}^{1} d\cos\theta \, R^2 \left(\frac{1}{R}\right)^2 = 4\pi \quad . \tag{4.51}$$

Willmore proved that 4π is the smallest value that the Willmore energy can attain among shapes of genus 0, thus showing that the 2–sphere minimizes W. The physical consequence is that the 2–sphere is the unique ground state (up to uniform scaling of the sphere's radius) of closed tensionless fluid membranes.

More solutions to (4.49) are given by surfaces whose mean curvature vanishes at every point:

$$H(\boldsymbol{\sigma}) = 0 \quad . \tag{4.52}$$

These surfaces most commonly appear as minimizers of the *Area* functional $\int_\Sigma dA$.

They are encountered for example in the physics of soap films. Surface tension controls the shape of soap films anchored to a fixed wire frame. The energy of the soap film is proportional to its area, and the equilibrium shape is given by equation (4.52). Surfaces that satisfy (4.52) are called minimal surfaces. The variational problem $\delta A = 0$ is briefly discussed in Appendix B. The stationary points of the Willmore functional provide a different way in which minimal surfaces appear.

The Willmore functional has many beautiful mathematical properties. Most importantly, it is invariant under conformal transformations of the space in which the surface is embedded. A proof of this fact is provided in section C. If $G_{\mu\nu}$ is the metric of the embedding space, a conformal transformation $\mathbf{X} \to \mathbf{X}'(\mathbf{X})$ leaves the metric $G_{\mu\nu}$ invariant up to a local scale factor

$$G'_{\mu\nu}(\mathbf{X}') = f(\mathbf{X}) G_{\mu\nu}(\mathbf{X}) \quad . \tag{4.53}$$

The conformal symmetry of (4.48) implies that given a fixed ground state shape $\mathbf{X}^0_h$, all its images under conformal transformations of $\mathbb{R}^3$ are also ground states. In other words, the ground state manifold of (4.35) is degenerate.

4.4 Bounds on the Willmore functional

In order to study the statistics of handle formation using (4.43) it is important to know the properties of the ground states, i.e. the shapes that minimize the Willmore functional (4.48). Determining the minimizers of W for all genera is a difficult open problem in mathematics. In the absence of known minimizing shapes, it is very useful to estimate genus-dependent lower bounds on the value of W. This program was started by Willmore [104] in 1965 and only recently completed by Marques and Neves (2012) [72].

In 1965 Willmore [104] proved that the energy (4.48) of all closed surfaces of genus

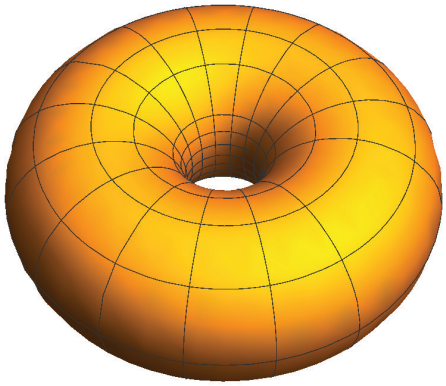

Figure 4.4: The Clifford Torus projected in $\mathbb{R}^3$.

0 must be greater than or equal to 4π [2]. A proof is given in Appendix D. From (4.51) we already know that the Willmore energy of the round 2–sphere (4.50) is 4π and therefore it saturates the bound. Willmore's conclusion was that for genus zero

$$W[\mathbf{X}_{h=0}] \geq 4\pi \quad ; \quad \text{equality holds for round 2–spheres.} \tag{4.54}$$

The next class of closed surfaces has genus 1 i.e. embedded tori. In the case of genus zero, the round 2–sphere is a natural candidate for the minimizer, thanks to its high symmetry, but it is harder to guess what class of toric surfaces have the lowest energy. Willmore started by considering a special class of tori of revolution, which are tubes of radius r whose central axis is bent to form a circle of radius R. Minimizing W over this class, Willmore found the optimal ratio $r/R = 1/\sqrt{2}$. The parametrization of this surface is

$$\Sigma_{\sqrt{2}} = \left((\sqrt{2} + \cos\theta)\cos\phi, (\sqrt{2} + \cos\theta)\sin\phi, \cos\theta\right) \quad . \tag{4.55}$$

Its Willmore energy has the value $W[\Sigma_{\sqrt{2}}] = 2\pi^2 > 4\pi$. The torus (4.55) is special,

[2] In other words 4π is the infimum of the Willmore energy among genus-0 surfaces.

because it is the stereographic projection into $\mathbb{R}^3$ of the Clifford torus[3]. Willmore's conjecture [104] states that the surface $\Sigma_{\sqrt{2}}$ is the minimizer of W among *all* closed surfaces of genus 1. In 2012, Marques and Neves [73] showed that this lower bound holds for any surface of positive genus:

$$W[\mathbf{X}_h] \geq 2\pi^2 \quad , \text{ for all } h \geq 1 \tag{4.56}$$

and equality holds only for stereographic projections of the Clifford torus.

4.5 Bounds on the partition function

We will now study the properties of the generating function of connected diagrams (4.43) using the bounds (4.54) and (4.56) on the Willmore energy. First, we separate the term $h = 0$ from $h \geq 1$ in the generating function of connected diagrams (4.43)

$$\log Z = \int \mathscr{D}\mathbf{X}_0 \, e^{-\frac{\widetilde{\kappa}}{2} W[\mathbf{X}_0]} + \sum_{h=1}^{\infty} g^{2h} \int \mathscr{D}\mathbf{X}_h \, e^{-\frac{\widetilde{\kappa}}{2} W[\mathbf{X}_h]} \quad . \tag{4.57}$$

The first term integrates over all possible shapes of spherical topology. In view of the inequalities (4.54) and (4.56), the statistical weight of all genus 0 configurations is smaller than

$$e^{-\frac{\widetilde{\kappa}}{2} W[\mathbf{X}_0]} \leq e^{-2\pi\widetilde{\kappa}} \tag{4.58}$$

For all surfaces of genus $h \geq 1$, the Boltzmann factor is bounded above by

$$e^{-\frac{\widetilde{\kappa}}{2} W[\mathbf{X}_h]} \leq e^{-\pi^2\widetilde{\kappa}} \quad \text{for all } h \geq 1 \quad . \tag{4.59}$$

[3]The Clifford torus is the cartesian product $S^1(1/\sqrt{2}) \times S^1(1/\sqrt{2})$ of 2 circles of radii $1/\sqrt{2}$. Its parametrization in 4–dimensional Euclidean space is $1/\sqrt{2}(\cos\theta, \sin\theta, \cos\phi, \sin\phi)$ with $\theta, \phi \in [0, 2\pi]$.

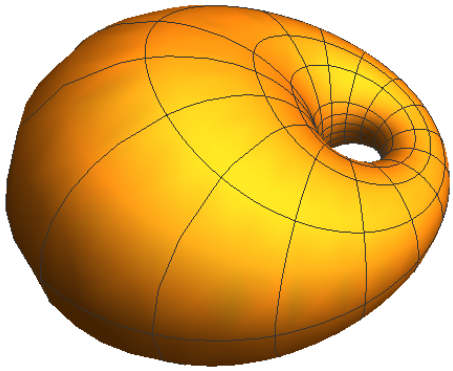

Figure 4.5: Deformation of the Clifford Torus (projected in $\mathbb{R}^3$) under the transformation (4.67) on (4.62). The transformation breaks the azimuthal symmetry of the Cifford torus.

Using (4.58) and (4.59) in (4.57) we find that $\log Z$ satisfies the following (formal) inequality:

$$\log Z \leq e^{-2\pi\widetilde{\kappa}} \int \mathscr{D}\mathbf{X}_0 + \sum_{h=1}^{\infty} g^{2h} e^{-\pi^2\widetilde{\kappa}} \int \mathscr{D}\mathbf{X}_h \quad . \tag{4.60}$$

On the right hand side of (4.60) we are left with the volume of integration over the space of shapes. These integrals are degeneracy factors that count the number of states with the same energy at every fixed genus. In the limit of low temperature, the ground states dominate the sums over configurations. The ground state shapes are Willmore surfaces. If we fix the most symmetric ground state as a reference state at each genus, all shapes obtained via conformal transformations of the reference state have the same energy. The parameters of the conformal transformations define a space of shapes. The volume of this space counts the degeneracy. It is necessary to establish whether this volume is finite (in which case (4.60) provides a genuine upper bound) or is infinite. Conformal transformations contain translations, rotations and scale transformations. The parameter λ of a scale tranformation, for example, ranges from 0 to ∞. This means that the direction λ gives an infinite degeneracy factor. Luckily, the integration in (4.60) runs over distinct shapes. Since scale transformations, rotations and translations don't change the shape of a surface, we disregard them. Then, we are

left only with special conformal transformations (SCT), which act on the embedding as

$$\mathbf{X} \to \mathbf{X}' = \frac{\mathbf{X}/X^2 - \mathbf{a}}{|\mathbf{X}/X^2 - \mathbf{a}|^2} \quad . \tag{4.61}$$

A SCT transforms spheres into spheres without deforming their shape. So at genus $h = 0$, the degeneracy factor is finite and equal to 1. At genus $h = 1$, we take as the reference ground state the surface $\Sigma_{\sqrt{2}}$ given by (4.55) and apply a SCT to it. This case was considered by Fourcade in [31] (see [51] for a review). The predictions of [31] were tested experimentally in [32]. The state $\Sigma_{\sqrt{2}}$ is azimuthally symmetric. SCTs breaks the azimuthal symmetry of $\Sigma_{\sqrt{2}}$ by moving the hole of the torus off-axis. The parametrization of the torus is most conveniently written in 4–dimensional Eucliden space as

$$x_1 = \sin\theta \sin\psi \tag{4.62}$$

$$x_2 = \cos\theta \sin\psi \tag{4.63}$$

$$x_3 = \cos\phi \cos\psi \tag{4.64}$$

$$x_4 = \sin\phi \cos\psi \tag{4.65}$$

where x_α, $\alpha = 1, 2, 3, 4$ are coordinates in $\mathbb{E}^4$, the angles θ, ϕ range from 0 to 2π and ψ is a fixed parameter. The Clifford torus corresponds to $\psi = \pi/4$. The transformations that deform the torus (4.62) leaving is Willmore energy invariant were found explicitly by Fourcade in [31]. There are two sets of deformations of the torus under SCT. One breaks the symmetry of the circular meridian cross-section:

$$\psi(u, v, \theta) = \frac{\pi}{4} + u \sin\theta + v \cos\theta \quad . \tag{4.66}$$

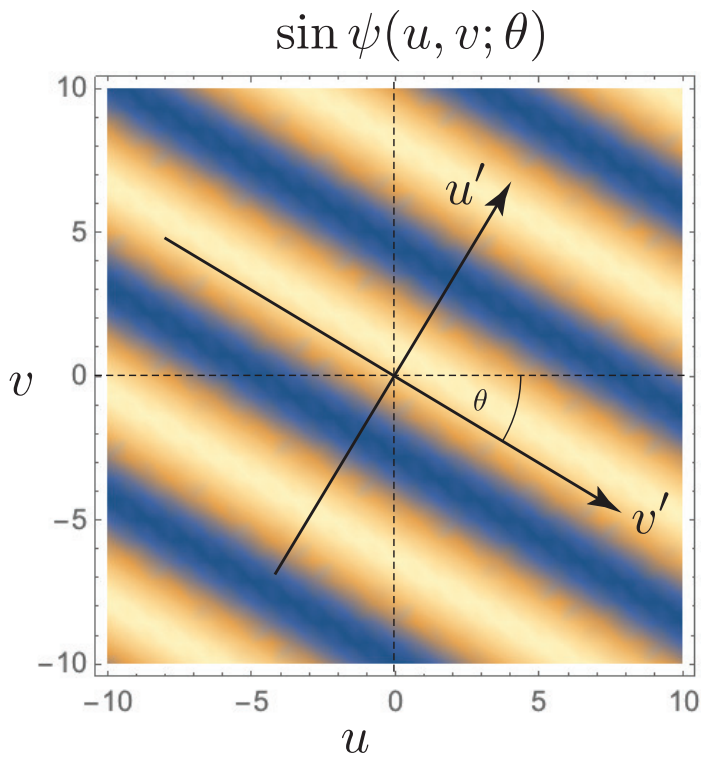

Figure 4.6: Pot of $\psi(u, v, \theta)$ (4.66) at fixed θ (here $\theta = \pi/6$) as function of u, v.

The other breaks azimuthal symmetry. It is obtained from (4.66) substituting θ with ϕ [31]:

$$\chi(w,z,\phi) = \frac{\pi}{4} + w\sin\phi + z\cos\phi \quad . \tag{4.67}$$

We want to study the transformation (4.66) as a function of u, v and prove that it generates a compact space of shapes. We note that the variable ψ enters (4.62) through the periodic functions sine and cosine. Starting from a shape (4.66) at a fixed value of ψ, we can change (u, v) and generate new shapes until $\psi \to \psi + 2\pi$. At this point, we reached again the initial shape. We generate the same shape every time (u, v) satisfy

$$\frac{\pi}{4} + u\sin\theta + v\cos\theta = 2k\pi \quad , \tag{4.68}$$

for all integers k. Equation (4.68) defines a set of straight lines in the (u, v) plane:

$$v(u) = -\tan\theta\, u + \frac{2k}{\sin\theta}\pi - \frac{\pi}{4\sin\theta} \tag{4.69}$$

Plotting ψ as function of u, v we find that it is periodic along stripes oriented by an angle $-\theta$ with the $u-$axis (see Fig. 4.6). As we change θ, the pattern of Fig. 4.6 rigidly rotates in the u, v plane. We can transform the coordinates u, v into a new set of coordinates u', v' such that u' is constant along the stripes and v' changes in the direction perpendicular to the stripes. Since $\psi(u')$ =constant, we conclude that the space of genus-1 ground states is a one-dimensional space parametrized by the compact coordinate v'. The range of v' is given by the period of the striped pattern in Fig. 4.6. Since the period is invariant with respect to θ, we can set $\theta = 0$ in (4.66). Since $\sin\theta$ vanishes at $\theta = 0$, $\psi(u, v, 0) \equiv \psi'(v, 0)$ is a function of v alone. Finally, we recall that ψ enters (4.62) as argument of trigonometric functions. We conclude that the fundamental domain of v' is 2π for every fixed θ. For every v' in $[0, 2\pi]$ we find a deformed torus of Willmore energy $2\pi^2$. The same argument can be applied to the second class of shape deformations (4.67). This suggests that degeneracy

factor at genus 1 is finite. This argument is only suggestive of the finiteness of the degeneracy factor but it can't be the final result. Its definition must be invariant under parametrizations of the space of shapes $\mathscr{S}$.

If similar arguments hold for all higher genus surfaces, and the dependence of the degeneracy factors do not increase too fast with the genus, maybe it is possible to sum the series on the right hand side of (4.60) to a finite number and establish a finite upper bound for the low-temperature limit of $\log Z$. Investigations in this direction are in progress.

A natural way to give an invariant meaning to the continuous degeneracy factor is to view the space of shapes

$$\mathscr{S} = \{\mathbf{X} : \Sigma \longrightarrow \mathbb{R}^3\} \tag{4.70}$$

as a metric space, and then compute its volume. $\mathbf{X}$ is the coordinates of a points in $\mathscr{S}$. The diffeomorphism invariance of a usual manifold needs to be modified in the case of (4.70). Clearly, only reprametrizations $\mathbf{Y} = \mathbf{X} + V^a \mathbf{t}_a$ that don't change the shape are to be considered valid reparametrizations of $\mathscr{S}$. The next step is to build the tangent vectors to $\mathscr{S}$. We notice that the space of degenerate ground states is the orbit of the group of SCT. So the infinitesimal deformation vector between two shapes $\mathbf{X}$ and $\mathbf{X} + \delta\mathbf{X}$ is given by an infinitesimal SCT

$$\delta_{\mathbf{a}}\mathbf{X} = X^2\mathbf{a} - 2\mathbf{X}(\mathbf{a}\cdot\mathbf{X}) \quad , \tag{4.71}$$

where $\mathbf{a}$ parametrizes the SCT and the X^2 is taken with the $\mathbf{R}^3$ norm. A shape is a function $\mathbf{X}(\boldsymbol{\sigma})$ so we further define the norm:

$$||\delta_{\mathbf{a}}\mathbf{X}||^2 = \int \sqrt{g(\boldsymbol{\sigma})}\, d^2\sigma\, \delta_{\mathbf{a}} X^\mu(\boldsymbol{\sigma}) \delta_{\mathbf{a}} X^\mu(\boldsymbol{\sigma}) \quad . \tag{4.72}$$

Note that we interpret the σ^a as components of the infinite dimensional vector $X^\mu(\boldsymbol{\sigma})$ for every fixed μ. To find the volume of $\mathscr{S}$, we need the Riemann-Lebesgue volume element on the normed space $(\mathscr{S}, ||\bullet||)$. This will be the object of future work.

4.6 Measuring the probability of handle formation

At low temperature, the largest contribution to the expansion (4.57) comes from the stationary points of $W[\mathbf{X}_h]$, that is, from the Willmore surfaces. Membranes with fluctuating topologies can be realized making microemulsions. From (4.57), the probability p_0 to find a spherical membrane of energy $W[S^2] = 4\pi$ is given by the Boltzmann weight

$$p_0 = \frac{\exp\left[-\frac{\widetilde{\kappa}}{2}(4\pi)\right]}{\log Z} \quad . \tag{4.73}$$

The probability p_1 to find toroidal membranes is

$$p_1 = \frac{N_1 g^2 \, \exp\left[-\frac{\widetilde{\kappa}}{2}(2\pi^2)\right]}{\log Z} \qquad , \quad g^2 = e^{\widetilde{\kappa}_{\mathrm{G}}} \quad . \tag{4.74}$$

where the factor N_1 is the number of toroidal ground states. Taking the ratio of (4.73) and (4.74) we find

$$\frac{p_1}{p_0} = N_1 g^2 e^{-\frac{\widetilde{\kappa}}{2}(2\pi^2 - 4\pi)} \tag{4.75}$$

and taking the logarithm on both sides

$$\log \frac{p_1}{p_0} = N_1 + 2\log g - \frac{\widetilde{\kappa}}{2}(2\pi^2 - 4\pi) \tag{4.76}$$

where $(2\pi^2 - 4\pi) = E_{\mathrm{handle}}$ is the minimum energy cost to attach a handle to a 2-sphere (if the sphere is deformed, its energy is higher than 4π). Experimental measurements of the relative abundance of toroidal membranes and spherical membranes can determine the left hand side of (4.76). Knowing the reduced bending rigidity $\widetilde{\kappa} = \beta\kappa$ of

the membrane and the factor N_1, equation (4.76) gives an indirect measurement of the parameter g.

Appendix A

Euler-Lagrange equations of the Willmore functional

In this appendix we derive the equations (4.49) satisfied by a stationary shape of the Willmore functional. The variational problem $\delta W[\mathbf{X}]$ with respect to a deformation $\delta\mathbf{X}$ is complicated by the non linear dependence of the quantities g_{ab}, K^{μ}_{ab} on the embedding $\mathbf{X}$. The treatment is greatly simplified by introducing Lagrange multipliers that enforce the definitions of tangent vectors, normal vector, metric and extrinsic curvature tensor. Then, following Capovilla and Guven [42] we can vary all the quantities independently, determine all the Lagrange multipliers and find the Euler-Lagrange equations. The new variational problem is

$$\begin{aligned} E_{CG}[\mathbf{X}, \mathbf{e}_a, \mathbf{N}, g_{ab}, K_{ab}; \mathbf{f}^a, \lambda^a, \lambda_N, \lambda^{ab}, \Lambda^{ab}] &= \frac{\kappa}{8}\int d^2\sigma\,\sqrt{g}\,(g^{ab}K^{\mu}_{ab})^2 \\ &+ \int d^2\sigma\,\sqrt{g}\,[\mathbf{f}^a\cdot(\mathbf{e}_a - \partial_a\mathbf{X}) + \lambda^a(\mathbf{e}_a\cdot\mathbf{N}) + \lambda_N(\mathbf{N}^2-1)] \\ &+ \int d^2\sigma\,\sqrt{g}\,[\lambda^{ab}(g_{ab} - \mathbf{e}_a\cdot\mathbf{e}_b) + \Lambda^{ab}(K_{ab} - \mathbf{e}_a\cdot\partial_b\mathbf{N})] \quad . \end{aligned} \tag{A.1}$$

All the quantities appearing in (A.1) can be varied independently. In particular, g_{ab} and K_{ab} depend on $\mathbf{e}_a$ and $\mathbf{N}$, but not on $\mathbf{X}$ explicitly. Note that $\mathbf{e}_a$ and $\mathbf{N}$ are collections of 6 scalar fields, so they are differentiated with the ordinary partial derivative rather than the covariant derivative. The only term that depends on the embedding is the constraint that forces the vectors $\mathbf{e}_a$ to be tangent vectors to the surface $\mathbf{X}$. So the variation of E_{CG} under a deformation of the embedding is simply

$$\delta_{\mathbf{X}} E_{CG} = -\int d^2\sigma \sqrt{g}\, \mathbf{f}^a \partial_a \delta\mathbf{X} = -\int d^2\sigma \sqrt{g}\, [D_a(\mathbf{f}^a \cdot \mathbf{X}) - (D_a \mathbf{f}^a) \cdot \delta\mathbf{X}] \tag{A.2}$$

Using the divergence theorem, the total divergence term is evaluated at the boundary of the surface. Since we are interested in surfaces with no boundaries, all the boundary integrals arising from the application of the divergence theorem will vanish identically. We are left with

$$\delta_{\mathbf{X}} E_{CG} = \int d^2\sigma \sqrt{g}\, (D_a \mathbf{f}^a) \cdot \delta\mathbf{X} \tag{A.3}$$

At the stationary points the variation vanishes ($\delta_{\mathbf{X}} E_{CG} = 0$), which implies that the vector $\mathbf{f}^a$ is covariantly conserved in the bulk:

$$D_a \mathbf{f}^a = 0 \quad . \tag{A.4}$$

Next, we require stationarity of E_{CG} with respect to $\mathbf{e}_a$, which gives $\mathbf{f}^a$ in terms of the remaining quantities:

$$0 = \delta_{\mathbf{e}_a} E_{CG} = \int d^2\sigma \sqrt{g}\, [\mathbf{f}^a + \lambda^a \mathbf{N} - \Lambda^{ab} \partial_a \mathbf{N} - 2\lambda^{ab} \mathbf{e}_b] \delta\mathbf{e}_a \tag{A.5}$$

The Lagrange multipliers λ^a, λ_N force $\mathbf{N}$ to be the normal vector to the surface so it satisfies the Weingarten equation

$$\partial_a \mathbf{N} = K_a^b \mathbf{e}_b \tag{A.6}$$

Since the variation $\delta \mathbf{e}_a$ in (A.5) is arbitrary, the term in parenthesis must vanish. Using (A.6) in (A.5) we find

$$\mathbf{f}^a = (\Lambda^{ac} K_c^b - 2\lambda^{ab})\mathbf{e}_b - \lambda^a \mathbf{N} \quad . \tag{A.7}$$

Substituting (A.7) in (A.4) we find

$$D_a \mathbf{f}^a = D_a(\Lambda^{ac} K_c^b - 2\lambda^{ab})\mathbf{e}_b + (\Lambda^{ac} K_c^b - 2\lambda^{ab}) D_a \mathbf{e}_b - (D_a \lambda^a)\mathbf{N} - \lambda^a D_a \mathbf{N} \tag{A.8}$$

Using the Weingarten equation (A.6) and its counterpart $D_b \mathbf{e}_a = -K_{ab}\mathbf{N}$, we find

$$D_a \mathbf{f}^a = [D_a(\Lambda^{ac} K_c^b - 2\lambda^{ab}) - \lambda^a K_a^b]\mathbf{e}_b - [D_a \lambda^a + K_{ab}\Lambda^{ac} K_c^b - 2\lambda^{ab} K_{ab}]\mathbf{N} = 0 \quad . \tag{A.9}$$

The component of (A.9) along the normal to the surface is the scalar Euler-Lagrange equation for the Willmore functional:

$$\mathbf{N} \cdot D_a \mathbf{f}^a = 0 \quad \Rightarrow \quad D_a \lambda^a + K_{ab}\Lambda^{ac} K_c^b - 2\lambda^{ab} K_{ab} = 0 \quad . \tag{A.10}$$

The Lagrange multipliers $\lambda^a, \Lambda^{ab}, \lambda^{ab}$ appearing in (A.10) are found by varying E_{CG} with respect to $\mathbf{N}, K_{ab}, g_{ab}$. The variation with respect to the normal vector gives

$$0 = \delta_{\mathbf{N}} E_{CG} = \int d^2\sigma \sqrt{g}\, [\lambda^a \mathbf{e}_a + 2\lambda_N \mathbf{N} - \delta_{\mathbf{N}}(\Lambda^{ab}\mathbf{e}_a \cdot \partial_b \mathbf{N})]\delta \mathbf{N} \quad . \tag{A.11}$$

The variation of the normal vector is arbitrary, so the term in square parenthesis must vanish. Since the Lagrange multipliear λ^a enforces orthogonality betweeen $\mathbf{e}_a$ and $\mathbf{N}$, the last term can be rewritten as $\Lambda^{ab}\mathbf{e}_a \cdot \partial_b \mathbf{N} = -\mathbf{N} \cdot D_b(\Lambda^{ab}\mathbf{e}_b)$. Then the integrand in equation (A.11) reduces to

$$\lambda^a \mathbf{e}_a + 2\lambda_N \mathbf{N} + (D_b \Lambda^{ab})\mathbf{e}_a + \Lambda^{ab} D_b \mathbf{e}_a = 0 \quad . \tag{A.12}$$

Using the Weingarten equation $D_b\mathbf{e}_a = -K_{ab}\mathbf{N}$, we finally obtain

$$(\lambda^a + D_b\Lambda^{ab})\mathbf{e}_a + (2\lambda_N - K_{ab}\Lambda^{ab})\mathbf{N} = 0 \quad . \tag{A.13}$$

This equation determines the Lagrange multiplier λ^a

$$\lambda^a = -D_b\Lambda^{ab} \quad . \tag{A.14}$$

The variation with respect to K_{ab} determines the Lagrange multiplier Λ^{ab}:

$$\delta_{K_{ab}}E_{CG} = \frac{\kappa}{8}\int d^2\sigma\,\sqrt{g}\,\delta(g^{ab}K_{ab})^2 + \int d^2\sigma\,\sqrt{g}\,\Lambda^{ab}\delta K_{ab} \tag{A.15}$$

$$= \frac{\kappa}{8}\int d^2\sigma\,\sqrt{g}\,2Kg^{ab}\delta K_{ab} + \int d^2\sigma\,\sqrt{g}\,\Lambda^{ab}\delta K_{ab} \tag{A.16}$$

$$= \int d^2\sigma\,\sqrt{g}\,\left[\frac{\kappa}{4}Kg^{ab} + \Lambda^{ab}\right]\delta K_{ab} \tag{A.17}$$

where $K = K^a_a$. Imposing $\delta_{K_{ab}}E_{CG} = 0$ for arbitrary variations of δK_{ab}, we conclude that

$$\Lambda^{ab} = -\frac{\kappa}{4}Kg^{ab} \quad . \tag{A.18}$$

Inserting (A.18) in (A.14), and noting the covariant derivative is compatible with the metric ($D_a g^{ab} = 0$), we find

$$\lambda^a = \frac{\kappa}{4}D^a K \quad . \tag{A.19}$$

The Lagrange multiplier λ^{ab} is determined by varying E_{CG} with respect to the tensor g_{ab}. Each term in (A.1) depend on the metric determinant so they should, in principle, be varied with respect to g_{ab}. But the terms proportional to $\mathbf{f}^a, \lambda^a, \lambda_N, \Lambda^{ab}$ don't depend on g_{ab} and are zero on the Euler-Lagrange equations thanks to the constraints.

Only two terms give non vanishing contributions:

$$\delta_{g_{ab}} E_{CG} = \delta_{g_{ab}} \left\{ \frac{\kappa}{8} \int d^2\sigma \, \sqrt{g} \, (g_{ab} K^{ab})^2 + \int d^2\sigma \, \sqrt{g} \, \lambda^{ab} (g_{ab} - \mathbf{e}_a \cdot \mathbf{e}_b) \right\} = 0 \quad . \tag{A.20}$$

Taking the variation into the integral sign and omitting the subscript g_{ab} in $\delta_{g_{ab}}$ for clarity of notation gives

$$\frac{\kappa}{8} \delta(\sqrt{g}) K^2 + \frac{\kappa}{8} \sqrt{g} \delta K^2 + \delta(\sqrt{g})(g_{ab} - \mathbf{e}_a \cdot \mathbf{e}_b) + \sqrt{g} \lambda^{ab} \delta g_{ab} = 0 \quad . \tag{A.21}$$

where $K = K^a_a$ denotes the trace of the extrinsic curvature tensor. The third term in (A.21) vanishes on the stationary point thanks to the constraint $g_{ab} = \mathbf{e}_a \cdot \mathbf{e}_b$. Using

$$\delta K^2 = 2K \delta K = 2K \delta(g_{ab} K^{ab}) = 2K K^{ab} \delta g_{ab} \tag{A.22}$$

and the variation of the area element

$$\delta(\sqrt{g}) = \frac{1}{2} \sqrt{g} g^{ab} \delta g_{ab} \quad , \tag{A.23}$$

we reduce (A.21) to

$$\sqrt{g} \left[\frac{\kappa}{16} K^2 g^{ab} + \frac{\kappa}{4} K K^{ab} + \lambda^{ab} \right] \delta g_{ab} = 0 \quad . \tag{A.24}$$

Relation (A.24) determines the last Lagrange multiplier:

$$\lambda^{ab} = -\frac{\kappa}{16} K^2 g^{ab} - \frac{\kappa}{4} K K^{ab} \quad . \tag{A.25}$$

Substituting (A.25), (A.18) and (A.19) in the Euler-Lagrange equation (A.10) and after simple algebraic manipulations we find

$$2D_aD^aK + K(2K^a_bK^b_a - K^2) = 0 \quad . \tag{A.26}$$

We can also write (A.26) in terms of the mean curvature H defined as $H \equiv K/2$. First, we note that

$$K^a_bK^b_a = k_1^2 + k_2^2 = (k_1 + k_2)^2 - 2k_1k_2 \quad . \tag{A.27}$$

Since the Gaussian curvature is $K_G = k_1k_2$ and $H = (k_1 + k_2)/2$, we have the useful relation

$$K^a_bK^b_a = 2(2H^2 - K_G) \quad . \tag{A.28}$$

Substituting (A.28) and $K = 2H$ in (A.26) we finally find the Euler-Lagrange equation for the Willmore functional

$$\Delta H + 2H(H^2 - K_G) = 0 \quad , \quad \Delta = D_aD^a \quad . \tag{A.29}$$

Appendix B

Minimal Surfaces

The aim of minimal surface theory is to find the surface Σ of minimal area bounded by a prescribed curve Γ. In 1760 Lagrange introduced the problem of finding the shape of minimal area bounded by a curve. The problem of minimal soap films was solved by Monge and Plateau. The energy of the surface Σ is proportional to its total area A:

$$E[\Sigma_\Gamma] = \gamma A = \gamma \int_{\Sigma_\Gamma} \sqrt{g}\, d^2\sigma \quad , \tag{B.1}$$

where γ is the surface tension, $g = \det g_{ab}$,

$$g_{ab} = \partial_a \mathbf{X} \cdot \partial_b \mathbf{X} \tag{B.2}$$

is the induced metric and $\sqrt{g}\, d^2\sigma$ is the area element induced by the embedding $\mathbf{X}$. The surfaces $\hat{\mathbf{X}}$ of minimal area are the absolute minima of the functional E. In order to find the stationary points of the functional E, we consider a variation of the embedding $\delta\mathbf{X}$. The surface is anchored to the boundary curve, so $\delta\mathbf{X} = 0$ on Γ. Under the deformation $\delta\mathbf{X}$, the area changes as

$$\delta A = \frac{\delta E}{\gamma} = \frac{1}{2} \int_{\Sigma_\Gamma} d^2\sigma \delta\sqrt{g} = \frac{1}{2} \int_{\Sigma_\Gamma} d^2\sigma \sqrt{g} g^{ab} \delta g_{ab} \tag{B.3}$$

where we used the variation of $\sqrt{g}$: $\delta\sqrt{g} = \frac{1}{2}\sqrt{g}g^{ab}\delta g_{ab}$. The variation of the induced metric (B.2) is

$$\delta g_{ab} = \mathbf{t}_a \cdot \partial_b \delta\mathbf{X} + \mathbf{t}_b \cdot \partial_a \delta\mathbf{X} \quad , \quad \mathbf{t}_a = \partial_a \mathbf{X} \quad . \tag{B.4}$$

Using (B.4) in (B.3) , the variation of the energy is

$$\delta E = \frac{1}{2}\int_{\Sigma_\Gamma} d^2\sigma \sqrt{g} g^{ab}(\mathbf{t}_a \cdot \partial_b \delta\mathbf{X} + \mathbf{t}_b \cdot \partial_a \delta\mathbf{X}) \quad . \tag{B.5}$$

integration by parts gives a bulk and a boundary term:

$$\delta E = -\frac{1}{2}\int_{\Sigma_\Gamma} d^2\sigma \sqrt{g} g^{ab}(D_b\mathbf{t}_a + D_a\mathbf{t}_b)\cdot\delta\mathbf{X} + \frac{1}{2}\int_{\Sigma_\Gamma} d^2\sigma\sqrt{g}\, D^a(\mathbf{t}_a\cdot\delta\mathbf{X}) \quad . \tag{B.6}$$

Using the divergence theorem, we convert the second term into an integral over the boundary curve Γ:

$$\delta E = -\int_{\Sigma_\Gamma} d^2\sigma\sqrt{g}\,(g^{ab}D_a\mathbf{t}_b)\cdot\delta\mathbf{X} + \frac{1}{2}\oint_\Gamma dn^a\,\mathbf{t}_a\cdot\delta\mathbf{X} \tag{B.7}$$

where n^a is the normal to Γ. The boundary term vanishes because the variation is zero on the curve Γ. Remembering that $\mathbf{t}_b = \partial_b\mathbf{X}$, in the bulk variation we recognize the the trace of the extrinsic curvature tensor, which is proportional to the mean curvature $\mathrm{Tr}(D_a\partial_b\mathbf{X}) = 2H$. The final form of the variation is

$$\delta E = -\int_{\Sigma_\Gamma} d^2\sigma\sqrt{g}\,\mathrm{Tr}(D_a\partial_b\mathbf{X})\cdot\delta\mathbf{X} = -2\int_{\Sigma_\Gamma} d^2\sigma\sqrt{g}\,H^\mu\delta X^\mu \quad . \tag{B.8}$$

We conclude that the mean curvature of stationary points of E must vanish locally:

$$\delta E = 0 \;\Rightarrow\; H(\boldsymbol{\sigma}) = 0 \quad . \tag{B.9}$$

The mean curvature is the sum of the local principal curvatures k_1, k_2, defined as the inverse of the principal radii of curvature. When the mean curvature vanishes everywhere, the principal curvatures have to be opposite. This means that every point on the surface must be a symmetric saddle point in the sense that the up-hill direction must have the same steepness as the down-hill direction. The condition $H = 0$ is a necessary but not sufficient to solve the Plateau problem. Only global minima of E are surfaces of least area. We can write condition (B.9) in terms of the Laplace-Beltrami operator $\Delta = D_a D^a$ on the surface as:

$$\delta E = 0 \Rightarrow \Delta \mathbf{X} = D_a D^a \mathbf{X} = 0 \quad . \tag{B.10}$$

The 3 components of the embedding are harmonic functions. The expression of the Laplacian in an arbitrary coordinate system is

$$\Delta \mathbf{X} = D_a D^a \mathbf{X} = \frac{1}{\sqrt{g}} \frac{\partial}{\partial \sigma^a} \left(\sqrt{g} g^{ab} \frac{\partial}{\partial \sigma^b} \mathbf{X} \right) \quad . \tag{B.11}$$

Thanks to a well-known result by Gauss, a 2-dimensional surface always admits orthonormal (isothermal) coordinates (ξ^1, ξ^2) such that the metric is locally proportional to the Euclidean flat metric:

$$g_{ab}(\boldsymbol{\xi}) = \rho(\boldsymbol{\xi}) \delta_{ab} \quad , \tag{B.12}$$

where ρ is called the conformal factor. In isothermal coordinates, the determinant and the inverse of the metric are given by

$$g = \rho^2(\boldsymbol{\xi}) \qquad g^{ab} = \rho^{-1} \delta^{ab} \quad . \tag{B.13}$$

Using (B.13) in (B.11), the Laplace-Beltrami operator becomes proportional to the Laplacian in flat space:

$$\Delta = \frac{1}{\rho}(\partial^2_{\xi^1} + \partial^2_{\xi^2}) \qquad , \quad \boldsymbol{\xi} \text{ isothermal} \tag{B.14}$$

so when parametrized with isothermal coordinates, the candidate mininmal surfaces are solutions to the flat-space Laplace equation.

Appendix C

Conformal invariance of the Willmore functional

Given a surface Σ embedded in $\mathbb{R}^3$ its Willmore energy is

$$W[\Sigma] = \int_\Sigma H^2 dA \tag{C.1}$$

Where the mean curvature H^μ is given by:

$$H^\mu = \frac{1}{2} K^\mu_{ab} g^{ab} = \frac{1}{2} K^{\mu a}_a \quad a, b = 1, 2 \quad \mu, \nu = 1, 2, 3 \tag{C.2}$$

where K^μ_{ab} is the extrinsic curvature (second fundamental form), g_{ab} is the metric induced by the embedding $\mathbf{X}$:

$$g_{ab} = G_{\mu\nu} \partial_a X^\mu \partial_b X^\nu \quad , \tag{C.3}$$

and $G_{\mu\nu}$ is the metric in the ambient space $\mathbb{R}^3$. We can introduce the tangent vectors $\mathbf{e}_a = \partial_a \mathbf{X}$ on the surface, and the unit normal

$$\mathbf{N} = \frac{\mathbf{e}_1 \times \mathbf{e}_2}{\sqrt{\langle \mathbf{e}_1 \times \mathbf{e}_2 \ , \ \mathbf{e}_1 \times \mathbf{e}_2 \rangle}} \quad . \tag{C.4}$$

The second fundamental form $\mathbf{K}$ is defined as

$$\mathbf{K}_{ab} = \nabla_{\mathbf{e}_a} \mathbf{e}_b \tag{C.5}$$

where ∇ is the covariant derivative in the ambient space. Notice that K^μ_{ab} is a vector in $\mathbb{R}^3$. It is possible to prove that the vector K^μ_{ab} is orthogonal to any vector tangent to the surface Σ:

$$\langle \mathbf{e}_c, \nabla_{\mathbf{e}_a} \mathbf{e}_b \rangle = 0 \quad \forall\, c, a, b \tag{C.6}$$

Hence, K^μ_{ab} lies entirely along the normal N^μ:

$$K^\mu_{ab} = K_{ab} N^\mu \quad , \quad K_{ab} \equiv \langle \mathbf{N}, \nabla_{\mathbf{e}_a} \mathbf{e}_b \rangle \tag{C.7}$$

Using this expression of the second fundamental form, we can write the mean curvature vector as

$$H^\mu = \frac{1}{2} K^a_a N^\mu \quad . \tag{C.8}$$

Since the normal vector has unit 3-dimensional norm, we also have $H^2 = (K^a_a)^2/4$.

We start by showing that the Willmore functional is invariant under a uniform scale transformation $X^\mu \to \lambda X^\mu$, where λ is a constant. The area element $dA = \sqrt{g} d^2\sigma$ depends on the induced metric trough the determinant. Since $g_{ab} = \partial_a \mathbf{X} \cdot \partial_b \mathbf{X}$, $g_{ab} \to \lambda^2 g_{ab}$ and the determinant transforms as $g \to \lambda^4 g$. Thus, the area element transforms as $dA \to \lambda^2 dA$. By (4.15), the mean curvature has dimension of inverse length, so it transforms as $H \to H/\lambda$. So $\mathrm{d}A\, H^2$ is invariant under uniform scaling.

We will now consider local conformal transformations of the coordinates in in 3–dimensional embedding space. A transformation

$$\mathbf{X} \to \mathbf{X}' \tag{C.9}$$

is conformal if the metric of the embedding space changes by a position-dependent prefactor

$$G_{\mu\nu}(\mathbf{X}) \longrightarrow e^{2\varphi(\mathbf{X})} G_{\mu\nu}(\mathbf{X}) \quad , \tag{C.10}$$

where we chose the exponential form for convenience of notation. Expression (C.8) is particularly convenient to find how the mean curvature changes under a conformal transformation of the ambient space. The normal vector, due to the scalar product in the denominator, acquires a factor of $e^{-\varphi}$:

$$N^\mu \to e^{-\varphi} N^\mu \tag{C.11}$$

The the extrinsic curvature changes as:

$$K_{ab} \to e^{\varphi}(K_{ab} + g_{ab}\, N^\nu \nabla_\nu \varphi) \tag{C.12}$$

Taking the trace, we find

$$K^a_a = K_{ab} g^{ab} \to e^{\varphi}(K_{ab} + g_{ab}\, N^\nu \nabla_\nu \varphi) e^{-2\varphi} g^{ab} = e^{-\varphi}(K^a_a + 2 N^\nu \nabla_\nu \varphi) \quad . \tag{C.13}$$

So the mean curvature changes as $H^\mu \to \frac{1}{2} e^{-2\varphi}(K^a_a + 2N^\nu \nabla_\nu \varphi) N^\mu$. Due to the presence of the normal derivative $n^\nu \nabla_\nu \varphi$, the mean curvature doesn't transform in a simple way. Fortunately, we can study an alternative expression. From the above relations, we see that the *traceless* part of the extrinsic curvature transforms in a

simple way under conformal transformation. Define

$$\hat{K}_{ab} \equiv K_{ab} - \frac{1}{2} g_{ab} K^a_a \tag{C.14}$$

Then, under a conformal transformation, we have:

$$\hat{K}_{ab} \to e^{\varphi}(K_{ab} + g_{ab} N^\nu \nabla_\nu \varphi) - \frac{1}{2} e^{-\varphi}(K^a_a + 2N^\nu \nabla_\nu \varphi) e^{2\varphi} g_{ab} \tag{C.15}$$

the terms containing the normal derivative of φ cancel, so the traceless part of the extrinsic curvature transforms simply with a pre-factor:

$$\boxed{\hat{K}_{ab} \to e^{\varphi} \hat{K}_{ab}} \quad . \tag{C.16}$$

Next, we need to find the relation between H^2 and $\hat{K}_{ab}$. Let us compute the norm squared of $\hat{K}_{ab}$:

$$\hat{K}_{ab}\hat{K}^{ab} = \left(K_{ab} - \frac{1}{2} g_{ab} K^a_a\right)\left(K^{ab} - \frac{1}{2} g^{ab} K^a_a\right) = K_{ab}K^{ab} - \frac{1}{2}(K^a_a)^2 \tag{C.17}$$

Using $H^2 = (K^a_a)^2/4$, we find

$$\hat{K}_{ab}\hat{K}^{ab} = \hat{K}^b_a \hat{K}^a_b = K^b_a K^a_b - 2H^2 \quad . \tag{C.18}$$

The matrix K^a_b can be conveniently represented in the basis of principal curvature (Gauss coordinates), where K^a_b is diagonal:

$$K^a_b = \begin{pmatrix} k_1 & 0 \\ 0 & k_2 \end{pmatrix} \tag{C.19}$$

In this coordinate system, $K^b_a K^a_b = (K^1_1)^2 + (K^2_2)^2$ and

$$\hat{K}^b_a \hat{K}^a_b = k_1^2 + k_2^2 - 2H^2 \tag{C.20}$$

we can add and subtract a multiple of the Gaussian curvature $2K_G = 2k_1k_2$ and use $4H^2 = (k_1 + k_2)^2$:

$$\hat{K}^b_a \hat{K}^a_b = (k_1 + k_2)^2 - 2K_G - 2H^2 = 2H^2 - 2K_G \tag{C.21}$$

We are now able to express the mean curvature squared in terms of the traceless second fundamental form and the Gaussian curvature:

$$\boxed{H^2 = \frac{\hat{K}^b_a \hat{K}^a_b}{2} + K_G} \tag{C.22}$$

The Willmore functional is then re-written as:

$$W[\Sigma] = \int_\Sigma H^2 dA = \int_\Sigma \frac{\hat{K}^b_a \hat{K}^a_b}{2} dA + \int_\Sigma K_G \, dA = \int_\Sigma \frac{\hat{K}^b_a \hat{K}^a_b}{2} \sqrt{g} \, \mathrm{d}u\mathrm{d}v + 2\pi\chi(\Sigma) \tag{C.23}$$

We are now in position to prove the invariance of the functional under conformal transformations of the ambient space. The topological term does not depend on the embedding $\mathbf{X}$. The first integral is locally invariant under a conformal transformation, in fact

$$\hat{K}^b_a \hat{K}^a_b \sqrt{g} = g^{cb} \hat{K}_{ac} g^{da} \hat{K}_{bd} \sqrt{g} \to (e^{-2\varphi} e^{\varphi} e^{-2\varphi} e^{\varphi} e^{2\varphi}) g^{cb} \hat{K}_{ac} g^{da} \hat{K}_{bd} \sqrt{g} \quad , \tag{C.24}$$

from which we see that the Willmore energy is invariant under conformal transformations of the ambient space.

Appendix D

Lower bound of the Willmore energy for genus 0 surfaces.

In this section we prove that $W \geq 4\pi$ for all closed surfaces of genus 0. The first observation in the proof is that the surface can be enclosed by a sphere $S^2(R)$ of sufficiently large radius R. Consider an arbitrary point P on S^2, and the plane Π tangent to S^2 at P. Let $\mathbf{n}$ be the normal vector in P. Bring the plane in contact with the compact surface Σ_0 keeping its normal vector parallel to the radius $R\mathbf{n}$. The plane Π will touch Σ_0 *for the first time* in a single point $P_{\mathbf{n}}$, where the Gaussian curvature is necessarily positive ($k_1 k_2 = K_G \geqslant 0$). We can repeat the procedure for all the tangent planes to $S^2(R)$, and build the set Σ^+ of all the 'first encountered' points $P_{\mathbf{n}}$. Now consider the Gauss map $\mathbf{N} : \Sigma_0 \to S^2$. Clearly, the image of Σ^+ under $\mathbf{N}$ is again the 2–sphere S^2. So we can identify $\mathbf{N}|_{\Sigma^+}$ resticted to Σ^+ with the embedding $\mathbf{n}$ of the unit sphere in $\mathbb{R}^3$. Consider orthogonal coordinates u, v on the unit sphere and the area integral

$$\int_{S^2} ||\mathbf{n}_u \times \mathbf{n}_v|| du dv = \int_{\Sigma^+} ||\mathbf{N}_u \times \mathbf{N}_v|| du dv = 4\pi \quad . \tag{D.1}$$

Since $\mathbf{N}$ is also the normal to Σ, we can write $\mathbf{N}_u$ as a combination of the tangent vectors to Σ: $\mathbf{N}_\alpha = K_\alpha^\beta \mathbf{t}_\beta$. After simplifying, we find the famous relation $||\mathbf{N}_u \times \mathbf{N}_v|| dudv = K_G dA$. We reached the result

$$4\pi = \int_{\Sigma^+} ||\mathbf{N}_u \times \mathbf{N}_v|| dudv = \int_{\Sigma^+} K_G \, dA \quad . \tag{D.2}$$

Next, we notice that $\Sigma^+ \subseteq \hat{\Sigma}^+ = \{Q \in \Sigma : K_G \geqslant 0\}$ which implies the inequality

$$\int_{\Sigma^+} K_G \, dA \leqslant \int_{\hat{\Sigma}^+} K_G \, dA \tag{D.3}$$

It is easy to prove that $K_G \leqslant H^2$ so we have:

$$\int_{\hat{\Sigma}^+} K_G \, dA \leqslant \int_{\hat{\Sigma}^+} H^2 \, dA \tag{D.4}$$

Finally, the surface $\hat{\Sigma}^+$ is contained in the surface Σ. Since H^2 is a positive quantity, we conclude that

$$\int_{\hat{\Sigma}^+} H^2 \, dA \leqslant \int_{\Sigma} H^2 \, dA = W[\Sigma_0] \quad . \tag{D.5}$$

Combining the inequalities from (D.2) to (D.5), we find that the Willmore energy of a closed surface of genus 0 cannot be smaller than 4π:

$$W[\Sigma_0] \geq 4\pi \quad . \tag{D.6}$$

Bibliography

[1] H. Aharoni, E. Sharon and R. Kupferman. Geometry of Thin Nematic Elastomer Sheets. *Phys. Rev. Lett.*, **113** 257801 (2014)

[2] J. Ambjørn, A. Sedrakyan and G. Thorleifsson. The 3D Ising model represented as random surfaces. *Physics Letters B*, **303** 327–333 (1993)

[3] D. J. Amit and V. Martin-Mayor. Field Theory, the Renormalization Group, and Critical Phenomena, (WORLD SCIENTIFIC2005), 3rd ed.

[4] P. W. Anderson. More is different. *Science*, **177**(4047): 393–396 (1972)

[5] Aristotle. Metaphysics. **7**

[6] A. P. Balachandran, F. Lizzi and V. G. J. Rodgers. Topological Symmetry Breakdown in Cholesterics, Nematics, and He3. *Physical Review Letters*, **52**(20): 1818–1821 (1984)

[7] V. L. Berezinskii. Destruction of Long-Range Order in 1- and 2-Dimensional Systems Possessing Continuous Symmetry - Classical Systems. *Jetp*, **32**(3): 493–500 (1971)

[8] M. J. Bowick and L. Giomi. Two-dimensional matter: Order, curvature and defects. *Advances in Physics*, **58**(5): 449–563 (2009)

[9] M. J. Bowick, D. R. Nelson and A. Travesset. Interacting topological defects on frozen topographies. *Physical Review B*, **62**(13): 8738–8751 (2000)

[10] M. J. Bowick and R. Sknepnek. Pathways to faceting of vesicles. *Soft Matter*, **9**(34): 8088–8095 (2013)

[11] P. B. Canham. The minimum energy of bending as a possible explanation of the biconcave shape of the human red blood cell. *Journal of Theoretical Biology*, **26**(1): 61–81 (1970)

[12] A. Carbone and N. Seeman. A route to fractal DNA-assembly. *Natural Computing*, **1** 469–480 (2002)

[13] J. Cardy. Fluctuating Geometries in Statistical Mechanics and Field Theory, vol. 4 (1996)

[14] S. R. Chandrasekhar and G. S. Ranganath. No Title. *Adv. Phys.*, **35** 507 (1986)

[15] J. H. Conway and S. Torquato. Packing, tiling, and covering with tetrahedra. *Proceedings of the National Academy of Sciences*, **103**(28): 10612–10617 (2006)

[16] F. David. Random surfaces and the statistics of membranes. *Physics Reports*, **184**(2): 221 – 227 (1989)

[17] F. David and S. Leibler. Vanishing tension of fluctuating membranes. *Journal de Physique II*, **1**(8): 959–976 (1991)

[18] J. A. Davies (Ed.) Mechanisms of Morphogenesis, (Academic Press, Boston2013), 2nd ed.

[19] P. G. De Gennes and C. Taupin. Microemulsions and the flexibility of oil/water interfaces. *The Journal of Physical Chemistry*, **86**(13): 2294–2304 (1982)

[20] M. W. Deem and D. R. Nelson. Free energies of isolated five- and sevenfold disclinations in hexatic membranes. *Phys. Rev. E*, **53** 2551–2559 (1996)

[21] G. A. DeVries, M. Brunnbauer, Y. Hu, A. M. Jackson, B. Long, B. T. Neltner, O. Uzun, B. H. Wunsch and F. Stellacci. Divalent metal nanoparticles. *Science*, **315**(5810): 358–361 (2007)

[22] D. E. Discher and A. Eisenberg. Polymer Vesicles. *J. Coll. Interface Sci*, **290**(23): 525 (2000)

[23] M. P. Do Carmo. Differential Geometry of Curves and Surfaces: Revised and Updated Second Edition, (Courier Dover Publications 2016)

[24] A. Donev, J. Burton, F. H. Stillinger and S. Torquato. Tetratic order in the phase behavior of a hard-rectangle system. *Physical Review B*, **73**(5): 19–28 (2006)

[25] G. Duclos, C. Erlenkämper, J. F. Joanny and P. Silberzan. Topological defects in confined populations of spindle-shaped cells. *Nature Physics*, **13**(1): 58–62 (2017)

[26] E. Efrati, E. Sharon and R. Kupferman. Elastic theory of unconstrained non-Euclidean plates. *Journal of the Mechanics and Physics of Solids*, **57**(4): 762–775 (2009)

[27] E. Efrati, E. Sharon and R. Kupferman. The metric description of elasticity in residually stressed soft materials (2013)

[28] L. Euler. Elementa doctrine solidorum. *Novi comm. acad. scientiarum imperialis petropolitanae*, **4** 109–160 (1758)

[29] L. G. Fel. Tetrahedral symmetry in nematic liquid crystals. *Physical Review E*, **52**(1): 702–717 (1995)

[30] A. Fernández-Nieves, V. Vitelli, A. S. Utada, D. R. Link, M. Márquez, D. R. Nelson and D. A. Weitz. Novel defect structures in nematic liquid crystal shells. *Physical Review Letters*, **99**(15): 157801 (2007)

[31] B. Fourcade. Theoretical results on toroidal vesicles. *Journal de Physique II*, **2**(9): 1705–1724 (1992)

[32] B. Fourcade, M. Mutz and D. Bensimon. Experimental and theoretical study of toroidal vesicles. *Physical Review Letters*, **68**(16): 2551–2554 (1992)

[33] J. R. Frank and M. Kardar. Defects in nematic membranes can buckle into pseudospheres. *Physical Review E*, **77**(4): (2008)

[34] Friedel, G. Les états mésomorphes de la matière. *Ann. Phys.*, **9**(18): 273–474 (1922)

[35] J. T. F.R.S. XXIV. On the structure of the atom: an investigation of the stability and periods of oscillation of a number of corpuscles arranged at equal intervals around the circumference of a circle; with application of the results to the theory of atomic structure. *The London, Edinburgh, and Dublin Philosophical Magazine and Journal of Science*, **7**(39): 237–265 (1904)

[36] J. Geng and J. V. Selinger. Theory and simulation of two-dimensional nematic and tetratic phases. *Physical Review E*, **80**(1): (2009)

[37] D. P. Gennes and J. Prost. The Physics of Liquid Crystals, vol. 2 (1993)

[38] S. Germain. Recherches sur la théorie des surfaces élastiques, (Mme. Ve. Courcier 1821)

[39] L. Giomi and M. J. Bowick. Defective ground states of toroidal crystals. *Physical Review E*, **78**(1): 010601 (2008)

[40] S. C. Glotzer and M. J. Solomon. Anisotropy of building blocks and their assembly into complex structures. *Nature Materials*, **6**(8): 557–562 (2007)

[41] R. Goetz, G. Gompper and R. Lipowsky. Mobility and Elasticity of Self-Assembled Membranes. *Physical Review Letters*, **82** 221–224 (1999)

[42] J. Guven. Membrane geometry with auxiliary variables and quadratic constraints. *Journal of Physics A: Mathematical and General*, **37**(28): L313–L319 (2004)

[43] B. I. Halperin and D. R. Nelson. Theory of Two-Dimensional melting. *Physical Review Letters*, **41**(2): 121–124 (1978)

[44] W. Helfrich. Elastic Properties of Lipid Bilayers: Theory and Possible Experiments. *Zeitschrift fur Naturforschung - Section C Journal of Biosciences*, **28**(11-12): 693–703 (1973)

[45] W. Helfrich. Elastic Properties of Lipid Bilayers: Theory and Possible Experiments. *Z. Naturforsch. C*, **28** (1973)

[46] P. J. Hilton. Book Review: Obstruction theory on homotopy classification of maps, vol. 1 of *Lecture Notes in Mathematics*, (Springer Berlin Heidelberg2008)

[47] C. Huang, D. Quinn, Y. Sadovsky, S. Suresh and K. J. Hsia. Formation and size distribution of self-assembled vesicles. *Proceedings of the National Academy of Sciences*, **114**(11): 2910–2915 (2017)

[48] D. Husemoller and D. Husemöller. Fibre Bundles, vol. 15 of *Graduate Texts in Mathematics*, (Springer1964)

[49] S. Jain and F. S. Bates. On the Origins of Morphological Complexity in Block Copolymer Surfactants. *Science*, **300**(5618): 460–464 (2003)

[50] L. Jia, A. Cao, D. Lévy, B. Xu, P. A. Albouy, X. Xing, M. J. Bowick and M. H. Li. Smectic polymer vesicles. *Soft Matter*, **5**(18): 3446–3451 (2009)

[51] F. Jülicher, S. W. Grill and G. Salbreux. Hydrodynamic theory of active matter. *Reports on Progress in Physics*, **81**(7): 076601 (2018)

[52] F. Jülicher and R. Lipowsky. Domain-induced budding of vesicles. *Physical Review Letters*, **70**(19): 2964–2967 (1993)

[53] F. Jülicher, U. Seifert and R. Lipowsky. Conformal degeneracy and conformal diffusion of vesicles. *Physical Review Letters*, **71**(3): 452–455 (1993)

[54] R. D. Kamien, D. R. Nelson, C. D. Santangelo and V. Vitelli. Extrinsic curvature, geometric optics, and lamellar order on curved substrates. *Physical Review E*, **80**(5): (2009)

[55] M. Kléman. Curved crystals, defects and disorder. *Advances in Physics*, **38**(6): 605–667 (1989)

[56] M. Kleman and O. D. Laverntovich. Soft matter physics: an introduction, (Springer Science & Business Media2007)

[57] M. Kléman, L. Michel and G. Toulouse. Classification of topologically stable defects in ordered media. *Journal de Physique Lettres*, **38**(10): 195–197 (2007)

[58] V. Koning, A. Fernandez-Nieves, V. Vitelli, T. Lopez-Leon and K. B. S. Devaiah. Frustrated nematic order in spherical geometries. *Nature Physics*, **7**(5): 391–394 (2011)

[59] J. M. Kosterlitz. The critical properties of the two-dimensional xy model. *Journal of Physics C: Solid State Physics*, **7**(6): 1046–1060 (1974)

[60] J. M. Kosterlitz and D. J. Thouless. Ordering, metastability and phase transitions in two-dimensional systems. *Journal of Physics C: Solid State Physics*, **6**(7): 1181–1203 (1973)

[61] L. Landau, E. Lifshitz, A. Kosevich, J. Sykes, L. Pitaevskii and W. Reid. Theory of Elasticity, vol. 7 of *Course of theoretical physics*, (Elsevier Science 1986)

[62] H. B. Lawson. Complete Minimal Surfaces in S¡sup¿3¡/sup¿. *Annals of Mathematics*, **92**(3): 335–374 (1970)

[63] H. B. Lawson. The Quantitative Theory of Foliations, vol. 27, (American Mathematical Society 1977)

[64] Y. Li, H. Miao, H. Ma and J. Z. Chen. Topological defects of tetratic liquid-crystal order on a soft spherical surface. *Soft Matter*, **9**(48): 11461–11466 (2013)

[65] G. Lim H. W., M. Wortis and R. Mukhopadhyay. Stomatocyte–discocyte–echinocyte sequence of the human red blood cell: Evidence for the bilayer– couple hypothesis from membrane mechanics. *Proceedings of the National Academy of Sciences*, **99**(26): 16766–16769 (2002)

[66] R. Lipowsky. The conformation of membranes. *Nature*, **349**(6309): 475–481 (1991)

[67] T. C. Lubensky and J. Prost. Orientational order and vesicle shape. *Journal de Physique II*, **2**(3): 371–382 (1992)

[68] P. L. Luisi and P. Walde. Giant Vesicles: Perspectives in Supramolecular Chemistry (2007)

[69] F. C. Mackintosh and T. C. Lubensky. Orientational order, topology, and vesicle shapes. *Physical Review Letters*, **67** 1169–1172 (1991)

[70] O. V. Manyuhina and M. J. Bowick. Forming a cube from a sphere with tetratic order. *Physical Review Letters*, **114**(11): 117801 (2015)

[71] F. Marques and A. Neves. Min-max theory and a proof of the Willmore conjecture. *ArXiv e-prints*, pp. 275–300 (2017)

[72] F. C. Marques and A. Neves. Min-Max theory and the Willmore conjecture. *Annals of Mathematics*, **179**(2): 683–782 (2014)

[73] F. C. Marques and A. Neves. The Willmore Conjecture. *Jahresbericht der Deutschen Mathematiker-Vereinigung*, **116**(4): 201–222 (2014)

[74] N. D. Mermin. The topological theory of defects in ordered media. *Reviews of Modern Physics*, **51**(3): 591–648 (1979)

[75] X. Michalet and D. Bensimon. Observation of Stable Shapes and Conformal Diffusion in Genus 2 Vesicles. *Science*, **269**(5224): 666–668 (1995)

[76] X. Michalet, D. Bensimon and B. Fourcade. Fluctuating vesicles of nonspherical topology. *Physical Review Letters*, **72**(1): 168–171 (1994)

[77] L. Michel. Symmetry defects and broken symmetry. Configurations hidden symmetry. *Reviews of Modern Physics*, **52**(3): 617–651 (1980)

[78] R. Mosseri. Visible points in a lattice. *Journal of Physics A: Mathematical and General*, **25**(1): L25–L29 (1992)

[79] M. Mutz and D. Bensimon. Observation of toroidal vesicles. *Physical Review A*, **43**(8): 4525–4527 (1991)

[80] D. Nelson and L. Peliti. Fluctuations in membranes with crystalline and hexatic order. *Journal de Physique*, **48**(7): 1085–1092 (1987)

[81] D. Nelson, T. Piran and S. Weinberg. Statistical Mechanics of Membranes and Surfaces, (World Scientific Pub. 2012)

[82] D. R. Nelson. Defects and geometry in condensed matter physics, (Cambridge University Press 2002)

[83] D. R. Nelson. Toward a Tetravalent Chemistry of Colloids. *Nano Letters*, **2**(10): 1125–1129 (2002)

[84] B. D. Olsen and R. A. Segalman. Self-assembly of rodcoil block copolymers. *Materials Science and Engineering: R: Reports*, **62**(2): 37 – 66 (2008)

[85] J. Park, T. C. Lubensky and F. C. Mackintosh. *n*-atic order and continuous shape changes of deformable surfaces of genus zero. *EPL (Europhysics Letters)*, **20**(3): 279–284 (1992)

[86] L. Peliti. Effective rigidity of membranes. *Physica A: Statistical Mechanics and its Applications*, **140**(1): 269 – 277 (1986)

[87] L. Peliti. Amphiphilic Membranes (1995)

[88] L. Peliti and S. Leibler. Effects of thermal fluctuations on systems with small surface tension. *Physical Review Letters*, **54**(15): 1690–1693 (1985)

[89] R. Penrose. The topology of ridge systems. *Annals of Human Genetics*, **42**(4): 435–444 (1979)

[90] V. Poénaru. Some aspects of the theory of defects of ordered media and gauge fields related to foliations. *Communications in Mathematical Physics*, **80**(1): 127–136 (1981)

[91] A. Polyakov. Fine structure of strings. *Nuclear Physics, Section B*, **268**(2): 406–412 (1986)

[92] A. M. Polyakov. Quantum geometry of bosonic strings. *Physics Letters B*, **103**(3): 207–210 (1981)

[93] A. M. Polyakov and M. E. Peskin. Gauge Fields and Strings , vol. 42 of *Contemporary concepts in physics*, (Taylor & Francis2008)

[94] S. Sacanna, D. J. Pine and G.-R. Yi. Engineering shape: the novel geometries of colloidal self-assembly. *Soft Matter*, **9** 8096–8106 (2013)

[95] J.-F. Sadoc. Geometrical Frustration, (Cambridge University Press 2008)

[96] U. Seifert. The concept of effective tension for fluctuating vesicles. *Zeitschrift für Physik B Condensed Matter*, **97**(2): 299–309 (1995)

[97] U. Seifert. Configurations of fluid membranes and vesicles. *Advances in Physics*, **46**(1): 13–137 (1997)

[98] H. S. Seung and D. R. Nelson. Defects in flexible membranes with crystalline order. *Physical Review A*, **38**(2): 1005–1018 (1988)

[99] H. Shin, M. J. Bowick and X. Xing. Topological Defects in Spherical Nematics. *Physical Review Letters*, **101**(3): 037802 (2008)

[100] G. Vernizzi, R. Sknepnek and M. Olvera de la Cruz. Platonic and Archimedean geometries in multicomponent elastic membranes. *Proceedings of the National Academy of Sciences*, **108**(11): 4292–4296 (2011)

[101] Virga, Epifanio G. Octupolar order in two dimensions. *Eur. Phys. J. E*, **38**(6): 63 (2015)

[102] V. Vitelli, J. B. Lucks and D. R. Nelson. Crystallography on curved surfaces. *Proceedings of the National Academy of Sciences*, **103**(33): 12323–12328 (2006)

[103] J. H. White. A Global Invariant of Conformal Mappings in Space. *Proceedings of the American Mathematical Society*, **38**(1): 162 (2006)

[104] T. J. Willmore. Note on embedded surfaces. *An. Şti. Univ. "Al. I. Cuza" Iaşi Secţ. I a Mat. (N.S.)*, **11B** 493–496 (1965)

[105] K. G. Wilson. Renormalization Group and Critical Phenomena. I. Renormalization Group and the Kadanoff Scaling Picture. *Phys. Rev. B*, **4** 3174–3183 (1971)

[106] K. G. Wilson and J. Kogut. The renormalization group and the ϵ expansion. *Physics Reports*, **12**(2): 75 – 199 (1974)

[107] M. Winterhalter and D. D. Lasic. Liposome stability and formation: Experimental parameters and theories on the size distribution. *Chemistry and Physics of Lipids*, **64**(1-3): 35–43 (1993)

[108] C. K. Wong, M. H. Stenzel and P. Thordarson. Non-spherical polymersomes: formation and characterization. *Chem. Soc. Rev.*, pp. – (2019)

[109] X. Xing. Topology and geometry of smectic order on compact curved substrates. *Journal of Statistical Physics*, **134**(3): 487–536 (2009)

[110] X. Xing, H. Shin, M. J. Bowick, Z. Yao, L. Jia and M.-H. Li. Morphology of nematic and smectic vesicles. *Proceedings of the National Academy of Sciences*, **109**(14): 5202–5206 (2012)

[111] B. Xu, R. Piñol, M. Nono-Djamen, S. Pensec, P. Keller, P. A. Albouy, D. Lévy and M. H. Li. Self-assembly of liquid crystal block copolymer PEG-b-smectic polymer in pure state and in dilute aqueous solution. *Faraday Discussions*, **143**(0): 235–250 (2009)

[112] D. Yllanes, S. S. Bhabesh, D. R. Nelson and M. J. Bowick. Thermal crumpling of perforated two-dimensional sheets. *Nature Communications*, **8**(1): (2017)

[113] E. H. Yong, D. R. Nelson and L. Mahadevan. Elastic platonic shells. *Physical Review Letters*, **111**(17): (2013)

[114] K. Zhao, R. Bruinsma and T. G. Mason. Supplementary Information Local Chiral Symmetry Breaking in Triatic Liquid Crystals. *Nat. Comm.*, **3** 1–3 (2012)

[115] O.-Y. Zhong-can. Anchor ring-vesicle membranes. *Phys. Rev. A*, **41** 4517–4520 (1990)

[116] F. Zhou, Z. Zhang, G. Jiang, J. Lu, X. Chen, Y. Li, N. Zhou and X. Zhu. Self-assembly of amphiphilic macrocycles containing polymeric liquid crystal grafts in solution. *Polymer Chemistry*, **7**(16): 2785–2789 (2016)

[117] L. Zhou, D. Zhang, S. Hocine, A. Pilone, S. Trépout, S. Marco, C. Thomas, J. Guo and M. H. Li. Transition from smectic nanofibers to smectic vesicles in the self-assemblies of PEG-: B -liquid crystal polycarbonates. *Polymer Chemistry*, **8**(33): 4776–4780 (2017)

Curriculum Vitæ

Francesco Serafin

Email: fserafin@syr.edu

Syracuse University
Physics Department *and*
Syracuse Soft and Living Matter Program
Syracuse, NY 13224, USA

KITP
Kavli Institute for Theoretical Physics
University of California
Santa Barbara, CA 93106, USA

Research Interests

Geometry and Topology in Soft Matter, Membranes, Topological Defects, Emergence of Shape.

Education

2015-present Ph.D. candidate at Syracuse University (NY)

2014 M.S. *cum laude* Theoretical Physics, Università degli Studi di Trieste

2011 B.Sc. Physics, Università degli Studi di Trieste

Professional Experience

Fall 2018 Affiliate Student at KITP

Fall 2017 Affiliate Student at KITP

Fall 2016 Affiliate Student at KITP

Teaching Experience

Main Instructor for *General Physics 1 – PHY211* (Summer 2015).

Teaching Assistant for *General Physics 1 – PHY211* at Syracuse University (Spring 2015-16-17-18, Fall 2015-16).

Grader for *Thermodynamics and Statistical Mechanics – PHY 731* and *Introduction to Modern Physics – PHY 361* at Syracuse University (Spring 2019).

Publications

4. **F. Serafin**, Mark J. Bowick, Sidney R. Nagel. *Topology and ground state degeneracy of tetrahedral smectic vesicles.* Eur. Phys. J. E 41 (12) 143 (2018) – Selected as EPJe Highlight article.

3. Mark J. Bowick, Oksana V. Manyuhina, **F. Serafin**. *Shapes and singularities in triatic liquid-crystal vesicles.* EPL, 117 (2017) 26001

2. **F. Serafin**, Mark J. Bowick. *An upper bound on the partition function of fluid vesicles.* – In preparation

1. **F. Serafin**, Suraj Shankar, Benjamin Loewe, Mark J. Bowick, M. C. Marchetti. *Activity driven buckling in early stages of organogenesis.* – In preparation

Posters and Presentations

Presentation at the *APS March Meeting 2019*. Title: A buckling model of an active epithelial tissue.

Presentation at the *APS March Meeting 2017*. Title: Topological defects and shapes of triatic liquid crystal vesicles.

Poster at the *5th Soft Matter Summer School and the 24th Innovative Workshop on Bio/Soft Materials: Membranes* at KAIST, Daejeon, South Korea. I received travel and lodging funding from the UCSB Materials Research Lab (MRL). (July 2017)

Awards

Summer Graduate Fellowship from the Syracuse Soft Matter Program. (Summer 2017)

Fellowship "Luciano Fonda" for Pyhsics from the University College for Sciences at Trieste University. (AYs 2008-09, 2009-10, 2010-11)

Last updated: March 2, 2019